SCALE AND COMPUTER MODELING OF WHEELED VEHICLES FOR PLANETARY EXPLORATION

by

HOWARD JAY EISEN
S.B., Massachusetts Institute of Technology
(1989)

Submitted in partial fulfillment of
the requirements for the degree of

MASTER OF SCIENCE
IN AERONAUTICS AND ASTRONAUTICS

at the

MASSACHUSETTS INSTITUTE OF TECHNOLOGY
June 1990

Signature of Author _____
Department of Aeronautics and Astronautics
May 11, 1990

Certified by _____
Prof. David L. Akin
Thesis Supervisor

Accepted by _____
Prof. Harold Y. Wachman
Chairman, Department Graduate Committee

SCALE AND COMPUTER MODELING
OF WHEELED VEHICLES
FOR PLANETARY EXPLORATION

by

Howard Jay Eisen

Abstract

Rovers are one of the options for acquiring surface information which would allow human exploration of planetary bodies. Our limited knowledge derived from the Viking landers and the Apollo and Surveyor programs indicate that Mars and the Moon possess rocky and sandy terrain. Any rovers sent there must therefore exhibit a high degree of mobility. This thesis develops a two-dimensional model of slow-speed vehicle mobility performance. Tests were also planned with a full-size vehicle but were not accomplished due to scheduling and technical problems. The scale model was, however, used to correlate the theoretical model with tested performance and validate the use of the two-dimensional quasi-static model.

Thesis Advisor: David L. Akin
Assistant Professor of Aeronautics and Astronautics

Acknowledgements

Many people have played an important role in my education at MIT and the events which led to the publication of this thesis. Yet among all those who have helped me on my way, some clearly stand out above the others.

First, I dedicate this thesis to the two people who have always had faith in me, my parents. Without their support and love, I could not have made it to and through MIT. Their constant help with all the red tape of living on two coasts, wake-up calls, and their visits, just for dinner. Now my dad isn't the only one in the family to publish.

Brian Muirhead and Don Bickler of JPL have guided me through my internship at JPL. I must thank Brian, for his patience with an inexperienced sophmore. Under his guidance, I grew in my technical, communicative and political skills. Don gave me my first introduction to the practical implementation problems that exist outside of the MIT theoretical engineering environment. Others at JPL such as Randy Lindemann and Carlos Moreno have contributed to this thesis both technically and with their friendship, especially through all the technical disagreements about the fine points no one really cares about anyway.

I am indebted to the faculty at MIT who have taken me from a teenager to an engineer in five years. But no other faculty member has been as much of an inspiration and a guide to me as the tremendous David L. Akin, who has demonstrated what I believe are the qualities of the finest of engineers. His broad base of knowledge defines what a systems engineer should be, and through his teachings I believe that I am now prepared to worry about every single aspect of a project. I am especially grateful for the opportunity to help impart some of his ideas mixed with my own perspective to the next graduating class of Astronautical engineers.

Finally, many friends have also provided support and fun during the good and bad that come with an MIT education. To them, all I have to say is, now that I have all my degrees, "I'll ask him, but I don't think he'll be very keen, you see, he's already got one" (and I got three).

This work was made possible by the NASA Mars Rover Sample Return and Pathfinder Planetary Rover Projects at the Jet Propulsion Laboratory, California Institute of Technology.

Table of Contents

List of Figures and Tables

1. INTRODUCTION

Roving vehicles will play an important role in the exploration of space as precursors to further manned exploration. Their design has not evolved appreciably since the 1960's, when rovers were planned to augment Apollo. Requirements placed on planetary rovers in terms of navigation and mobility are very different from those placed on Earth trucks, tanks and farm equipment. Rovers must exhibit a high degree of mobility to accommodate rough terrain, yet they must be capable of accurate position and orientation to allow for precision sampling. They must be robust to handle the extremes of the Lunar and Martian environments, and must be capable of a significant lifetime and range.

One of the most important rover subsystems is mobility. Both the terrains of Mars and the Moon are rough, with many large (> 0.5 m) boulders, slopes and other irregular features [Moore87a]. A failure in the mobility system would render the rover stationary; it would then be little more than a fixed lander, incapable of collecting samples and returning them to the ascent module for return to Earth, exploring geological formations, examining potential human landing sites and many other rover functions. Furthermore, increasing the obstacle negotiating capabilities of a vehicle will reduce the need to navigate around obstacles which are below the mobility limits, or may compensate for errors in navigation and terrain sensing.

Commercially available computer dynamic modelling codes have been proposed for use in the design and evaluation of rovers. Such modelling tools have limitations and still require custom user-developed subroutines to handle vehicle parameters (e.g. "tire"/terrain interfaces). Furthermore, dynamic systems are used primarily for high speed vehicle work where a steady state ratio of rotational velocity to forward velocity

is assumed. This assumption as implemented in standard dynamic codes is not valid for large obstacles and low speed vehicles [Bernard87].

Physical scale models can be used in the design process to verify and compare various designs. The models are relatively inexpensive, and can save the designer from building a costly full scale brassboard and then discovering a design flaw. Multiple scale models can also be built and tested under conditions outside that to which a full scale model could be subjected. However, the precise scaling of every parameter of the prototype may not be feasible. For example, in a model it may not be possible to produce the same flexibility in a given member as in the prototype design. If performance similitude can be established with a minimum number of constraints on the physical model design, then the models can be fabricated at little cost in local machine or hobby shops.

The purpose of this thesis is to establish similitude between the JPL Pathfinder Planetary Rover Navigational Systems Testbed ("Navtest") and a 1/7 scale model made for this thesis. In addition, 2-D computer models using quasi-static equilibrium techniques have been created which predict the performance limit of the Navtest and the scale model. The computer code can be used to investigate the sensitivity of mobility performance to changes in the vehicle geometry. The diagram below shows the scope of the thesis and the correlations used to establish similitude.

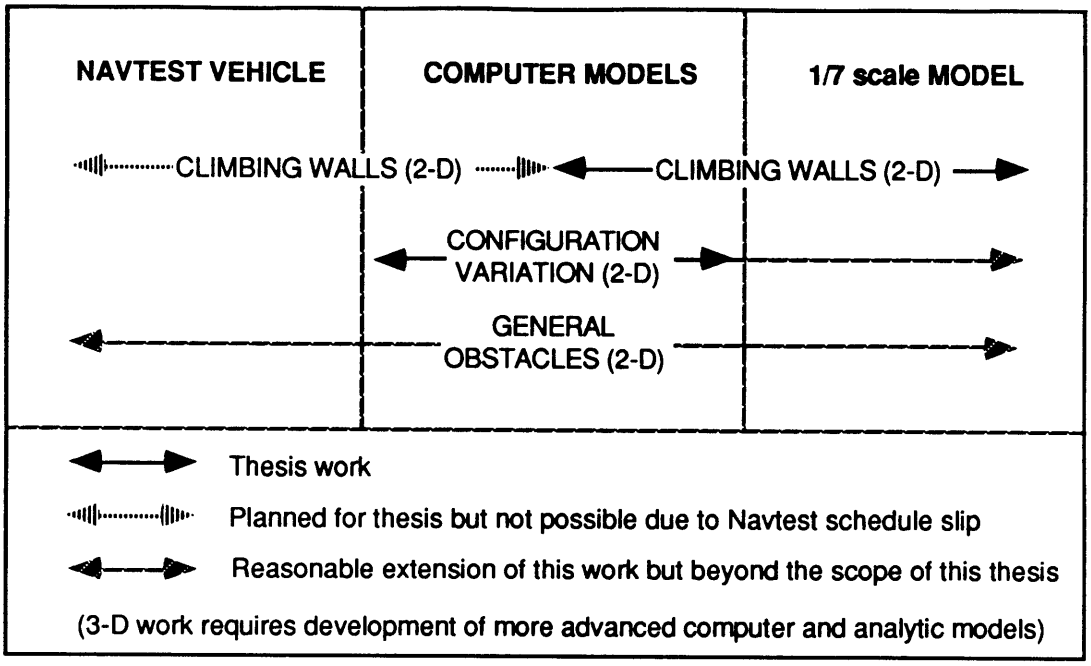

Figure 1-1
Scope of Thesis

2. BACKGROUND

The continuing exploration of the solar system, both manned and unmanned, is an evolving process. The general strategy for planetary exploration has been in three stages: flyby, orbiter and lander. The first non-earth based observations have occurred from the flyby missions such as Pioneer and Voyager. The next step involves the planetary orbiters and mappers, such as Mariner, Mars Observer, Galileo and Magellan. Orbiters can provide global perspective on the physical, chemical and electromagnetic structure of a celestial body. They do not, however, have the resolution to determine small scale surface features. They cannot determine physical and electrical surface and near-surface properties. Such information is necessary for design of human exploration missions. Landers such as Surveyor, Apollo, and Viking have been sent to the moon and Mars to acquire and return (Apollo) surface samples. These landers have been limited in their area coverage as they did not have roving capabilities to wander from beyond the locale of the landing site. (Apollo did have the lunar rover, but the astronauts were limited in their stay time, so significant distances could not be covered.)

Mobile vehicles, when coupled with sample return, have the potential to return a wealth of information about the foreign environments, as do robotic divers which probe the depths of the ocean floor. These vehicles can discover the information necessary to properly plan and execute manned exploration. The Apollo missions were preceded by the unmanned Surveyor lander program, which gave the first detailed pictures of the lunar surface and soil bearing strength measurements, assuring NASA that the lunar soil could support the bearing pressure of a human. Each lander was, however, only able to produce one data point and gave little information about the rest of the moon. The same is true on Mars, where Viking has investigated two isolated points on the

Martian surface about which a little is now known. Rovers could navigate larger terrain, aiding in global characterization and human landing site selection.

2.1 Mars Rover Sample Return Development Flight Project

For the past three years, NASA's Jet Propulsion Laboratory (JPL) has headed an effort to study a Mars Rover Sample Return (MRSR) mission to be launched to Mars beginning in 1998. This mission set has been modified recently to incorporate President Bush's call for the human exploration of the surface of Mars, beginning with rover precursors in the 2001-2005 time frame. The primary objectives of the MRSR mission are to:

1) Reconstruct the geological, climatological and biological history of Mars

2) Determine the composition and possible toxicity of its surface materials, so as to establish whether the surface is safe for human exploration, as well as to assess what natural resources might be available to assist in the preservation of human life

3) Test key technologies necessary to maximize the safety and effectiveness of human exploration [Bourke89]

These objectives are stated here in their official order, although the Human Exploration Initiative (HEI) is emphasizing the second and third objectives more. Mission studies conducted by JPL, Lyndon B. Johnson Space Center (JSC) and the Science Applications International Corporation (SAIC) have led to a set of requirements for Martian rovers.

These requirements led to a series of studies by JPL, Martin Marietta Astronautics Group and the FMC Corporation to determine candidate designs for Martian rovers. The JPL team focused its efforts on wheeled vehicles with passive suspension systems. The work related to this thesis was either part of or the result of that study [Piv89].

The Rocker-Bogie suspension which is the JPL baseline for the precursor phase of the Human Exploration Initiative (also known as Exploration Initiative Studies) is shown in Figure 2-1.

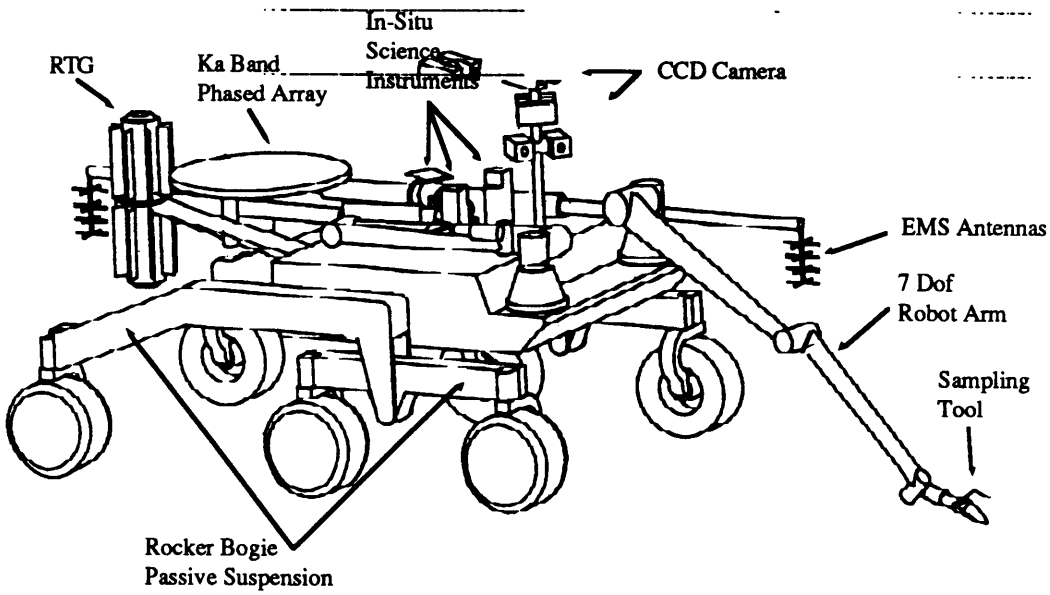

Figure 2-1
NASA/JPL Exploration Initiative Studies
Baseline Planetary Rover Configuration

A trade exists between mobility robustness and accuracy of the navigational systems. The rover designer has the option of sensing and avoiding an obstacle, or just selecting a mobility system which can handle the obstacle. The navigation requires large amounts of computation and storage, as well as accurate camera pointing and attitude sensing. Complex navigation also takes time and reduces the average speed of the vehicle. Mobility is limited primarily by size and reliability. A larger rover, in general, will be able to handle larger obstacles. Size is, however, limited by available launch mass and the aeroshell envelope. Rovers which are larger than the volume allowed by

the aeroshell are possible, if deployable structures are used. Such structures must have some form of actuation, which is another failure point and thus reduces system reliability.

Mobility can also be enhanced by using actively articulated suspension systems, which change the mobility configuration on command to better accommodate obstacles. Such suspensions have the same problem as the deployable structures: actuators can fail and reduce system reliability. Passive articulation is the compromise studied by the JPL rover team, possibly to be augmented by active elements in the future. Active suspensions must be designed to function passively in the event of actuator failure. Furthermore, independent control of drive motors also lends flexibility to obstacle traverse capabilities.[Piv89]

The standard model of the Martian surface [Moore87a] contains statistical probabilities of encountering slopes and obstacles. The data used for this model includes albedo measurements from orbit and Viking lander photos. A picture of the surface taken by the Viking 2 Lander is shown in Figure 2-4. Note the large quantity and variety of the rocks, as well as the flow of drift material. This terrain would be very challenging to a wheeled or legged rover and demonstrates the need for mobility research.

Present knowledge indicates that obstacles 0.5m in size will be encountered by a 2m wide rover approximately every 19m of traverse on the "nominal" terrain and every 4 m on "rocky" terrain. By configuring the rover to be able to climb meter size obstacles, the need to detect and avoid obstacles by the navigation system is reduced by a factor of six as compared to the requirements for 0.5m obstacles. The MRSR project has established in its requirements that rovers must be able to traverse obstacles defined as a 1.0 m high square step, a 1.0 m boulder and a 0.5 m wide bottomless ditch.

2.2 Pathfinder Planetary Rover Project

In FY'89, NASA started the Pathfinder Technology Program under the Office of Aeronautics and Space Technology, a series of small projects to foster the development of technologies which would enable the next generation of space exploration. One such project is the Pathfinder Planetary Rover (PPR), administered by JPL. Among the goals of PPR are to develop and validate analytical tools for vehicle design, local navigation and controls design. The tool developed in this thesis is an early step toward the generalized 3-D vehicle terrain/vehicle interaction simulator, which is an eventual goal of the program [Moreno89b].

One of the more advanced areas within the PPR project is the development of local navigation algorithms which use stereo camera/overhead image correlation. To validate these algorithms, PPR has fabricated the Navigational Systems Testbed (Navtest). This vehicle is approximately full scale, has six wheels, four bodies and five degrees of freedom (the wheel rotations are not considered to be free in this formulation, as they are fixed by the constraint that the vehicle is in contact with the terrain and slip is ignored). Variations in terrain are accommodated through three passively articulated joints. Two roll axles account for differences in terrain height across the width of the vehicle and one pitch axle accommodates variations in terrain slope [Moreno89a]. Steering can be accomplished via a steering motor located in the steering axle location indicated, or by leaving the axle free and driving wheels in opposite directions to cause the front and rear bodies (1 and 4) to rotate. The steering and roll provisions were not used in this study. The relevant geometry is shown in Figures 2-2 and 2-3.

The Navtest was assembled in the summer of 1989, and was used as a reference configuration for the models in this thesis. The vehicle was, however, not debugged and running at specifications as of March, 1990, and thus the vehicle was not available

for experimental use in this thesis. Nominal vehicle testing began in April and the vehicle is assumed to be operational in the summer of 1990. Test equipment designed for this thesis has been fabricated and is available for use as a continuation of this work as soon as the vehicle is ready (currently estimated to be August, 1990). These tests are described in chapter 5 and results will be published in an upcoming NASA Pathfinder report.

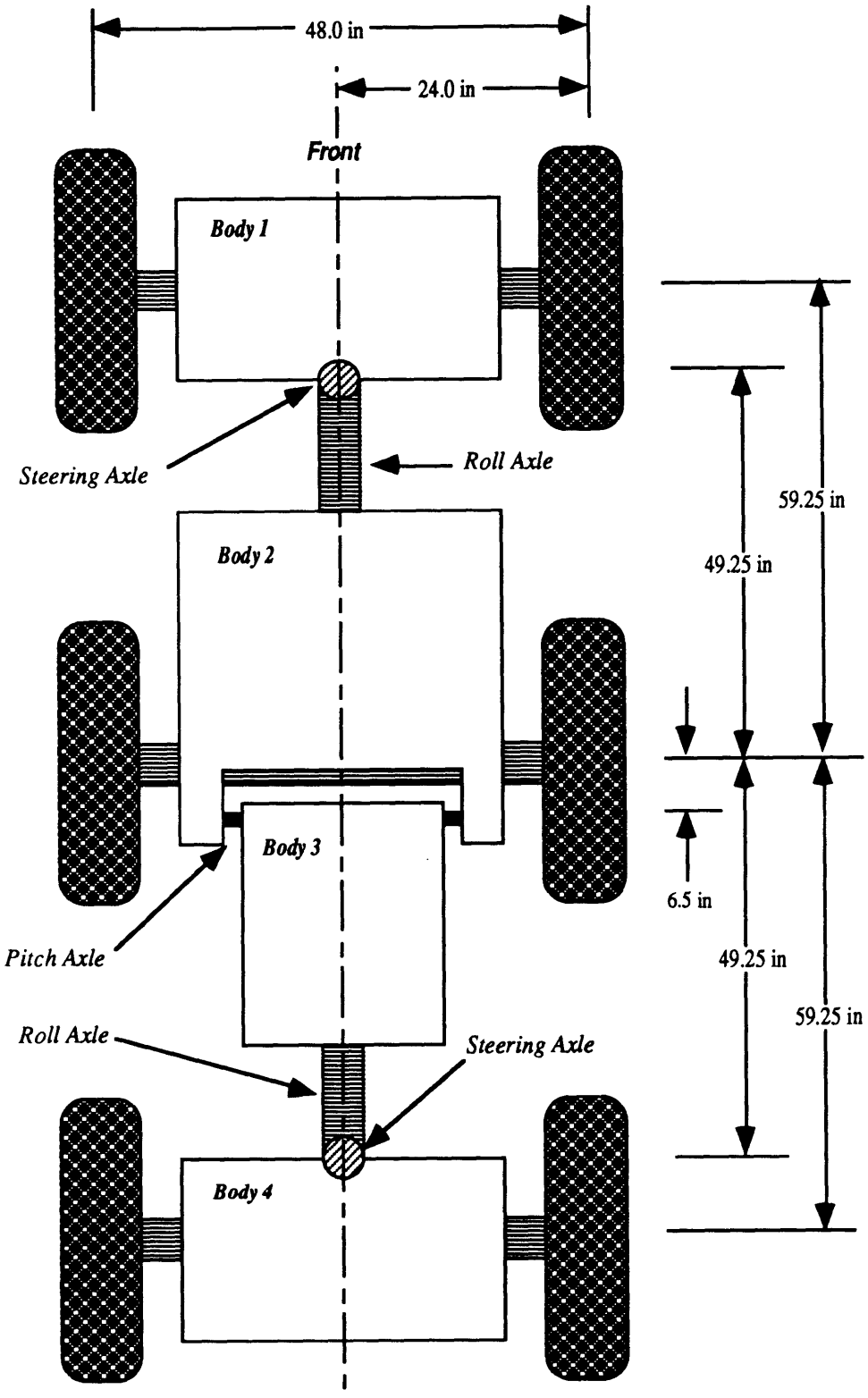

Figure 2-2
Navigational Systems Testbed
Top View

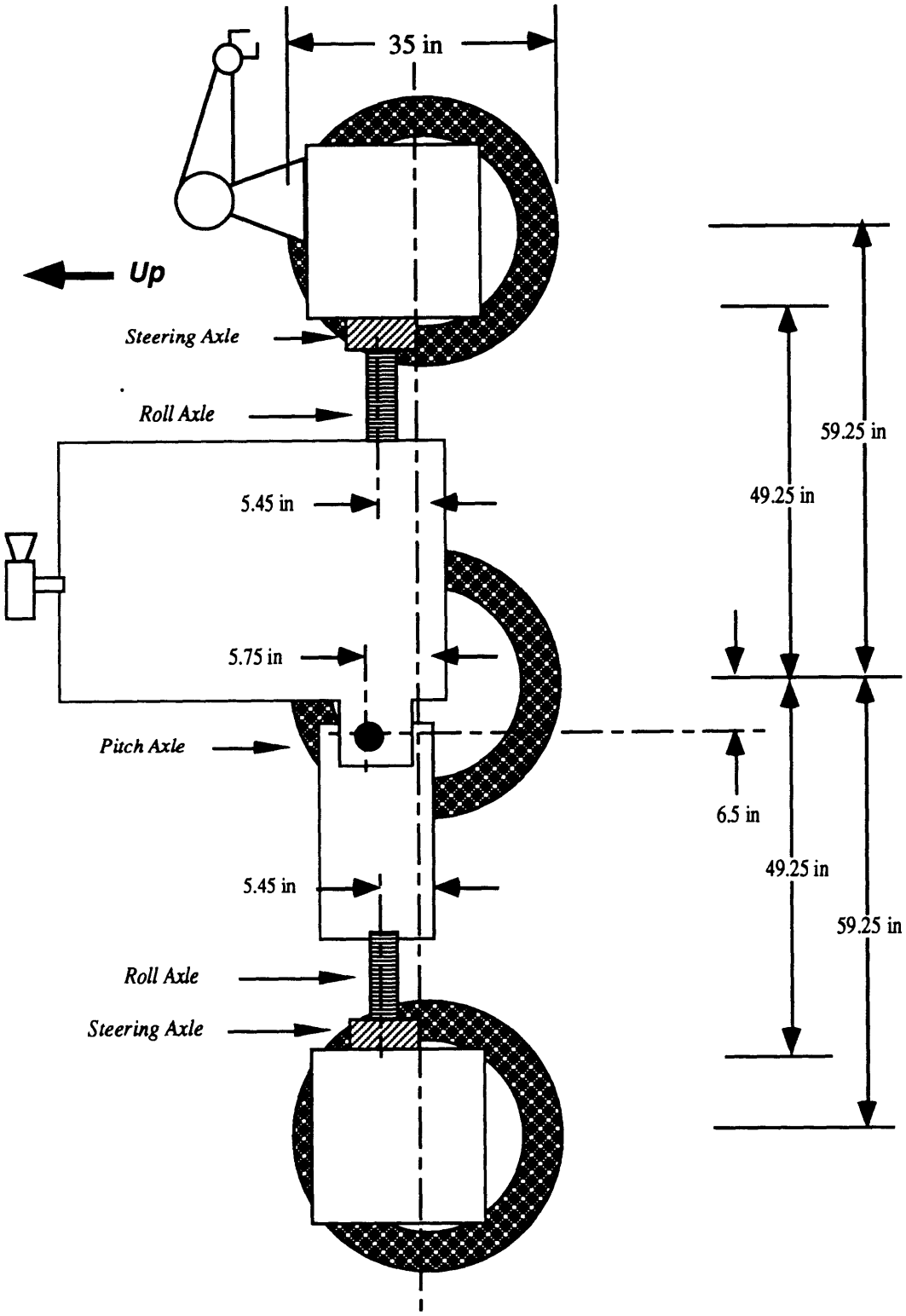

Figure 2-3
Navigational Systems Testbed
Side Cut-Away

2.3 Historical Perspective

Planetary vehicles have been studied in the past for the Moon (1960's) and Mars (1970's). While the US has flown unmanned landers, but not rovers, the USSR successfully teleoperated the Lunokhods on the moon in 1970 and 1973. Rover technology has progressed since the 1960's, especially in the field of navigation, where the development of computers and artificial intelligence has fueled the design of image recognition and correlation schemes used in many navigation designs.

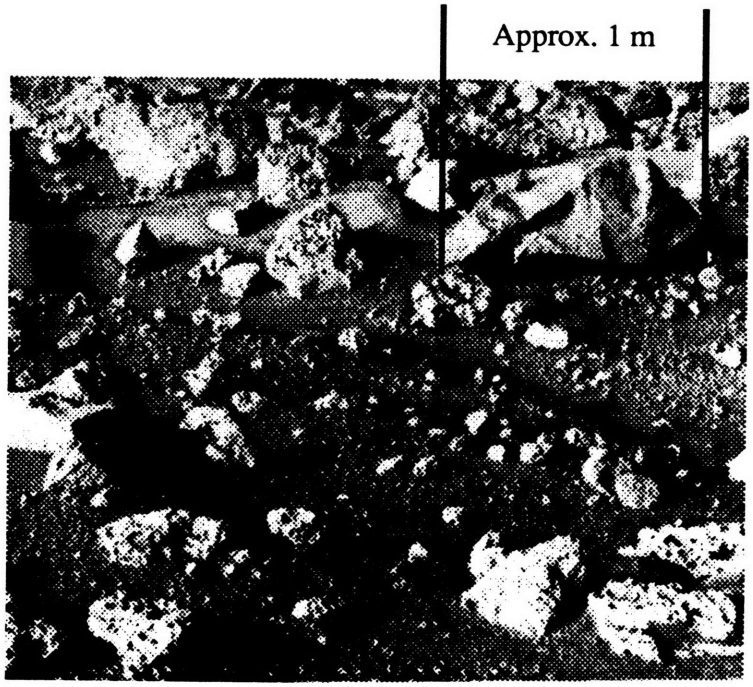

Figure 2-4
The Surface of Mars from the Viking 2 Lander [Carr81]

The design of vehicles employing legged locomotion has also progressed, due to similar advances in electronic technologies. Wheeled locomotion, however, has not changed much since the early pre-Apollo studies. Most of the studies related to tracked and wheeled vehicles were administered by the US Army Automotive Tank Command Waterways Experiment Station; these examine go/no go performance of heavy vehicles

in highly cohesive soils (e.g. a tank going through mud)[Baladi84]. Martian soil, is however, believed to be cohesionless by terrestrial standards due to a lack of water both in bulk and at the molecular level [Moore87b]. Furthermore, rovers will be lightweight due to requirements of earth launch and interplanetary transfer vehicles, as well as the low Martian gravity (0.38g). The primary focus of the Army work was in the characterization of soil properties rather than in improving vehicle design. Army efforts concentrated on tire/terrain interaction in order to create empirically based models of vehicle flotation and traction, not obstacle surmounting capabilities. M.G. Bekker developed a soil bin test facility (at GM Defense Research Labs in Santa Barbara) in which candidate wheels were driven or towed over various soils to determine those properties. A soil test facility was also developed where soils were characterized in terms of empirical parameters related to the vehicle models. Very little integrated vehicle work was done. That which was accomplished focused on verifying the characterization process, without regard to obstacle performance of that particular configuration. [Bekker69]

The US automotive industry has also spent a great deal of time and money developing models of wheeled vehicle performance. These models, however, were designed primarily to investigate comfort and handling properties of vehicles at high speed on relatively smooth roads to influence tire and suspension design. Martian vehicles will be tackling very rough terrain encountering slopes, crevasses, boulders and other obstructions that exists on the surface. High speed is not possible, nor is it desired due to the limited speed of the computationally intensive autonomous navigation subsystems or the 20-40 minute round-trip signal time between Earth and Mars for teleoperated navigation.

It has been found, historically, that three axle vehicles have a definitive advantage over two axle vehicles of the same wheel size. When one of three axles is confronted by an

obstacle, the other two help to push or pull it over or out of the obstacle. As a result, a lower coefficient of traction is required between the wheels and the surface being traversed. [Jindra66] showed this by employing a quasi-static equilibrium model to describe how a six-wheeled vehicle with four or six-wheel drive handles small steps. This approach was, however, limited by the lack of computational power at the time. It was necessary to reduce the equations of static equilibrium by hand for each case with a minimum of geometry variation. It is this approach which has been rethought in this thesis utilizing modern computation. Furthermore, Jindra did not verify his results experimentally, but left his results as correlated through intuition.

3. THEORETICAL AND COMPUTER MODEL

3.1 Model Assumptions

The modelling of six-wheeled vehicles can be quite complex, considering the many degrees of freedom, variations in terrain and vehicle geometry, surface and vehicle material properties and other factors which exist in real systems. To make the problem manageable and produce useable results, a few assumptions are made. The first is that a vehicle can be modelled quasi-statically, where at each time step the vehicle is in equilibrium with its surroundings. This is directly tied to the primary goal of this model, finding the mobility limits. At the mobility limit, the vehicle is at the threshold of negotiating the obstacle. This limit implies that the vehicle has lost all of its kinetic energy and momentum earlier in the traversal. Otherwise, the excess energy would carry the vehicle over. Only the ground tractive forces supplied to the vehicle through reactions to the motor torques allow the vehicle to remain in equilibrium. While the vehicle is not moving translationally, it is not statically fixed to the terrain. Rather, all the rover tires may be spinning, as maximum traction occurs at some finite relative velocity between the terrain and the tire. The situation may thus be described as quasi-static.

The next assumption is that the wheel drive system is always capable of delivering a torque, $\tau \geq \mu Nr$. Classical physics states that μN is the maximum friction force that an object can generate where μ is the net coefficient of traction (friction) of the soil, r is the tire radius and N is the normal force exerted by the ground on any wheel. This is a safe assumption since any flight hardware would have an available torque margin of safety that would insure a positive margin of torque against any foreseeable tire load. If the motor is commanded to supply more torque than the soil can handle, the wheel will accelerate due to the non-reacted torque, but the soil will provide no more thrust. A

consequence of this is that a vehicle could be tied to ground and would be able to spin its wheels at large rotation rates with no forward velocity; the ground would still supply a force of only μN. Note that the coefficient of traction may be a function of the relative velocity between the tire surface and the ground. Since the vehicle must move uniformly (all wheels must have the same average speed over ground), the terrain is considered to have a homogeneous distribution of materials; since the vehicle is quasi-static when it is studied, it is assumed that all wheels see the same coefficient of traction.

This model also assumes that all linkages in the vehicle are rigid, except for the tires. This is a valid assumption for the physical models which are fabricated from aluminum without consideration of scaled rigidity. For flight hardware, chassis flexibility will be determined by pointing requirements for cameras and other instruments, as well as for surviving landing loads and roving into ditches. No shocks or springs are planned for these mobility configurations. If the flexibility is desired, as in the case of tires which deflect as springs, it can be added to the model.

Pneumatic tires are often modelled as a series of linear extensional springs mounted to a rigid wheel hub [Baladi84]. This spring model should prove even more useful for planetary rovers where it is assumed that the tires will indeed be springs and not pneumatic, although they may possess non-linear characteristics. Tire deflection in the 2-D model is thus dependent only on the tire spring deflection characteristics and the normal force exerted on the tire. It will be shown in section 5.1 that even though tire deflection can be modelled in this manner, it has a minor effect on obstacle performance and was omitted from the final model in order to increase computational efficiency.

The vehicle is modelled in two dimensions only. The interaction of the tires and the terrain in the transverse direction is more complicated and is more sensitive to the

deflection and torque distribution characteristics of a given suspension.. An attempt to model the side-slipping of tires was undertaken using a rivet/plate analogy and will be published shortly by Don Bickler, but is not included within this thesis. It was hypothesized by the author that constraining a a 3-D rover such that a pair of wheels must move together is a more challenging test than where the wheels can move independently at different angles and rates. This was demonstrated during testing of the scale model (described in section 4.3). Thus, the 2-D analysis case can serve as a conservative estimate of actual performance.

When a vehicle is modelled in 2-D, it appears in a free-body diagram as in figure 3-1 below. Note how the tractive ability of each tire is proportional to the normal force exerted upon it. The mass locations on the vehicle can be grouped into a center-of-mass for each body through the method described in the next section. The normal forces on each wheel are thus a function of the location of the mass centers and the torques reacted by the soil interface.

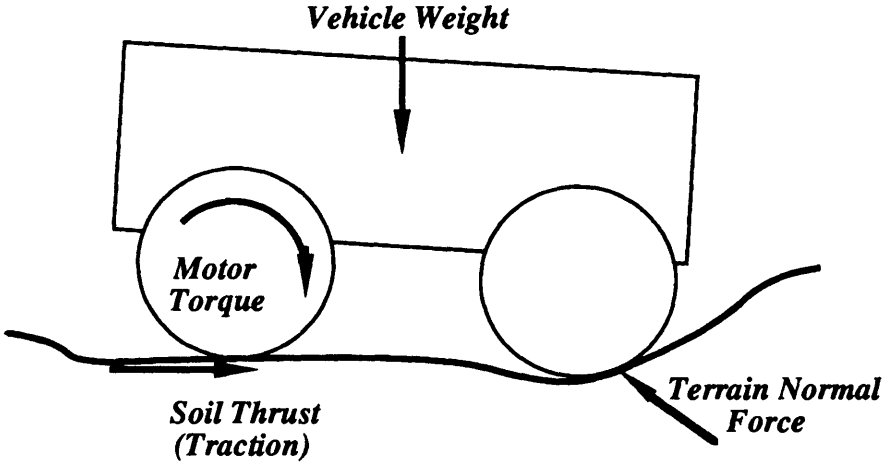

Figure 3-1
Vehicle/Terrain Equilibrium

3.2 Mass-Distance Method of Center-of-Mass Determination

The prediction of the quasi-static mechanical behavior of a vehicle through computer calculations of the equations of equilibrium requires knowledge of its various mass-centers. Likewise, for a physical scale model to perform as the prototype, it must possess the same mass distribution. The mass center must therefore be determined before computer or scale models can be used. Multiple-body vehicles have several centers-of-mass, which all must be found in order to model the behavior of the vehicle when it is deformed from its nominal, level configuration.

The Navtest vehicle as described earlier possesses four bodies with five degrees of freedom (the wheel rotations are not independent as they are constrained by loads and torques), two of which (front and rear steering) will be locked during testing. The current limitations of computer modelling restrict the analysis to a two-dimensional representation of the vehicle with all effects pertaining to the vehicle width and the roll axles ignored. This is not significant as the vehicle is symmetric about its longitudinal center-line. The remaining three DOF are thus reduced to the one pitch degree of freedom and two effective bodies, each with their own center-of-mass. Kinematic deflections through rotation of the pitch DOF result in movement of the overall vehicle center-of-mass.

It is assumed that all relevant vehicle geometry can be measured. The simplest and most direct method for determining the center-of-mass of an existing vehicle would be to decouple the bodies at the pitch axles to weigh and suspend them separately. This requires disassembly of the vehicle, which was not permitted in the case of the Navtest vehicle used for this thesis. A more complicated but also direct method would be to weigh each component and note its orientation and placement before assembly. To be precise the mass list would have to contain dimensions and masses for all components,

down to each bolt. Such a level of detail would be cumbersome to maintain; furthermore, in the present case, no mass list exists.

It was therefore necessary to develop a method to handle the problem of deriving the two center-of-mass locations from analytic formulations which use only measurements of the assembled vehicle on simple scales and overall vehicle dimensions as inputs.

A conventional approach to such a problem would involve the equations of static equilibrium. If a system of six independent equations could be found which relate the six variables involved, the problem could be solved. However, all formulations which were attempted were unsolvable. Most of these formulations contained dependencies between equations which were revealed through careful study of the system. Other formulations were less obviously dependent; yet when a solution was attempted, they were found to be dependent through a zero determinant matrix. As the equations were non-linear, a variable substitution to a new set of linear parameters was used. The new variables led to the idea that perhaps the actual masses and distances were not necessary to describe the system, but instead, the product of mass and distance would suffice. Figure 3-2 shows the basic situation and the variables used. Note that the distances a,b,A,B are written from the pitch axis (pin joint) between the two effective bodies, which here is drawn at the middle wheel axle for simplicity. The front and rear body masses are denoted as MF and MB, respectively.

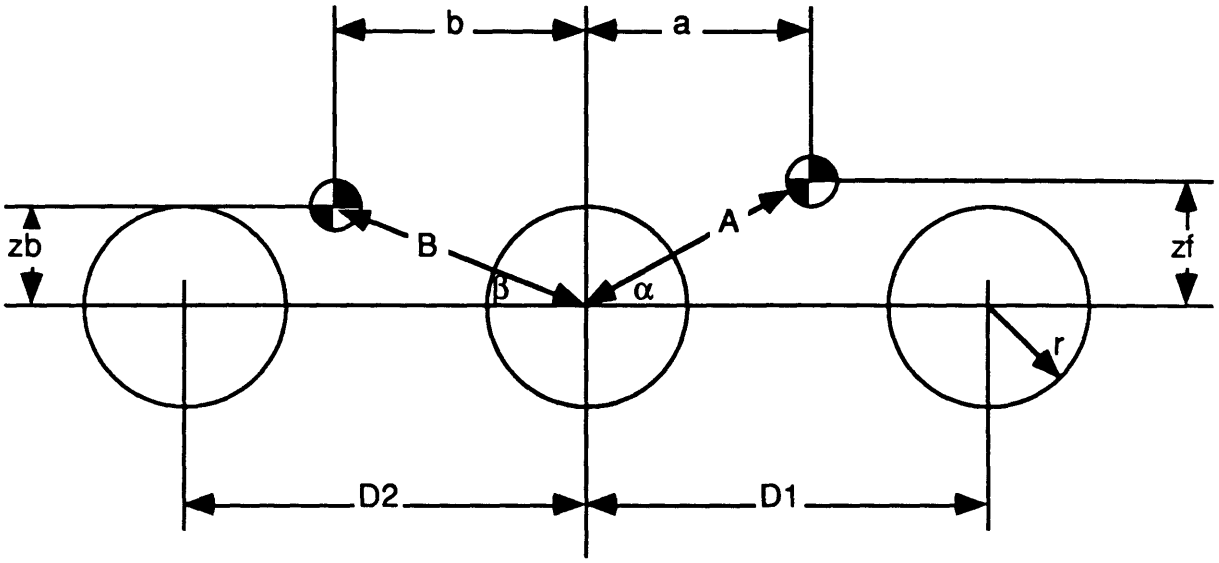

STANDARD VARIABLES	LINEAR VARIABLES	PRODUCT VARIABLES
MF	*MF*	*MFA*
MB	*MB*	*MBB*
a	*MFa*	α
b	*MBb*	β
zf	*MFzf*	
zb	*MBzb*	

Figure 3-2

Geometry of Vehicle and c.g. Locations

In this new system of product variables, two lines are defined, along which the c.g.'s must lie. These lines are at angles α and β which yield the ratios of a to zf and b to zb. Along these lines, the products (MF)(A) and (MB)(B) are constant, and the system is thus reduced to four variables. This reduction leaves ambiguity. The location of the c.g.'s along these lines are not known, and therefore neither are their magnitudes. If

the composite c.g. for the whole vehicle on level ground is superimposed, the result is Figure 3-3.

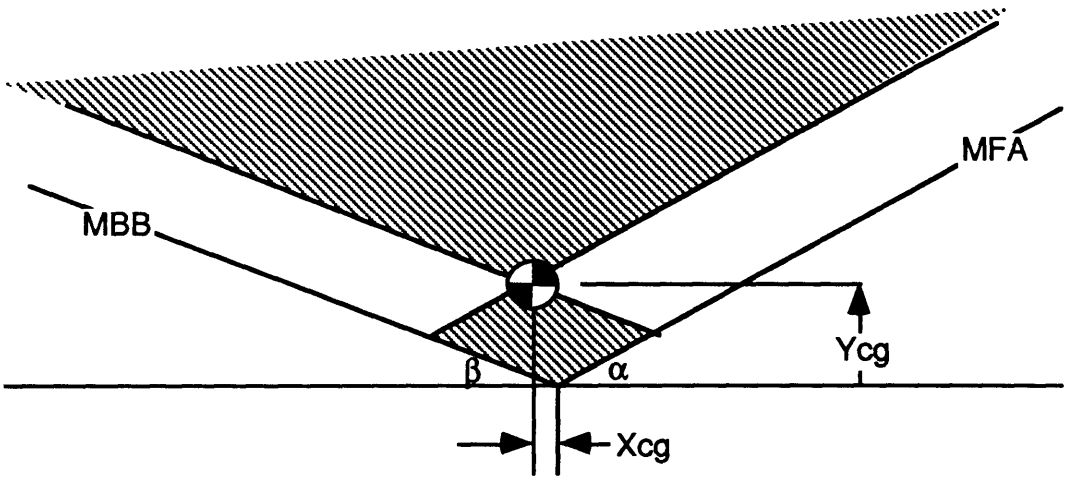

Figure 3-3

Mass-Distance Product Space

For any two point masses (which is a valid representation for the two minor c.g.'s), it should be obvious that their combined c.g. must lie on a line between them. Therefore, the intersection points of the mass-product lines and any line which passes through the c.g. form a valid set of masses and distances which are indistinguishable from any other valid set. Lines drawn parallel to the mass-product lines through the composite c.g. represent the maximum mass/minimum distance of one minor c.g. and an infinitesimal mass at infinite distance for the other. Only finite distances are possible, so the area outside these lines (shaded) is not valid. The allowable area can be further confined if a maximum distance of the c.g. is known due to geometric limits of the vehicle length, i.e. $a = A \cos \alpha < D$.

A corollary to the idea that only the mass-product lines can be detected and only the mass-product lines are necessary for a quasi-static formulation, is that various mass distributions which produce the same mass-product lines are indistinguishable. Figure 3-4 illustrates this argument. All three of the rovers shown have the same values of the

four variables: MFA, MBB, α,β, yet different mass distributions. For example, consider a vehicle whose total mass is measured as 900 kg by placing scales under all six wheels. The longitudinal location of the composite center-of-mass can then be found by considering the weight observed under each wheel and summing the moments about the location of the center-of-mass to zero. Next, raise the front wheels until scales placed under them read no weight. This angle indicates that the front center-of-mass is over the pitch axis, and this produces α. Performing the same operation on the rear wheels yields β. The magnitudes of the mass-product lines are now easily found by rewriting the first moment equation in terms of the mass-product variables and the angles α, β. So for the three configurations shown in Figure 3-4, say:

$$a = 30°$$

$$b = 15°$$

$$W1 = W2 = W3 = 300kg$$

$$D1 = D2 = 2m$$

Then sum the moments about the pitch axis to yield:

$$MFA = 693 \text{ kg·m}$$

$$MBB = 621 \text{ kg·m}$$

The height of the composite center-of-mass can then be calculated as:

$$Z = (MFA \sin\alpha + MBB \sin\beta)/W = 0.56 \text{ m}$$

The three situations in Figure 3-4 may have the following values:

(i) MF = 400 kg MB = 500 kg

(ii) MF = 500 kg MB = 400 kg

(iii) MF = 630 kg MB = 270 kg

yet they are indistinguishable as they would each have the same MFA and MBB, and would have the same results if scales were placed under the wheels on arbitrary terrain geometry.

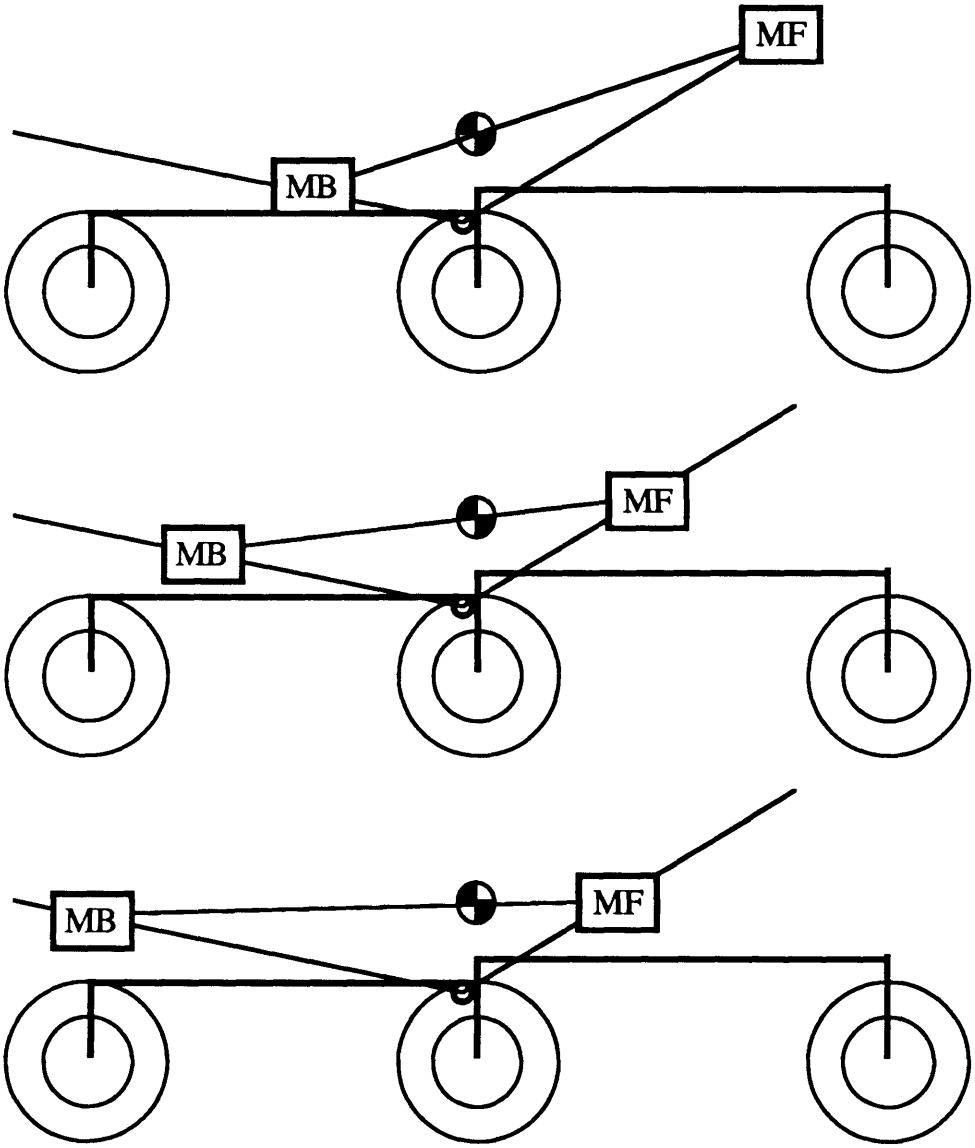

Figure 3-4

Indistinguishable Mass Distributions

3.3 Four-Wheel Implementation

The basic analytic model of the vehicle is based on the equations of static equilibrium. To demonstrate this approach, first examine a simple four-wheeled vehicle against a vertical wall, then generalize to a more complex four-wheeled vehicle on arbitrary terrain. The complex six-wheeled case will be presented in a similar fashion in the next section.

3.3.1 Wall Climbing

First consider a simple four-wheeled vehicle ("Simple 4") with the following variable geometry parameters as shown in Figure 3-5:

L = wheelbase

r = radius of both wheels

z = height of center-of-mass from axle height

a = location of center-of-mass from front axle

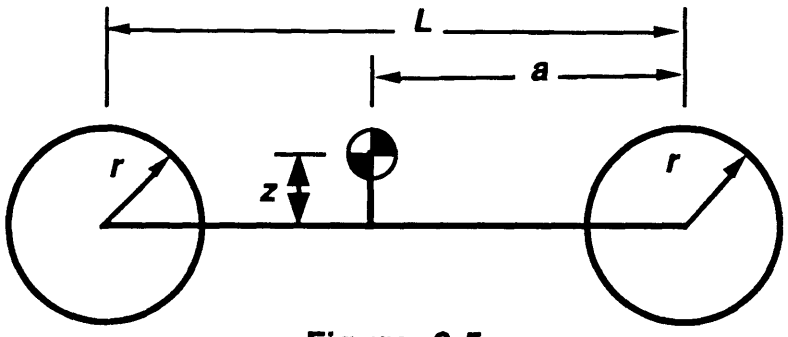

Figure 3-5
Simple Four-Wheeled Vehicle

If the vehicle is driven with the front wheels up against a wall (Figure 3-6), as in the front wall of a vertical step, (direction of travel is to the right), to a height, h, the vehicle horizontal is now at an angle, θ, to the ground horizontal. These last two parameters are related through

$$\theta = \text{Arcsin}\left(\frac{h}{L}\right) \tag{3-1}$$

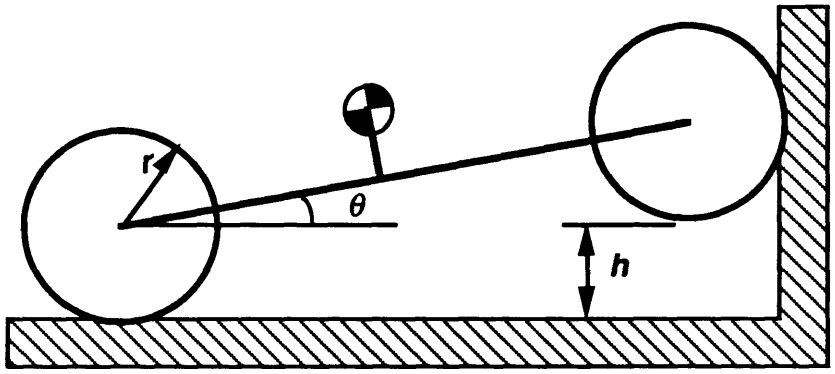

Figure 3-6
Simple 4 Against Wall

The mobility limit in this situation is such that for given surface properties, such as tractive coefficient, μ, the vehicle is quasi-static at height, h. Recall the quasi-static condition allows the wheels to spin, each such that the maximum available traction of the terrain is generated. The normal forces are represented as N_i and the motor torques which are reacted by the soil as $\mu N_i r$ (where μN_i is the resulting soil thrust). The basic equations of static equilibrium are that the sums of the forces in each direction and the moments must be zero. These forces are shown in the free-body representation of the vehicle in Figure 3-7.

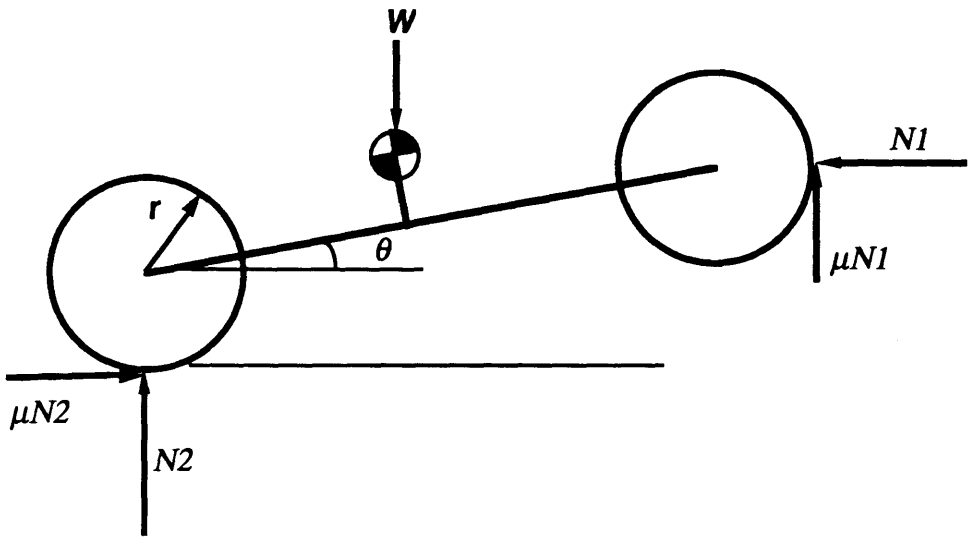

Figure 3-7
Forces acting on Simple 4 Against Wall

These static equations are written as:

Sum of Vertical Forces: $\mu N_1 + N_2 - W = 0$ (3-2)

Sum of Horizontal Forces: $\mu N_2 - N_1 = 0$ (3-3)

Sum of Moments (about rear axle):

$$\mu N_2 r + N_1 L \sin\theta + \mu N_1 (r + L \cos\theta) - W ((L-a) \cos\theta - z \sin\theta) = 0 \quad (3\text{-}4)$$

The three simple equations can be solved simultaneously with the three unknowns (μ, N_1, N_2). The normal forces are just proportional to the weight of the vehicle, so as the actual magnitudes are unimportant, W may be normalized. The weight of the vehicle then drops out of the equation (as the relevant forces are a function of friction which is proportional to the weight, regardless of what it may be). The result is a quadratic equation for μ in terms of L and θ (or h). A plot of the solutions where h is measured in radii, is shown in Figure 3-8 below.

This data was generated by solving equations (3-2) through (3-4) in the Mathematica symbolic mathematics manipulation environment as implemented on a Macintosh IIcx computer. This approach allows easy manipulation of vehicle geometry and rapid data generation. The capabilities of this system are described in [Wolfram88] and the code for solving these equations is shown in Appendix A.

It is readily apparent that this method shows the sensitivity of obstacle performance to vehicle geometry. In Figure 3-8, several curves are plotted; both have L/a = 2, and z=r, but vehicle length is varied. Shorter vehicles have an easier time than the longer ones at climbing the vertical wall.

Figure 3-8: Simple 4 Equilibrium Traction Requirements

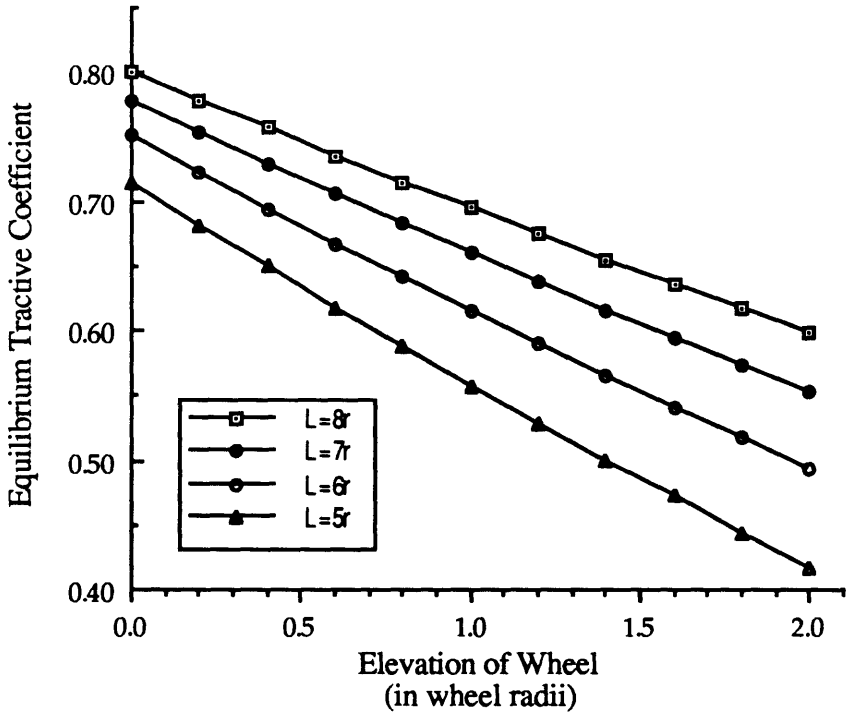

If these seems counter-intuitive, the explanation can be derived easily from (3-4) which at h=0 becomes:

$$\mu N_2 r + \mu N_1 (r + L) - W (L/2) = 0 \qquad (3\text{-}5)$$

Since a = L/2, approximate $N_1 \sim N_2 \sim W/2$ and (3-5) becomes:

$$\mu (2r + L) - L = 0 \qquad (3\text{-}6)$$

and therefore, as L/r increases, $\mu \rightarrow 1$. For smaller values of L/r, the 2r term becomes more important and the required friction is less. Thus, for shorter vehicles, the wheel torque plays a more important role in lifting the front wheel. Notice how the curves for the shorter vehicles have a higher slope. This is because at the same height, they experience a larger value of θ.

3.3.2 Bump/Slope Model

A more difficult case is a vehicle encountering an obstacle of height, h, less than a wheel radius as shown in Figure 3-9. A complete solution to such a problem would involve solving the equations of equilibrium at each point in the path. There are many variables which must be considered including the length and profile of the obstacle. In this example, just the first point of contact will be modelled. At that instant, the vehicle is still level and the ground no longer supports that wheel which is in contact with the obstacle.

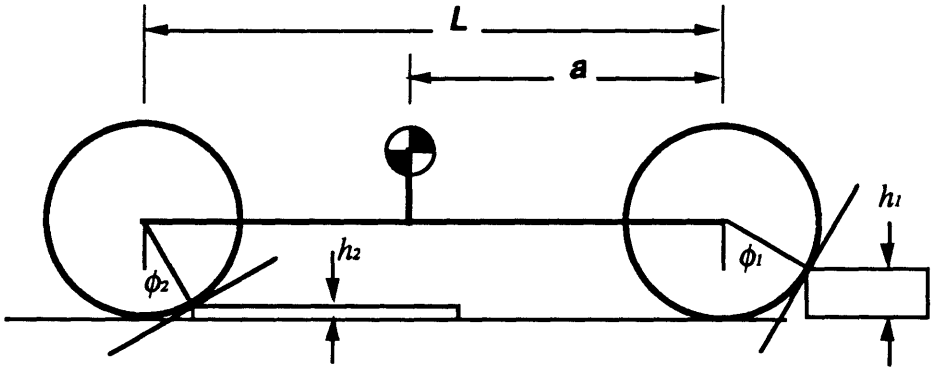

Figure 3-9
Simple 4 Against Bumps/Slopes

The problem is very similar to the vertical wall, except that now the obstacle normal is not horizontal. The normal force is at an angle ϕ which is related to the obstacle height through:

$$\phi = \text{Arccos}\left(\frac{r-h}{r}\right) \tag{3-7}$$

The obstacle is thus similar to an inclined wall. Wall angle proves to be a useful way of assessing mobility performance. (Just as steps relate to angles between 0 and 90 degrees, crevasses can be correlated to wall angles between 90 and 180 degrees). The equations of static equilibrium are now written more generally, allowing the solution of the system for both front and rear wheels encountering obstacles of arbitrary height (h<r).

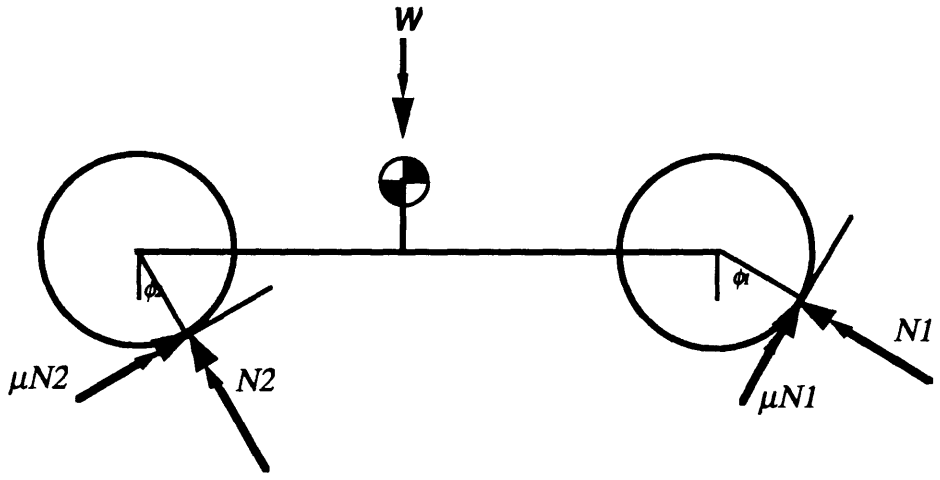

Figure 3-10
Forces acting on Simple 4 Against Bumps/Slopes

The equations of static equilibrium are again written:

Sum of Vertical Forces:

$$\mu N_2 \sin\phi_2 + N_2 \cos\phi_2 + \mu N_1 \sin\phi_1 + N_1 \cos\phi_1 - W = 0 \qquad (3\text{-}8)$$

Sum of Horizontal Forces:

$$\mu N_2 \cos\phi_2 - N_2 \sin\phi_2 + \mu N_1 \cos\phi_1 - N_1 \sin\phi_1 = 0 \qquad (3\text{-}9)$$

Sum of Moments (about rear axle):

$$(\mu N_2 r - W (L-a) + N_1 L \cos\phi_1 + \mu N_1 (r + L \sin\phi_1) = 0 \qquad (3\text{-}10)$$

Figure 3-11: Simple 4 Against Bumps

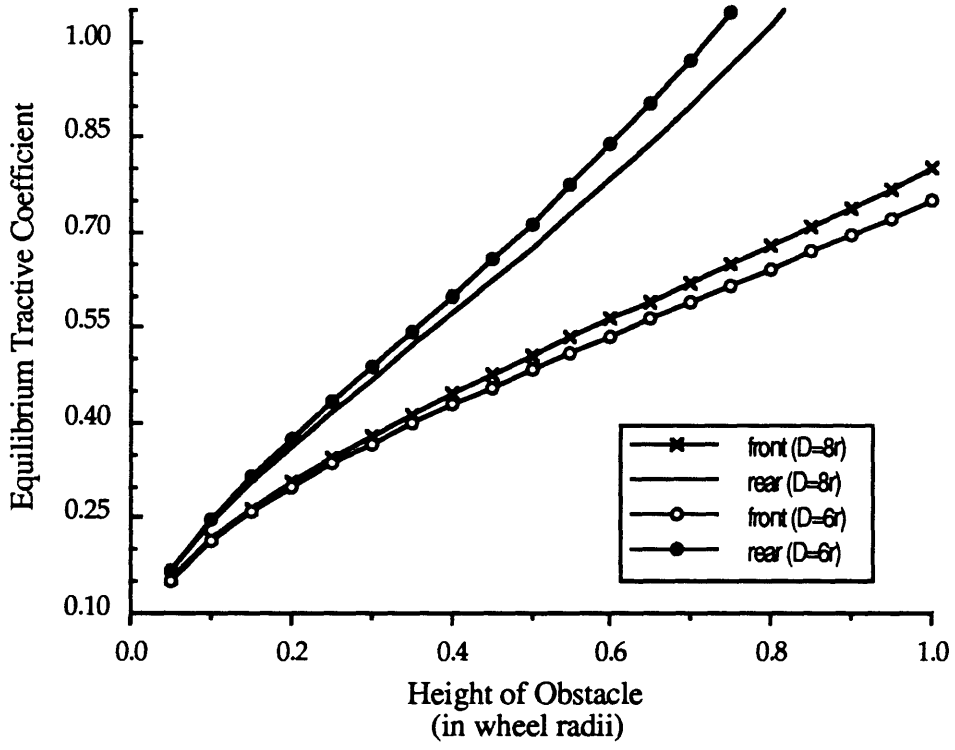

As expected, the vehicle finds it easier (requires less traction from the tire/soil interface) to traverse small bumps than large ones. The shorter vehicle (D/r = 6) has an advantage over the longer one when the obstacle is encountered at the front wheel. Note the point

where the obstacle height is 1.0 radii is the same as the vehicle against a vertical wall with its front wheels off the ground by a height of zero (see Figure 3-8). The rear wheels require much more traction than the front to surmount bumps. Furthermore, a longer wheelbase helps the rear wheels get over the bump.

For example, if the soil/vehicle interface has a tractive coefficient of 0.8, the front wheels can get over a 1 wheel radius obstacle, but the rear would become stuck. The longer wheelbase vehicle could start to bring its rear wheels over a 0.6 radii obstacle and the shorter vehicle cannot begin to bring up its rear wheel unless the obstacle is shorter than 0.55 radii. Elevation of the front wheel was shown above to make it easier to push the vehicle. Therefore, the first encounter traction (Figures 3-11,12) should be the largest requirement for the front wheels. The rear behave differently and have a harder time when they are elevated. Note how due to the vehicle symmetry (L=2a), the front wheels forward are the same as the rear wheels in reverse. Conversely, the front wheels in reverse would behave the same as the rear wheels do here moving forward. While this is not a complete analysis (elevation of the rear wheels must be included next), it can be immediately seen that a longer wheelbase is better for climbing bumps smaller than a radius.

Figure 3-12: Simple 4 Against Slopes

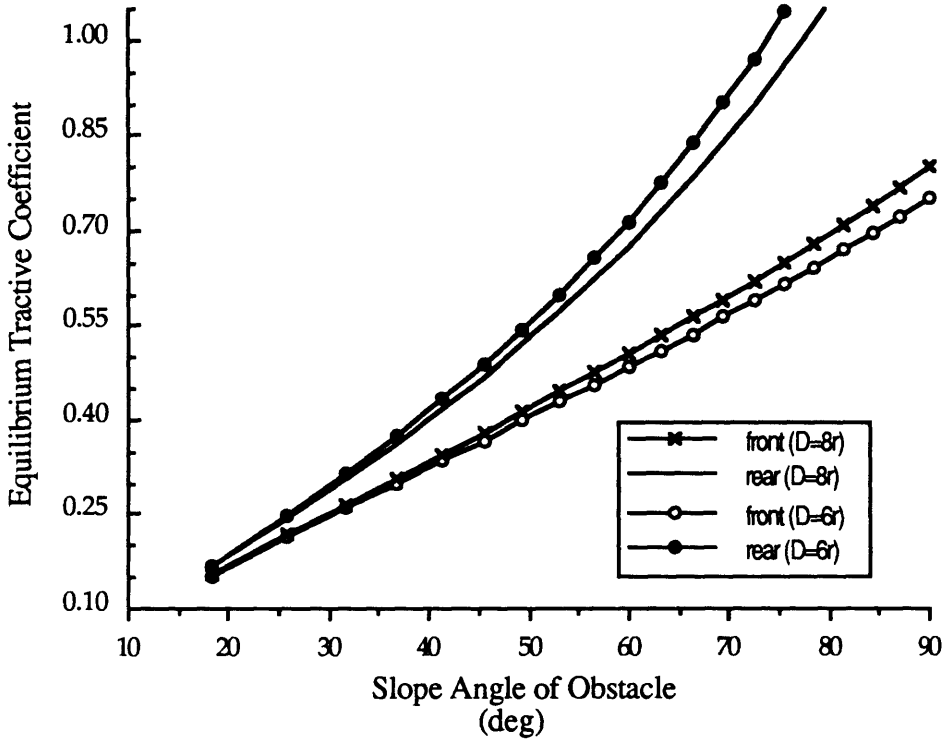

The same data found for Figure 3-11 is replotted in Figure 3-12 in terms of the angle, ϕ, using (3-7). The scale and distribution of points along the ordinate of the graph has changed, but the general trends have not, and the same conclusions may be drawn about the performance of the vehicle and its sensitivity to length.

3.4 Six-Wheel Implementation

This quasi-static technique was also applied to two six-wheeled configurations. The method was applied by the author and other JPL engineers to the rocker-bogie conceptual configuration. A physical model was built and tested to demonstrate its capabilities. The rocker-bogie study was conducted in parallel with the work presented in this thesis [Lind90]. The theoretical model was then used to predict the slope climbing performance of the Navtest and its physical scale model.

Specific six-wheeled configurations were implemented in the Mathematica environment using the technique as described above and building on the work of [Jindra66]. Discrete problems such as the front wheels against a wall, as in (3-2) through (3-4), were analyzed first, both by hand and computer. These, along with some logical boundary conditions, such as the vehicle on level ground with no obstacles has an equilibrium $\mu \sim 0$ (with negligible rolling resistance, any slight traction above zero would result in thrust and thus motion, breaking static equilibrium), led to the development of some vehicle trends which were used in refining designs such as the rocker-bogie. Once these capabilities were demonstrated, Randy Lindemann at NASA/JPL developed a generic computer six-wheel code which included contact angles, wheel elevations, tire deflection and all variable geometry at each equilibrium. For ease and speed of operation, a subset of this package was adapted by the author to execute in batch with the constraints that the vehicle rests on flat terrain, with tire deflection ignored and contact angle varied (as in Figure 3-12).

3.4.1 Vertical Wall

The six-wheeled case can be analyzed to see how it performs against a vertical wall in much the same way as the four-wheeled case was analyzed in the previous section. The variables needed to define the geometry of the Navtest for the purposes of this model are shown in Figure 3-13 and the situation analyzed here is shown as Figure 3-14. The equations of equilibrium are written for the middle wheel of a level vehicle against a vertical wall as:

Sum of Vertical Forces:

$$N_3 + \mu N_2 + N_1 - Wf - Wb = 0 \qquad (3\text{-}11)$$

Sum of Horizontal Forces:

$$\mu N_3 - N_2 + \mu N_1 = 0 \qquad (3\text{-}12)$$

Sum of Moments (front body, about pitch axis):

$$\mu N_1 (r + e) + N_1 (a + b + c) + \mu N_2 (r + c) + - N_2 e - Wf (b+c) = 0 \qquad (3\text{-}13)$$

Sum of Moments (rear body, about pitch axis):

$$Wb\, d + \mu N_3 (r+e) - N_3 (d+f) = 0 \qquad (3\text{-}14)$$

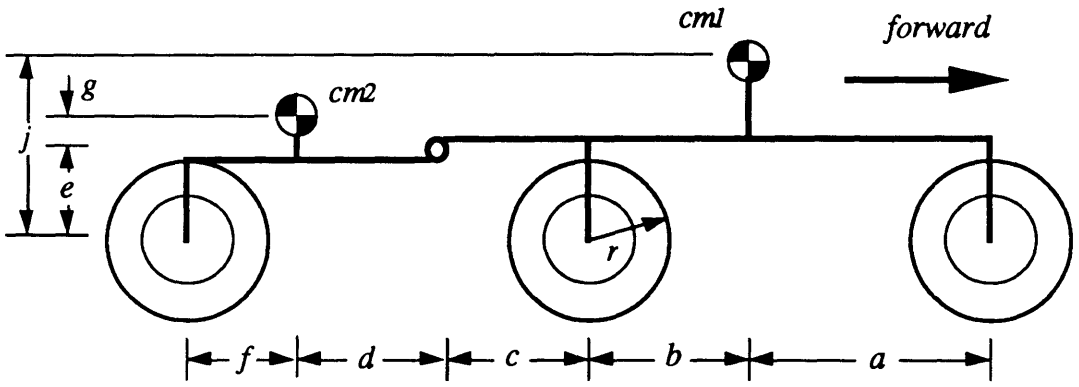

Figure 3-13
Navtest Configuration Variables

Notice how the vehicle weights, Wf and Wb only appear in the moment equations coupled with a distance (thus corresponding to the mass-distance products of section 3.2) or summed in the vertical force balance (Wf + Wb = Wtotal). These equations now include a second moment equation due to the rotational degree-of-freedom associated with the free pitch axis. The following values for the variables shown in Figure 3-13 were measured from the Navtest (Figure 2-4) and work accomplished in sections 3.2 and 5.2:

a	=	29.25
b	=	30.0
c	=	6.5
d	=	39.3
e	=	5.75
f	=	13.45

Note how the *g* and *h* variables do not appear on this list. Since the vehicle is level, the heights of the centers-of-mass do not matter and do not appear in equations (3-11) to (3-14).

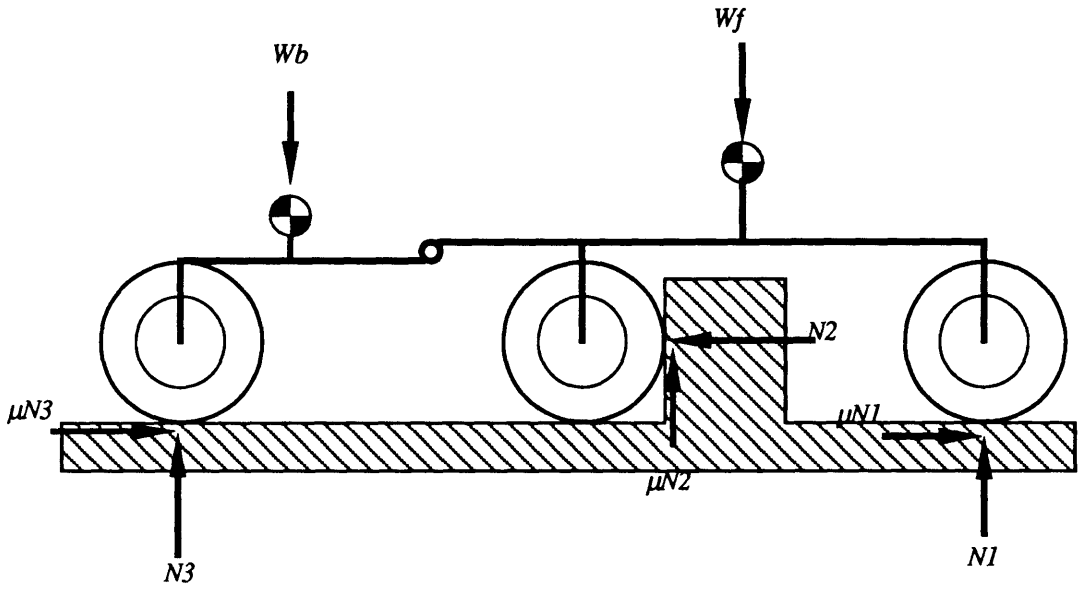

Figure 3-14
Navtest Middle Wheel Against a Vertical Wall

The complexity these equations has increased greatly in the step from four to six wheels. Note that they are not written here in terms of an independent variable such as wheel height or contact angle, so the numerical values given apply to only one test point. These equations were solved and found to yield a traction requirement of μ = 0.777. Therefore, if such a vehicle were to attempt to climb a vertical wall positioned in front of its middle tires, it would only be successful if the coefficient of traction in the tire/terrain interface exceeded 0.777. For any smaller value, the vehicle would fail this test.

3.4.2 Generalized Slope Model

The model was then extended to accommodate variable contact angle on each wheel, as

well as non-level terrain. The vehicle is shown in equilibrium on such a generalized terrain in Figure 3-15. The equations to solve such a generalized system were developed directly from those presented earlier, but have many more complex terms to handle the more complicated contact geometry. The full solution (for arbitrary single pitch axle, six-wheeled vehicles) was written compactly with the use of intermediate variables which represent combinations of dimensions, forces and geometry. This formulation was then implemented in Mathematica (code shown in Appendix A) and the reader is referred to [Lind90] for more details on the generalized implementation.

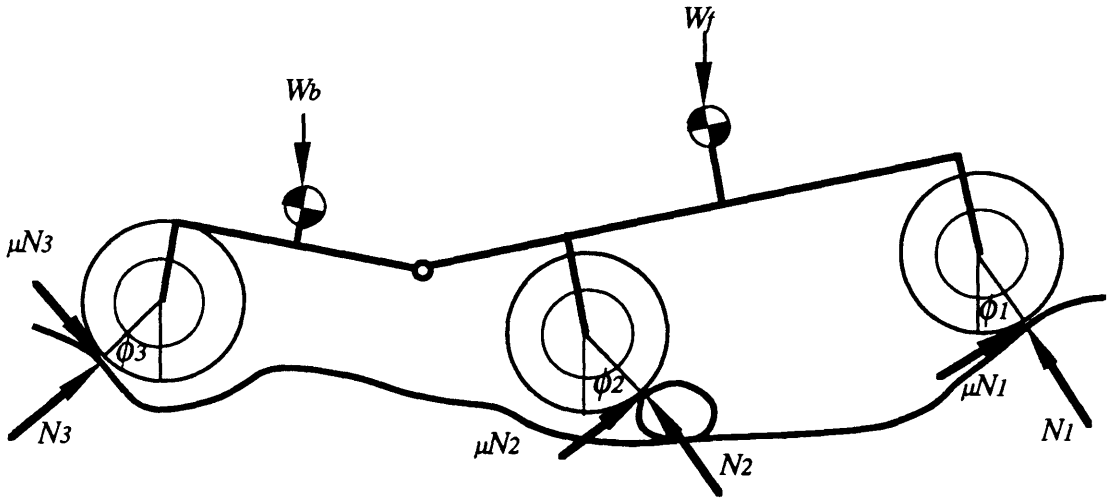

Figure 3-15
Navtest Vehicle Force Diagram

3.4.3 Testing Predictions

While a complete formulation for arbitrary terrain exists, it is difficult to use for sensitivity analysis and validation through testing. It is more difficult to assess the contributions of each of the wheels when on arbitrary terrain. Simpler tests where only one of the contact angles, heights, or vehicle parameters are varied prove to be more useful in gaining insight for vehicle design.

A number of standard evaluation tests have been developed during the course of JPL rover design efforts. One which clearly shows a great variation in capability with traction, is slope climbing ability. This is evident even in the simple case of Figure 3-12 where the curves have a large slope and are not linear. This type of curve is difficult to match and should provide a robust test for validation of the theory. The vehicle on level ground with one wheel against an inclined wall is easy to study, requires less computation than arbitrary terrain, and is easy to test. As the safety of the Navtest and the design of the test apparatus were concerns during the development of this model, the level vehicle angled wall tests were favored as they did not require elevation of the vehicle. They also did not require the construction of elaborate steps or bumps which would have to be anchored to the floor for stability, yet would also be adjustable to find the mobility limits would have to be strong enough to support vehicle weight. This test allows investigations of a wide range of tractions with minimal motion or reconfiguration of the test equipment. The level-vehicle sloped wall was thus chosen as the standard evaluation test.

The computer package was run for the Navtest vehicle over a wide range of frictions and wall angles, centered around typical tire/soil tractions. Actual testing of the vehicle is described in section 4.2. The vehicle is always positioned on level ground, with one set of wheels against a slope of a given angle (with all forces acting through the contact angle, no wheel contact with the level floor) and the other two axles are run on the ground as shown in Figure 3-16. In other words, in each case, only the angle, ϕ, as specified in the figure is changed. The results (Figure 3-17) form a set of calculated data which describes the mobility performance of the vehicle geometry. Individual dimensions can be (and were) varied to study the sensitivity of a variety of performance measures (i.e. front wheel traction, middle wheel traction) to the configuration.

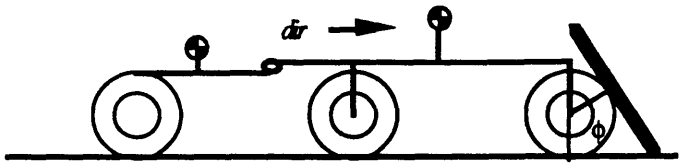

Front Wheel Forward

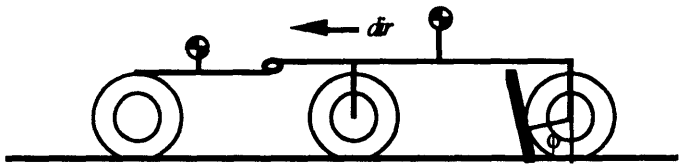

Front Wheel Reverse

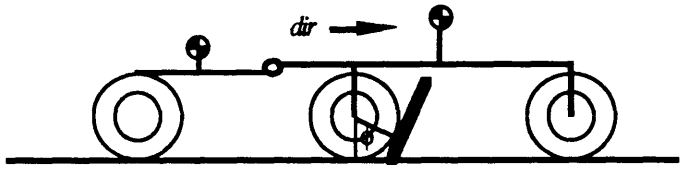

Middle Wheel Forward

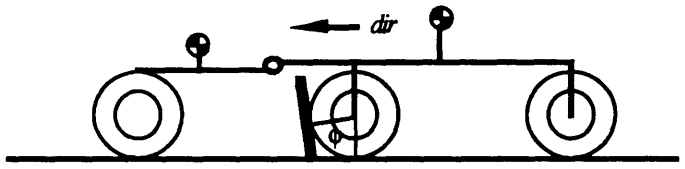

Middle Wheel Reverse

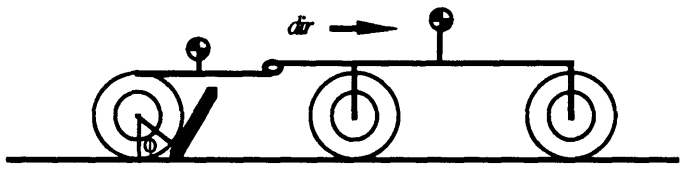

Rear Wheel Forward

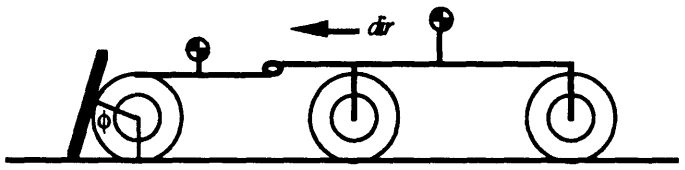

Rear Wheel Reverse

Figure 3-16
Vehicle Testing Configurations

Figure 3-17: Navigation Testbed Inclined Wall Climbing Traction

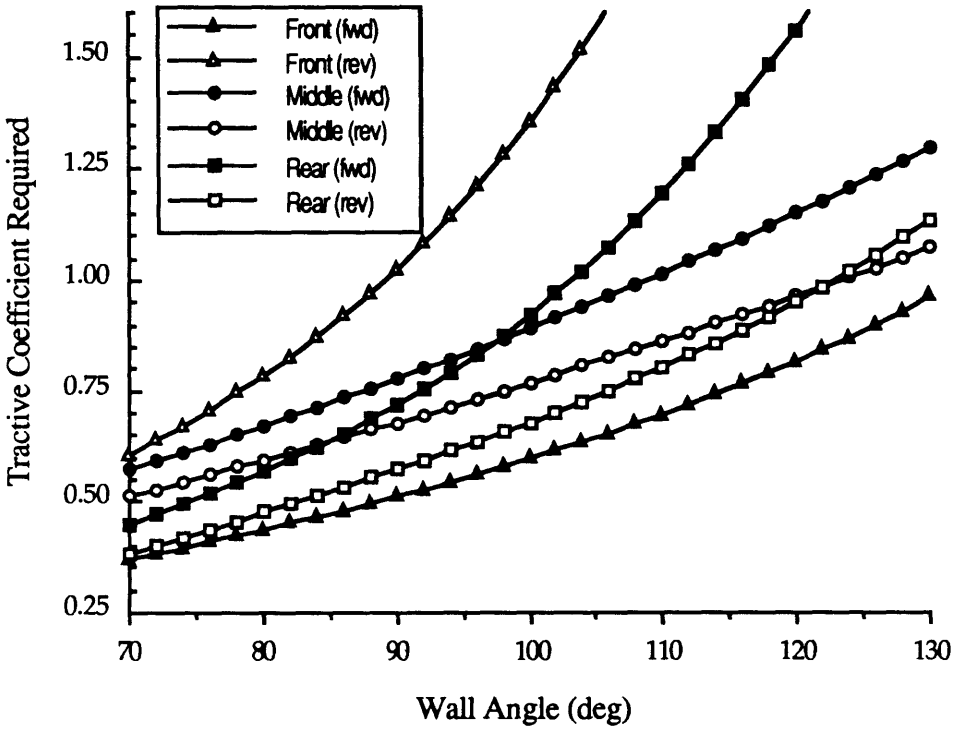

The curves are coded with closed symbols indicating all wheels driving in the forward direction and open symbols when all wheels are driving in reverse. The wheels which are against a slope are indicated by the symbol on the data point. Note how the performance curves seem to be grouped in three classes; outside extremes, inside extremes and centers. The vehicle has an uneven mass distribution and the pitch axis is not located directly above the geometric center. Therefore, the vehicle should not behave symmetrically.

The vehicle performs best with the front wheel in the forward direction where the minimum soil traction is needed at any slope. This is no surprise, as the front wheel had an advantage in the four-wheeled case. The rear wheel driving in reverse would perform identically if the vehicle were symmetric. As it is not, decreased performance in seen in this case, although the curve follows the shape of the front-forward curve.

Thus, these outside extreme cases offer the best performance over most of the indicated range.

The second class involves driving the insides of the extreme wheels. The rear wheel forward is difficult to raise (as was the rear wheel in the four-wheeled vehicle). However, as the front wheel forward has an advantage in this configuration, the front wheel in reverse is hindered even more. This is comparable to the four-wheel slope climbing, where modifying the configuration to help the forward motion of the front wheel hindered the performance of the front wheel in reverse. Thus the worst performing of the six wheels is the front when the vehicle moves in reverse. For a fully reversible vehicle, the lowering of this traction requirement would be a design driver. This is not, however, necessarily a problem, as vehicles can be designed to perform best in a preferential direction, allowing better nominal performance. The danger in practical operations is that a vehicle may begin to traverse a patch of terrain, decide to abort the maneuver due to unfavorable conditions and then not be able to back out. Despite these shortcomings, a quick look back at Figure 3-12 shows that this six-wheeled vehicle still clearly outperforms the four-wheeled vehicle.

The last of the three classes is the center wheels, which behave approximately the same in both directions. They behave essentially as the front wheel forward (as they are pushed by the wheels behind them), although they are also dragged back down a bit by the wheels ahead of them. The center wheel has the largest traction requirement of any of the wheels for the forward driving vehicle until a 98° angle when the rear wheel surpasses it. As it is unlikely that many reentrant walls will exist on Mars or the Moon, vehicle design work should consider reducing this center wheel requirement which is the toughest over most of the foreseeable range.

Many of the insights derived from data such as that plotted in Figure 3-17 have been used in the development of new configurations. This work was done by Don Bickler, Randy Lindemann and the author with the goal of reducing the coefficient of traction needed when any of the wheels was against a vertical wall. Reducing the traction necessary for the front wheel to move backwards necessitated a geometry change which increased other requirements. The resulting configurations require the same coefficient of approximately 0.7 in all test cases. One is the "rocker-bogie" configuration (baseline for MRSR) which is shown in Figure 2-1. One advantage of this configuration is that smaller wheels (than the previous baselines, such as the Navtest) give greater mobility performance. A scale model of this vehicle has demonstrated its superior abilities. Another new development is the "split-bogie" which is an enhancement of the rocker-bogie and uses pantograph linkages to move the torque reaction moments to further reduce the traction requirement on all wheels.

4. PHYSICAL SCALE MODEL AND TESTING

4.1 Physical Model Description

The computer model was to be validated through testing of the prototype vehicle and a 1/7 physical scale model. The prototype Navtest vehicle was unavailable for use in this thesis due to problems with the drive subsystem. This problem was not discovered until late in the study, so test equipment fabricated has been unused to date.

The physical scale model was based on the specifications of the Navtest vehicle as shown in Figures 2-2 and 2-3. These values were measured from the fabricated Navtest hardware, not from the design plans (as they were not available) and there may have been measurement errors of up to $\pm$ 0.5 inches.

A basic goal of the model design was to reproduce the essential aspects of the vehicle only. As the computer model assumes rigid members, flexibility in the physical model was not a consideration. Furthermore, the quasi-static nature of the model discards all inertial relationships. The designer was therefore free to use whatever materials were available and easy to use in the fabrication. As a result, most of the model was fabricated from aluminum with selected components purchased off the shelf.

The width of the vehicle does not appear in the 2-D formulation, but was preserved in the scale model to allow for further use of the model in 3-D scaling studies, which are beyond the scope of these computer models. It is also possible that at some future date the scale model may be outfitted with steering actuators allowing a fuller representation of the prototype, especially in areas of resistance to tip-over when steering under power.

The remaining essential aspects of the vehicle were only those which appear in the computer formulation of the equations of static equilibrium. The physical dimensions of the vehicle were scaled by a factor of 1/7 from the prototype (35" wheels) thus placing this physical model at the same scale as other physical models produced by the Advanced Spacecraft Development Group. The other models are all at 1/8 the standard MRSR scale of 1 meter ground clearance and 1 meter wheels (except the rocker-bogie configuration which uses smaller wheels but other factors place it on the same scale). The Navtest vehicle uses 35 inch wheels so it is at approximately 7/8 standard MRSR scale. Therefore the 1/7 scale Navtest is a 1/8 scale MRSR candidate.

While inertial properties are not important, the mass distribution is. The weight distribution shifts with changes in the suspension configuration when the vehicle encounters an obstacle. It was therefore necessary to determine the mass distribution of the Navtest vehicle through the method described earlier in section 3-2. This mass distribution (given in section 5.2) was then imposed upon the physical model by applying lead weighting to the front cab until the proper ratio was established. Note that a complete scaling would require that the model mass, M_m, be related to the prototype mass, M_p, through

$$M_m = \left(\frac{1}{s}\right)^3 M_p$$

where s is the scale factor (7 in this case). Three key assumptions caused this relationship to be disregarded when preparing this model. The first is that the system is composed entirely of rigid bodies except for the tires. To model the system kinematically, the deflection of the scale tires must be 1/7 the deflection exhibited by the full-scale tires. Therefore, if the scale tires do not have a spring rate which is 1/49 that of the prototype tires, the model weight should be adjusted to provide the proper tire deflection, if this deflection is significant.

Secondly, the forces which interact in the model do not depend on the total mass of the vehicle. The interacting forces are either the distributed weight, normal forces, or the friction forces which arise from the wheel torques and normal forces. These can all be expressed as a fraction of the total mass, and therefore vary linearly with any changes of the total vehicle mass which do not affect distribution. In fact, during reduction of the equations of static equilibrium, the vehicle weight is treated as a variable which is absent from the final solution; in some cases (no tire deflection) the weight is normalized to ease computation. Therefore, two vehicles of identical dimensions and mass distributions but differing total mass would behave the same in the computer model.

Thirdly, it has been assumed that the vehicle is operating on "engineering surfaces" where the coefficient of friction does not vary spatially or with load. This classical invariance of the coefficient of friction is a valid assumption for standard materials. It is not valid, however, for soils where a greater surface bearing pressure implies a greater depth of soil compaction. This linear increase in compaction depth results in a non-linear increase of shear strength. For a further discussion of this phenomenon, the reader is referred to the work of Prof. Ronald Scott of the California Institute of Technology. [Scott89]

A properly scaled vehicle would therefore need to have adjusted tire spring constants and total mass to accommodate both the first and last phenomenon. Once these assumptions were made, the mass of the vehicle was not set by any global parameters. It was, however, adjusted to approximately the proper scale weight to allow some degree of compatibility on non-engineering surfaces and tire spring rate scaling.

A great deal of freedom existed in designing the scale model so that it functioned kinematically as the prototype without the need for scaling dynamic properties. This is

one of the goals of the applicability of this thesis. It is far easier to construct a model which is kinematically correct than it is to scale masses, spring constants, tire width and tread, chassis flexibility and other parameters which are generally considered necessary for a functioning scale model. This thesis demonstrates how the design and fabrication of simple and cheap models yields a very useful addition to the vehicle evaluation process.

The model which has been fabricated for this thesis is shown in Figures 4-1 through 4-4. The shop drawings as prepared by the author are shown in Appendix B. Note the use of shoulder bolts and hobby shop wheels and tires. These parts were readily available at a substantially reduced cost compared to the time and cost associated with the design and fabrication of custom components. The model was built with the same three independent degrees of freedom as the prototype (2 roll, 1 pitch). While the roll axles do not appear in the 2-D computer model, they are useful in non-computer related correlations of the prototype and physical model. The model was also used to evaluate, qualitatively, the tipover limits of the various vehicle bodies, which are dependent only on center-of-mass locations and vehicle and terrain geometry.

The model is powered by six gearmotors as modified by Donald Bickler of JPL. The components were purchased at a surplus store so their original purpose and specifications are not available. The motors are from a small DC gearmotor with parallel shaft spur gearing. These 2048:1 gearboxes were found to strip under impact conditions when tested on other models. When proceeding across an obstacle, a wheel would often undergo some form of impact. An example is when surmounting a square bump, the wheel would usually fall off the trailing edge of the bump. This impact would cause an instantaneous torque which often stripped the final stage high-torque gear. The steady torque provided by these gearmotors was approximately 20 in-lbs before slippage occurred.

Globe AC gearmotors were discovered which use 900:1 planetary gearing. These gearboxes provide enough torque as they allow the assumption that $\tau > \mu Nr$ to be valid. Assuming the final model would weigh in around 15 lbs with tires of radius 2.5 inches and leaving significant margin for impacts and weight shifting, it was determined that torque capability greater than 35 in-lbs/wheel was desirable. After Mr. Bickler mated the Globe planetary gearbox to the DC motor they were tested by the author using a torque load cell in an Instron testing machine. The gearmotors were able to achieve 120 in-lbs of torque before failure. Even then, the failure was due to torsional bending of the output shaft and not due to any gear failure. [Bickler89]

The power source is a simple 6V lantern battery. The left and right sides of the vehicle were wired separately to allow for differential "skid" steering. Each side was controlled through a switch which allowed forward or reverse motion of that set of wheels.

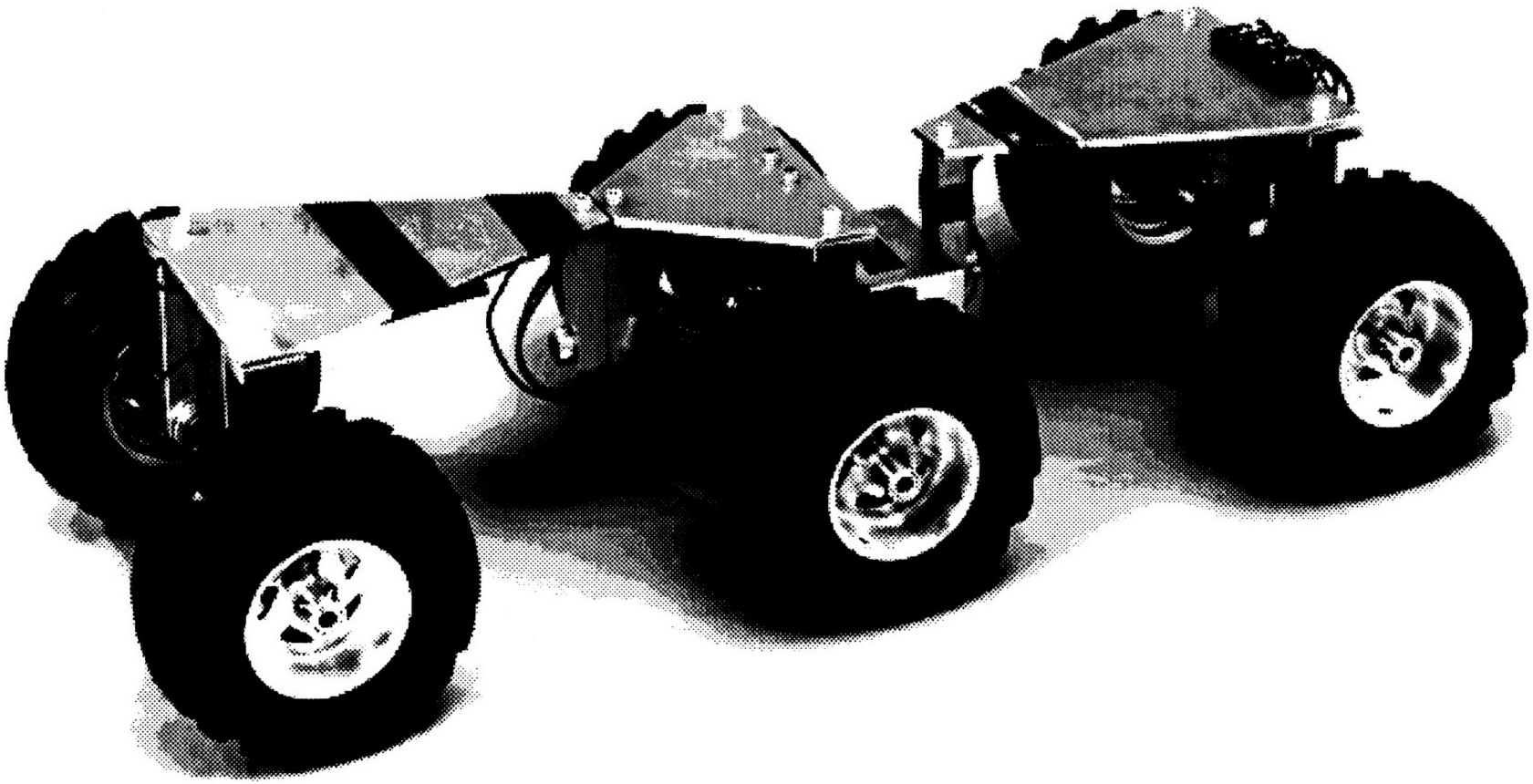

Figure 4-1
Scale Model Configuration

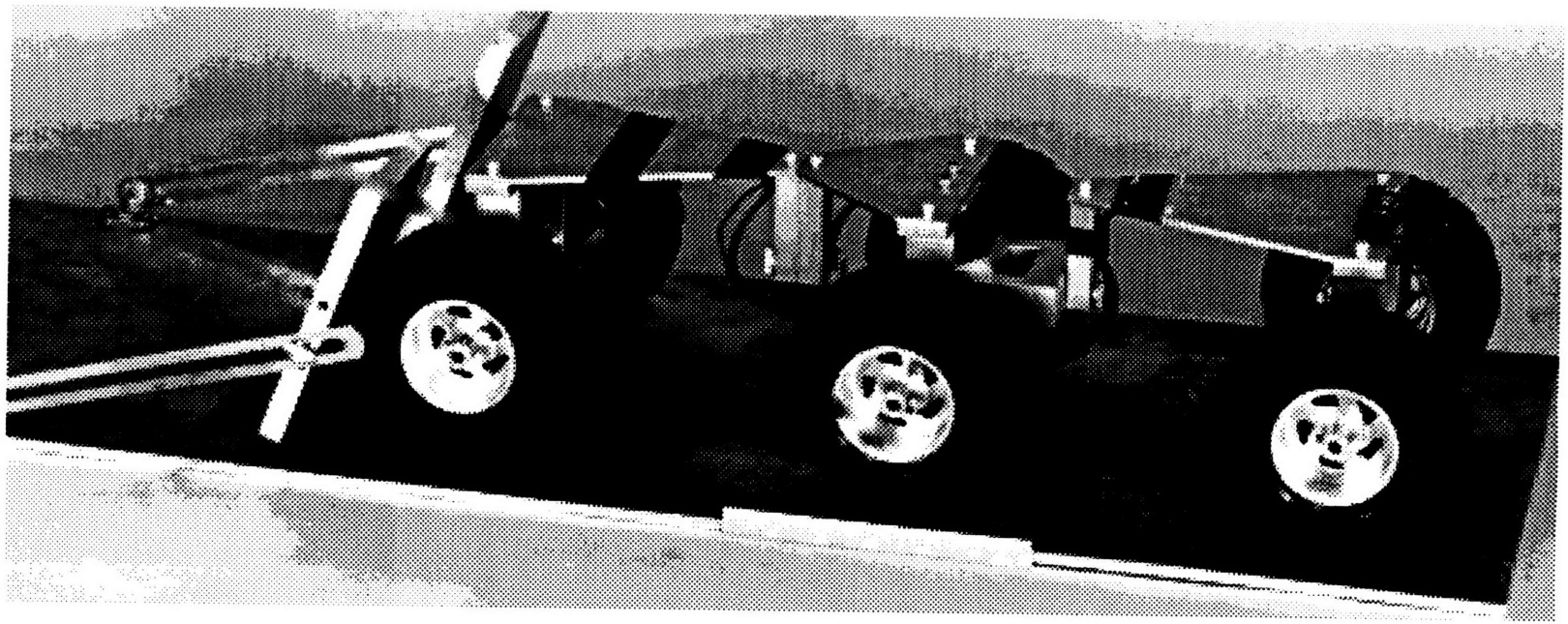

Figure 4-2
Front-Forward Test

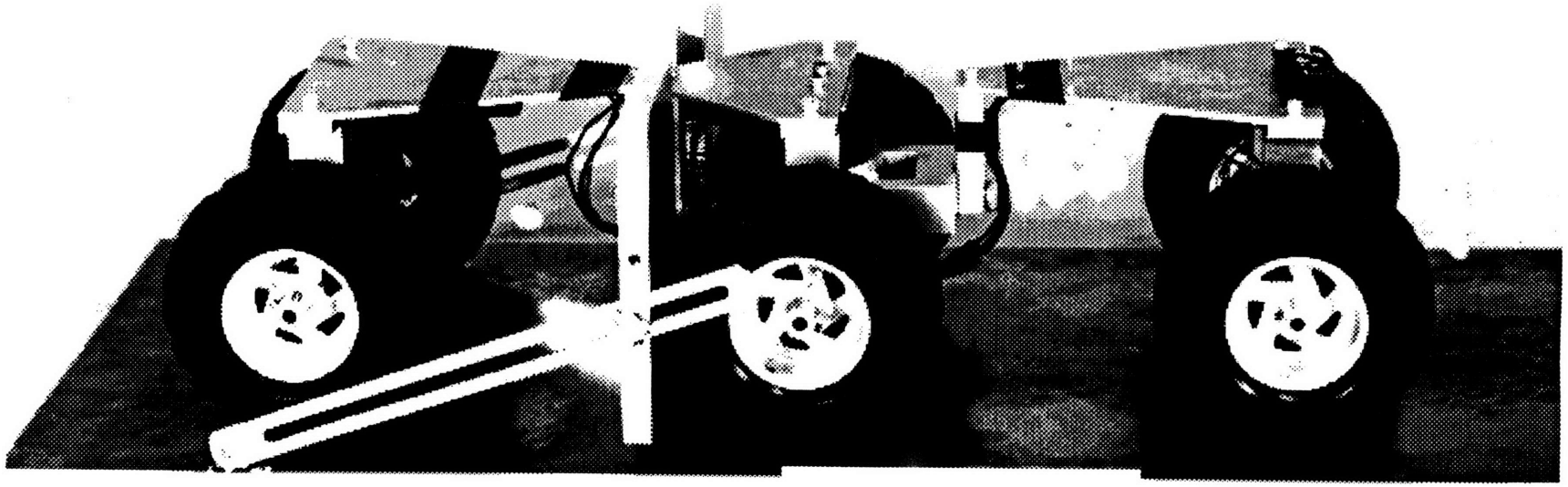

Figure 4-3
Middle-Forward Test

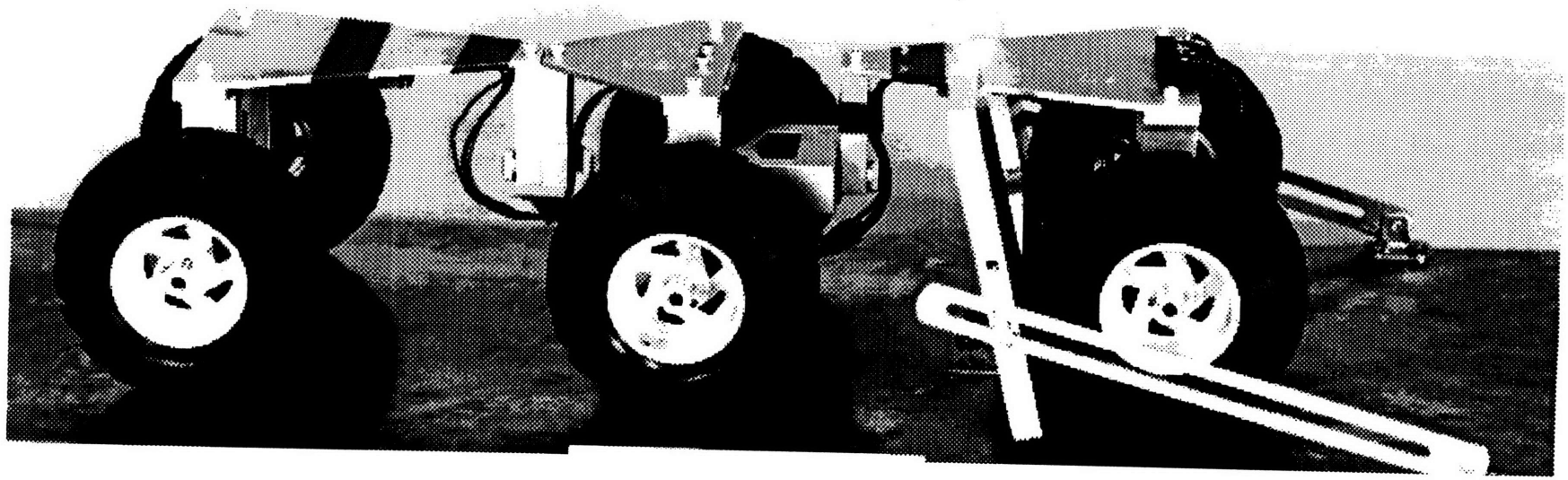

Figure 4-4
Rear-Forward Test

4.2 Test Equipment Design and Procedure

The requirements placed on the small test apparatus were simple. The vehicle had to be tested over a range of angles commensurate with the friction of the surface and the angles predicted in Figure 3-17. It was also necessary to provide the same coefficient of friction on the ramp as on the floor, allowing the transfer between the floor normal and obstacle normal regimes to be continuous, as well as to satisfy the computer model assumption that all surfaces provide the same tractive coefficient.

The test equipment was designed with a minimum of cost and effort in mind. The components were aluminum and standard shelf hardware. The finished hardware can be seen in Figures 4-3 and 4-4. The wall angle measurement is not built into the hardware, but rather is measured through the use of a machinists' protractor. This system allowed measurements of wall slope to within 0.5 degrees.

The testing procedure is straightforward. The first step must be the determination of the coefficient of traction which exists. This is not simply the static or sliding coefficient of friction between aluminum and rubber. There is a considerable variation in this parameter due to the specific properties of the rubber compound (which were not known from the off-the-shelf tires). Furthermore, contrary to the idealized classical theory of Coulomb friction, it has been shown [Gao89] that at low speeds, friction may have a velocity dependence. Tests conducted during this study revealed that increasing speed could increase friction, but trends were difficult to distinguish and were dependent on other parameters such as tire heating and surface degradation as well.

The selected friction test was thus an inclined plane (as in a classic Coulomb block sliding down an angled floor whose tangent corresponds to the frictional coefficient), but with tires spinning, rather than sliding locked. With the wheels locked, the tires

exhibited some form of viscous damping as the vehicle slid slowly down the plane, rather than possessing a sharp static/kinetic friction boundary. As motor speed was reasonably constant, except for the more difficult complex obstacles (the slopes used in this thesis were simple), it was decided that the traction encountered on the inclined plane was comparable to actually achievable traction. The measurement error was approximately 0.5 degrees. Due to uncertainties in determining the actual point of slippage, this error is treated as 1.5°. The coefficient was also determined at the start and end of each set of data, so the traction could be linearly interpolated through the tests.

The vehicle was then placed on the aluminum floor of the apparatus with the wheel set which is being tested resting up against the angled wall. The position of the wall was then set to approximately the predicted value. The vehicle was powered up and observed. If it proceeded up the wall, it possessed excess traction, and the available coefficient was higher than needed. The wall angle was then increased until the vehicle could not climb. If the initial wall setting was not climbed, then the angle was decreased until the equilibrium threshold was found.

It was sometimes difficult to determine exactly which setting was the threshold. If one wheel got a head start on the other, the problem became a three-dimensional case not handled in this thesis. The small initial lead one has over another can be difficult to detect, even on video. It has also been demonstrated informally that vehicles perform better in a three-dimensional mode than they do in the 2-D mode being enforced here. The traction requirements which result from these tests are thus a little conservative. More testing and modelling of three-dimensional vehicles will be necessary before this margin can be quantized. The range over which this uncertainty exists does not appear to be large; it is assumed that an error of one degree exists in detecting the threshold.

4.3 Test Results

These simple tests were run for all six cases (each axle against the wall in the forward and reverse direction) with several coefficients of friction. The materials used and the values determined experimentally are shown in Table 4-1. The angles of the limiting inclined walls were measured with an inclinometer with a precision of 5 arcminutes, although accuracy of the measurement was deemed to be only 0.5 degrees. This was partially due to the error in table levelling of up to 20 arcminutes. Note that the design of the testing apparatus limited the testing angle to 55-180° in one direction and 35-130° in the other, and thus rubber angles were not available for the easier tests or teflon angles for the harder tests. In some cases, the tractive coefficient measured before and after the six test differed by more than 0.02. In such cases, the minimum and maximum are both noted.

Table 4.1: Observed Equilibrium Angles

Material	μ	Front		Middle		Rear	
		Fwd	Rev	Fwd	Rev	Fwd	Rev
Teflon	0.3	57°10'	<56°	38°50'	40°	<56°	54°30'
aluminum	.67-.72	107°30'	72°30'	80°30'	90°	89°	99°30'
polished al	0.83	121°55'	81°25'	91°	103°20'	92°15'	110°
paper	.87-.93	123°10'	86°	103°	117°	95°	118°20
rubber	1.40	>125°	>125°	98°55'	>125°	113°10	>125°

Several errors exist in the modelling and testing effort. They have been mentioned earlier and are summarized in Table 4-2.

Table 4-2 : Errors Applicable to Scale Model Tests

ERROR SOURCE	MAGNITUDE
Angle Measurement	0.5 deg
Threshold Determination	1.0 deg
Traction (Measured as $\mu=\tan(\theta)$)	1.5° (0.03-0.07)
Model Geometry Fabrication	2 mm

These errors are plotted as error bars on the following graphs (Figures 4-5 through 4-7). Each of these three graphs represents the theory and experimental data for one of the three classes as defined in section 3.4. In all cases, the data clearly follows the trend of the theory; 92% of the data points lie within known error of the theoretical curve. This correlation exists over the whole range of $\mu = 0.3$ (teflon) to 1.4 (rubber). It is therefore concluded that the experimental data verifies the computer model for these two-dimensional cases. One interesting phenomenon noticed during these tests as well as others while investigating traction properties is the dependence of traction on surface dirt. Note the dirty aluminum offered lower traction than cleaned and polished aluminum. It has been theorized that this decrease is due to the fact that dirt degrades the adhesion of the rubber to the smooth metal surface. Furthermore, it was observed that friction increased over time with the dirty aluminum. The tests seemed to be cleaning the surface below the wheels of loose dirt.

Another interesting phenomenon falls outside the applicability of the computer model. The vehicle behaved differently as a 3-D vehicle, where the vehicle would roll the body which was against the inclined wall to allow it to climb easier. Raising just the port or starboard sides of the vehicle provided more forward thrust (as five wheels were in

contact with the ground), which provided a larger normal force on the wheel which was elevated. This larger normal provided more climbing traction, and the roll angle allowed more transfer of weight from the elevated wheel to the grounded one (as the center-of-gravity remained between the two). This would usually continue until either the grounded wheel developed enough traction to rise too, or the elevated wheel would roll until the vertical component of its traction diminished to the point where it could not support the vehicle, and then the wheel fell to the ground. This three-dimensional roll occurred at angles both above and below the critical 2-D threshold. It was therefore necessary to lock the roll axles during the 2-D tests. This is, however, an interesting 3-D phenomenon which deserves further study.

Figure 4-5: Outside-Extreme Wheel Tests

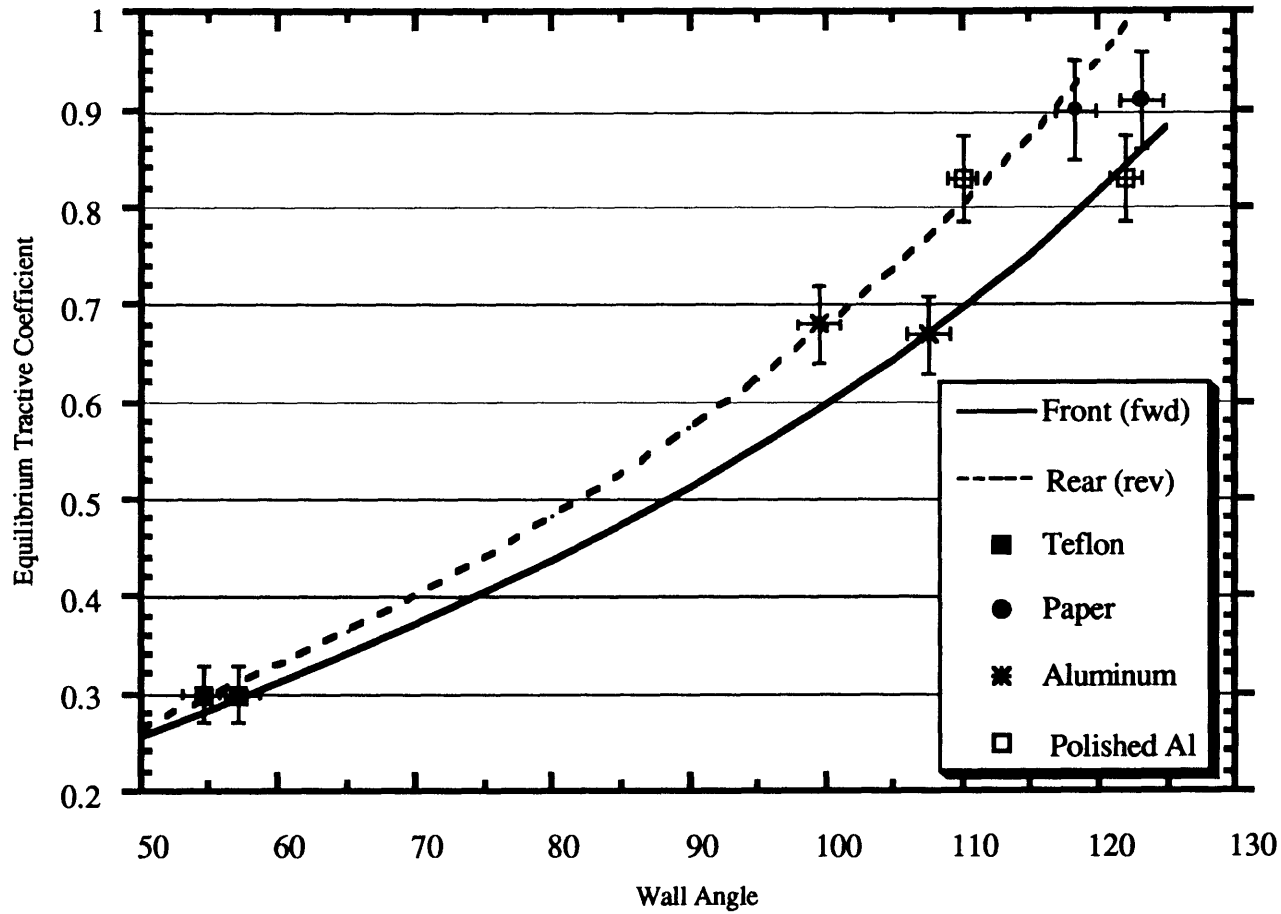

Figure 4-6: Inside-Extreme Tests

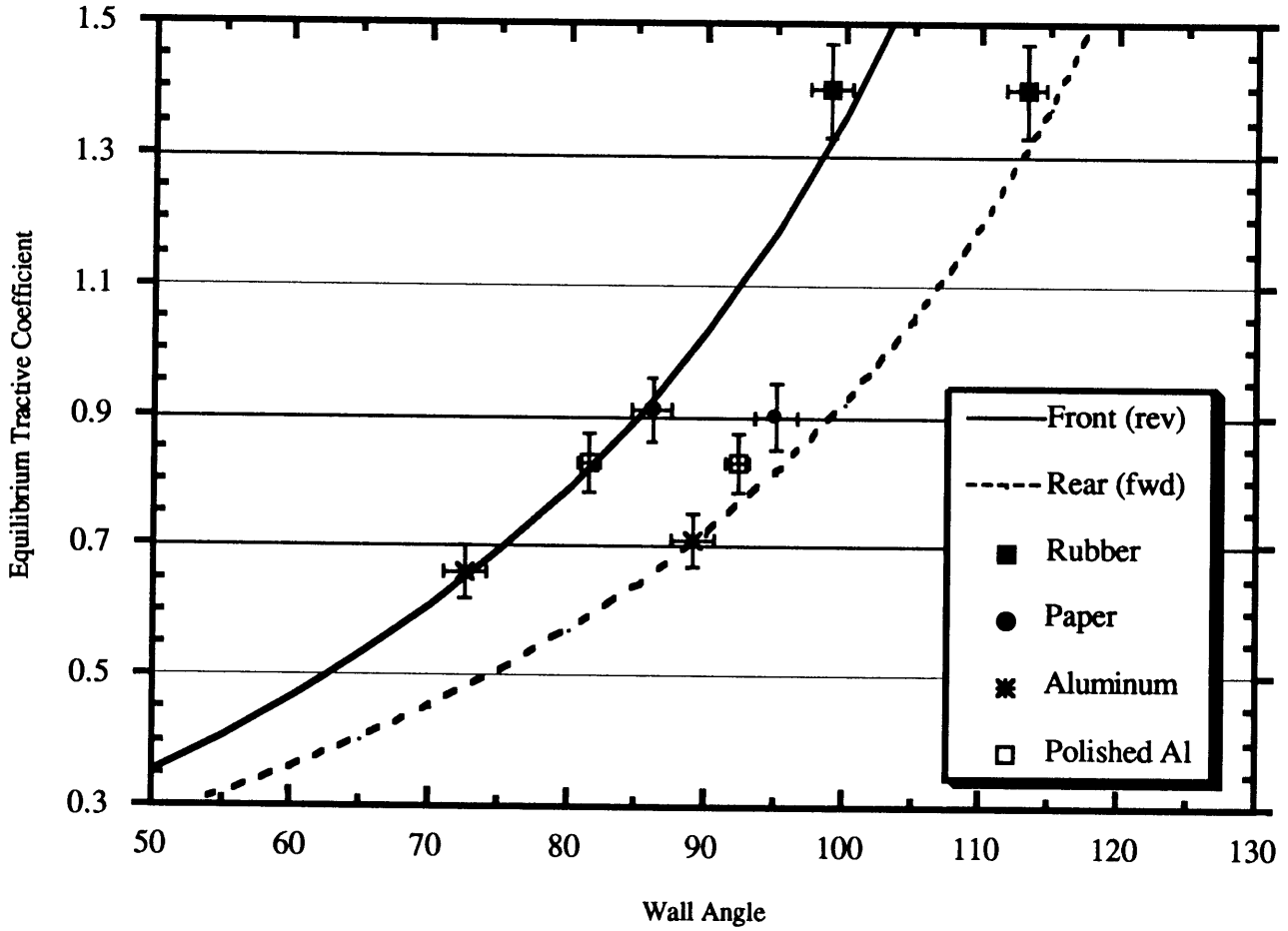

Figure 4-7: Middle Wheel Tests

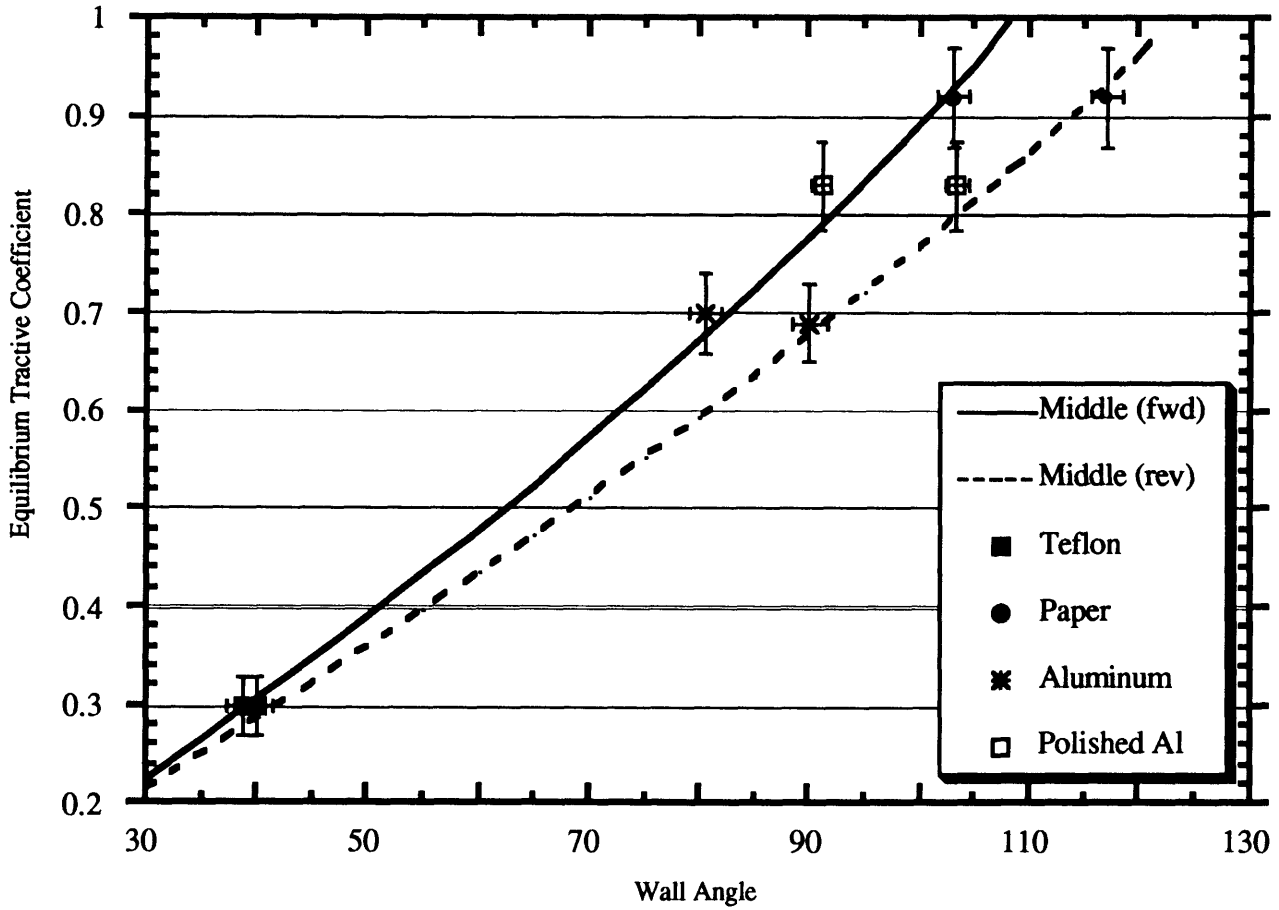

5. PROTOTYPE NAVTEST TESTING

A goal of this thesis was to correlate performance of the full-scale Navigational Systems Testbed with the test results obtained from the 1/7 scale model and the computer predictions. While the Navtest was not available for actual testing in time to be included, the necessary test equipment was fabricated and installed and some tests were accomplished. This chapter describes the intended use of the full-scale vehicle.

5.1 Tire Deflection Testing

The radius of a tire has a strong impact on vehicle performance. The tires on Navtest were measured at 34.5 inches in diameter when no load was applied. The radius included in the tire model would thus be r = 17.25 inches if they were infinitely rigid. As real tires do have some flexibility, they can be modelled as springs [Baladi, 1966]. Thus, for a spring whose behavior is linear with deflection

$$r = r_o\left(1 - \frac{N}{k}\right) \tag{5-1}$$

where r = radius of the tire at the contact point

r_o = undeformed radius of tire

N = Normal force acting on tire

k = linear effective spring constant of tire

Thus, for a more accurate model of vehicle performance, equation (5-1) must be included in the set of equations of static equilibrium for each set of tires. This increases the number of equations which must be solved simultaneously for the six-wheeled Navtest to nine (sum of vertical forces, sum of horizontal forces, two moment equations, three tire deflection equations, and two more which keep the tires on the terrain when they deflect) which increases the complexity of the solution process greatly and requires much more computer time. With the current processing available

(Mathematica implementation on Apple Macintosh IIcx), this problem must be handled iteratively in order to obtain solutions at a reasonable rate.

To determine the spring constant, k, tests were performed on Navtest wheels and tires. The tire was arranged in an Instron testing machine in building 158 at JPL in the configuration shown below in Figure 5-1. This testing lab has tested motorcycle and bicycle wheels before by placing them between two flat plates. This is fine for a balloon type structure where the carcass stiffness is not significant compared to the stiffness generated by the air pressure. These truck tires were, however, quite stiff, even with no internal pressure, so another method was needed. The author designed the following setup with the requirement of applying the load to one area of the tire only, in a fashion where deflection in the direction of the normal force could be directly measured.

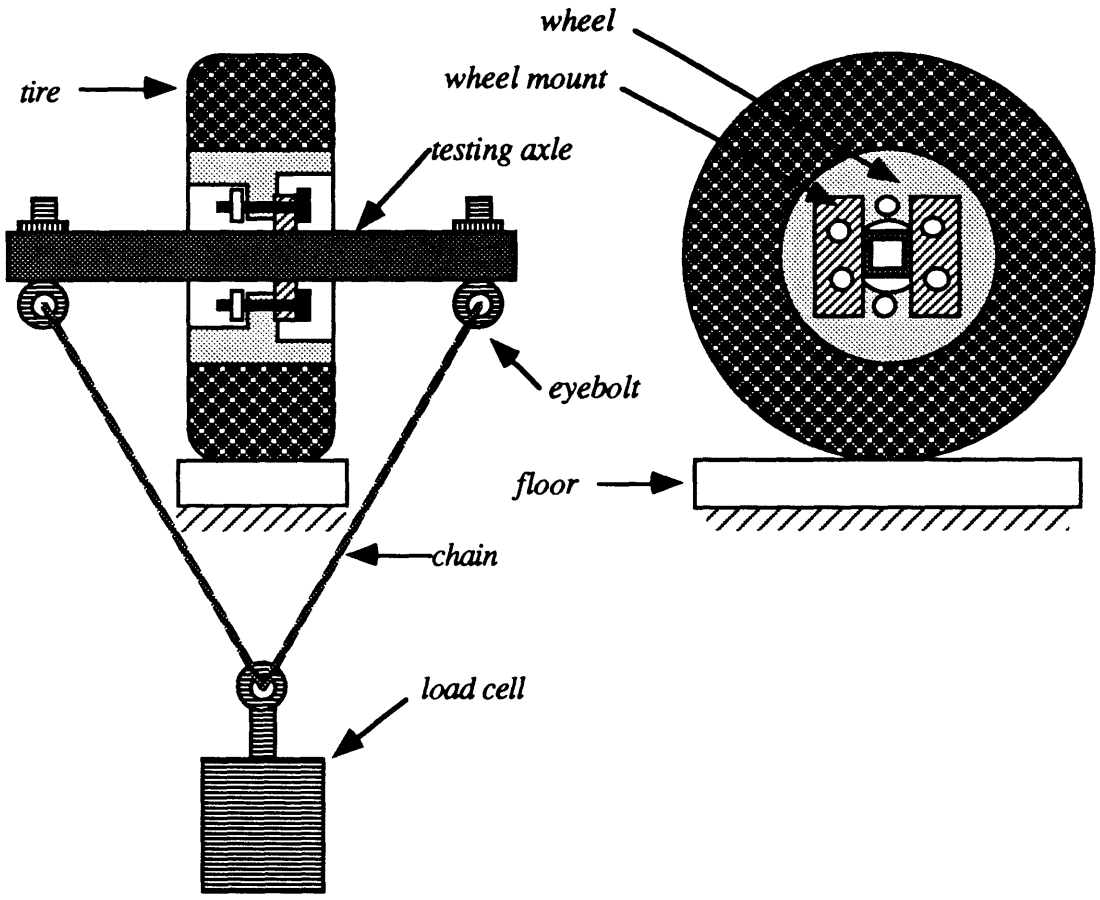

Figure 5-1

Tire Deflection Test Setup

The tire rests on the "floor", which is a platform built upon the Instron machine which is tied to ground. A testing axle was fabricated from some square aluminum tubing. The wheel mount is composed of two sections of aluminum angle which are welded to the axle. Four holes were then drilled in the angle which corresponded to four of the six mounting locations on the wheel's 5.5 inch bolt circle. This axle and wheel mount was then passed through the wheel center and bolted to the wheel. The axle was then levelled and restrained through large chains which ran from the ends of eyebolts at the ends of the axle to the load cell mounted below. The chains were set to equal lengths and the tire was centered over the cell so that the applied force was vertical. The tire's

inner tube was hooked up to a tank of nitrogen and a regulator, so internal pressure could be measured and controlled. Safety analysis and fabrication drawings for this test apparatus is shown in Appendix C.1.

Table 5-1: Spring Constants for Navtest Tires

Air Pressure (at start) (psig)	*Spring Constants* (lb/in)	
	Low-Load	*High Load*
16	660	660
8	420	440
4	270	400
2	170	320
1	130	270
0	130	300
open	130	600

The candidate chains were tested past the expected loads beforehand both for safety and to estimate their rate of extension so that the actual deflection could be corrected. The selected chain showed negligible extension under the tested loads. The test was controlled by moving the load cell under stroke control. An IBM-based data acquisition system allowed the monitoring and recording of load and tire pressure vs. deflection. The was close to linear (except for the open valve case) so the simple form of equation (5-1) was sufficient to describe the deflection behavior. Table 5-1 shows the spring constants that were found for the tire as a function of air pressure.

Figure 5-2: Tire Deflection Due to Normal Force (Middle Wheel Encountering a Vertical Wall)

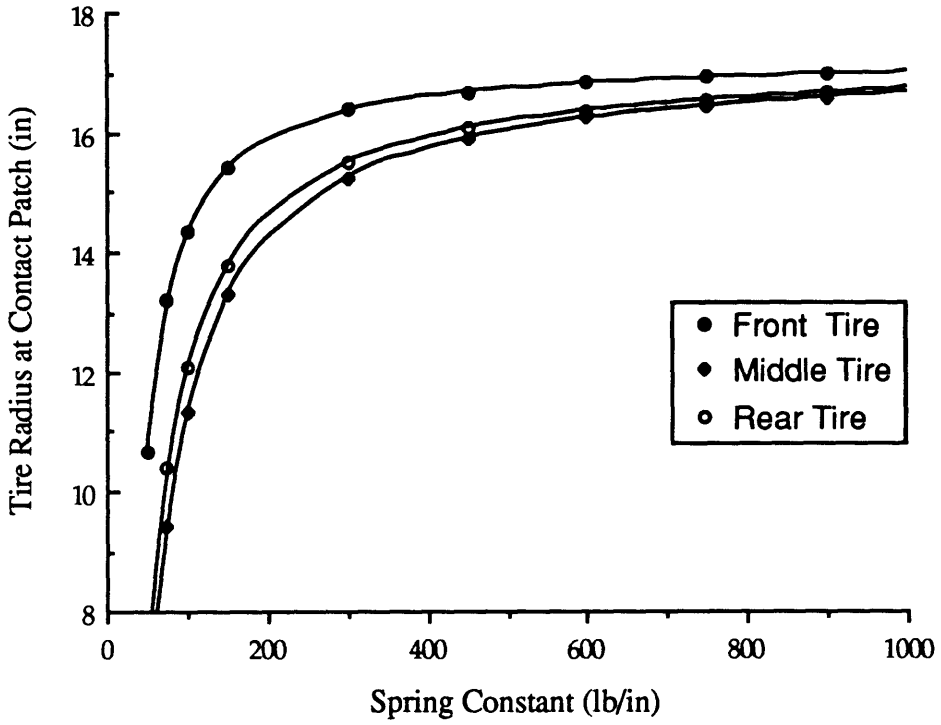

When spring constants are considered in the model for climbing performance, as in Figures 5-2 and 5-3, the deflections of the tires affect the vehicle when the middle wheel is against a vertical wall. Figure 5-2 shows how the radius of the tires change with tire stiffness. For spring constants less than 150 lb/in there is danger of hitting the wheel rim. A conservative requirement would be to specify that k must be greater than 300 lb/in when loaded to avoid damage to the rims on dynamic loading. One may thus conclude that the Navtest should be run with its current tires pressurized to at least 2 psi (suggested 4 psi).

Figure 5-3: Effect of Tire Flexibility on Tractive Performance (Middle Wheel Encountering a Vertical Wall)

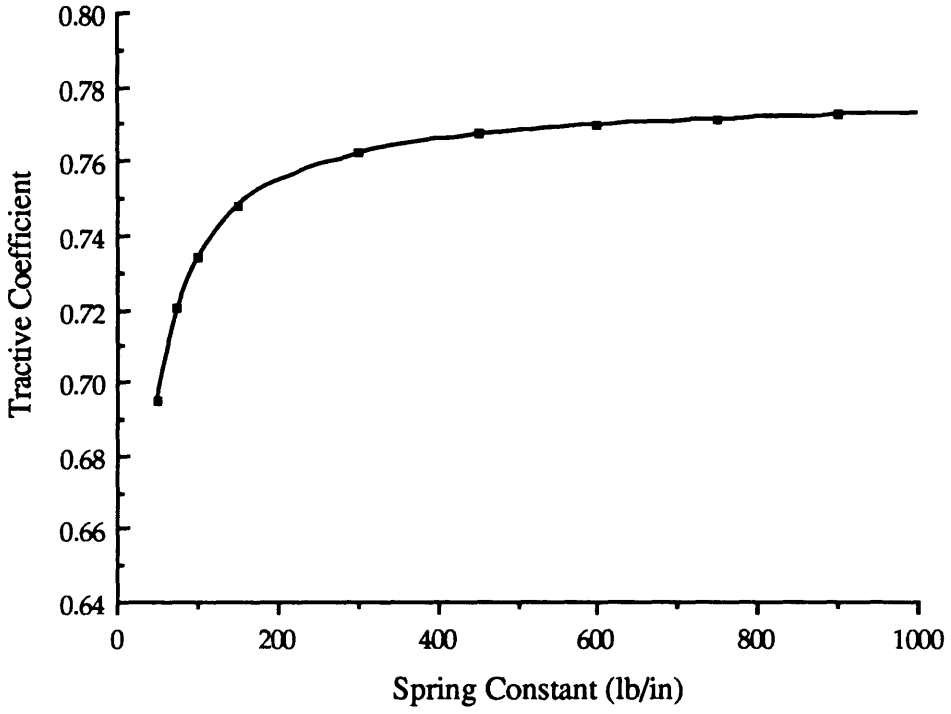

It is clear from Figure 5-3 that for stiff tires (k > 200 lb/in), the flexibility results in negligible changes (less than 4%) in the tractive coefficient. Similar results were obtained when these numbers were used in the model for the rocker-bogie configuration. It was decided that the small perturbations caused by such quasi-rigid tires was not worth the computer time to include them. The graphs shown in chapter 3 were therefore prepared without the use of equation (5-1). Furthermore, the scale model tires were tested and found to have a stiffness of approximately 7 lb/in which corresponds to over 340 lb/in for a full-scale vehicle, so they are not affected by flexibility either

5.2 Mobility Slope Testing

Testing equipment for the slope-climbing capabilities of the Navtest was designed similar to that for the scale model. Due to the size of the Navtest vehicle, and the potential hazard posed by testing such a vehicle to its mobility limits, a large factor of safety of 5.0 was used in designing the test apparatus. Three sets of data are needed to compare the Navtest to the 1/7 scale model: mass distribution, friction, and slope performance.

5.2.1 Mass Distribution

The mass distribution of the two mass centers of the vehicle could not be determined explicitly in three dimensions as explained in section 3.3. It was, however, possible to determine the weight supported by each of the tires when the vehicle was level through the use of a portable truck scale. The scale would be placed under any wheel and wood blocks were placed under the other wheels to ensure that the vehicle remained level. Figure 5-4 below shows the result of this test. The mass distribution of the 1/7 scale model and the computer code were accordingly adjusted. The determination of the heights of the c.g's would have been possible through measuring the weights under the wheels when the front or rear axles were raised above level. As the computer modelling was predicting only slope starting performance (vehicle level) and the Navtest was not available for slope tests, this was not accomplished.

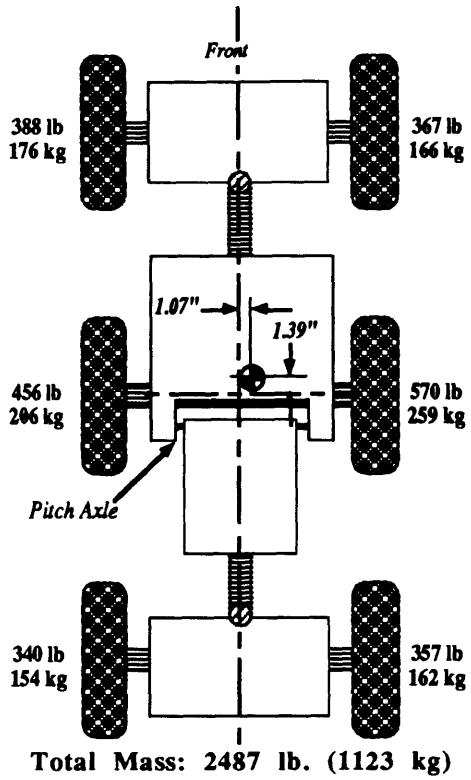

Figure 5-4
Measured Mass Distribution of Navtest

5.2.2 Tire/Aluminum Friction

Determining the coefficient of friction of such a vehicle is also more complex, as it is not possible to use a sliding block test. The alternate plan for such a measurement is to attach a yoke to the rear cab of the vehicle, which leads to heavy chains which are attached to a load cell. The vehicle would then drive forward on the aluminum testing rails (described below) until the chains were tight and then the wheels would start to spin in place. Knowing the level weight of the vehicle from above, the coefficient of friction could be easily determined by reading the pull on the load cell and dividing by the weight.

5.2.3 Angled Wall Equipment

The most important tests for the Navtest would be the slope performance. The equipment designed for the Navtest is similar to that for the 1/7 scale model. The vehicle would be required to drive against an angled wall with each set of tires. The floor of the room in which the Navtest is stored is linoleum tile. It was decided that wear and dirt would make the linoleum an unrepeatable surface. The desire to minimize the errors associated with the surface friction and the need for safety lead to the decision to use aluminum rails.

The Navtest is shown on the test equipment in Figures 5-4 through 5-6 and the fabrication drawings and safety analysis is in Appendix C. It is composed of aluminum plates with angle welded upward. The equipment was attached to the ground by floor bolts mounted through the angle and the plate. The upright angle section was drilled with holes of various spacing and formed the bottom leg of a triangular truss. The walls attached to one face of the truss and the other two legs were moved into different holes in the aluminum angle to vary the wall slope. The equipment was easily reconfigurable by pulling pins, moving the truss legs and reinserting the pins. A schematic of this system is shown in Figure 5-7.

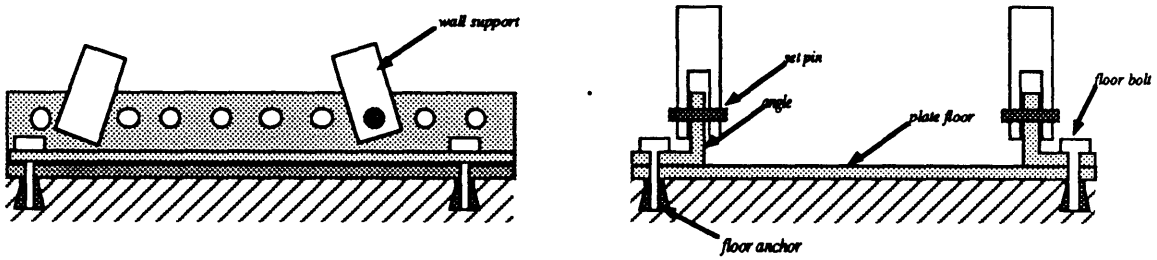

Figure 5-7

Floor-Mounted Slope Support Equipment

Tests were not run due to problems with the Navtest drive system. The planned activities were analogous to those conducted for the scale model and described in chapter 4.

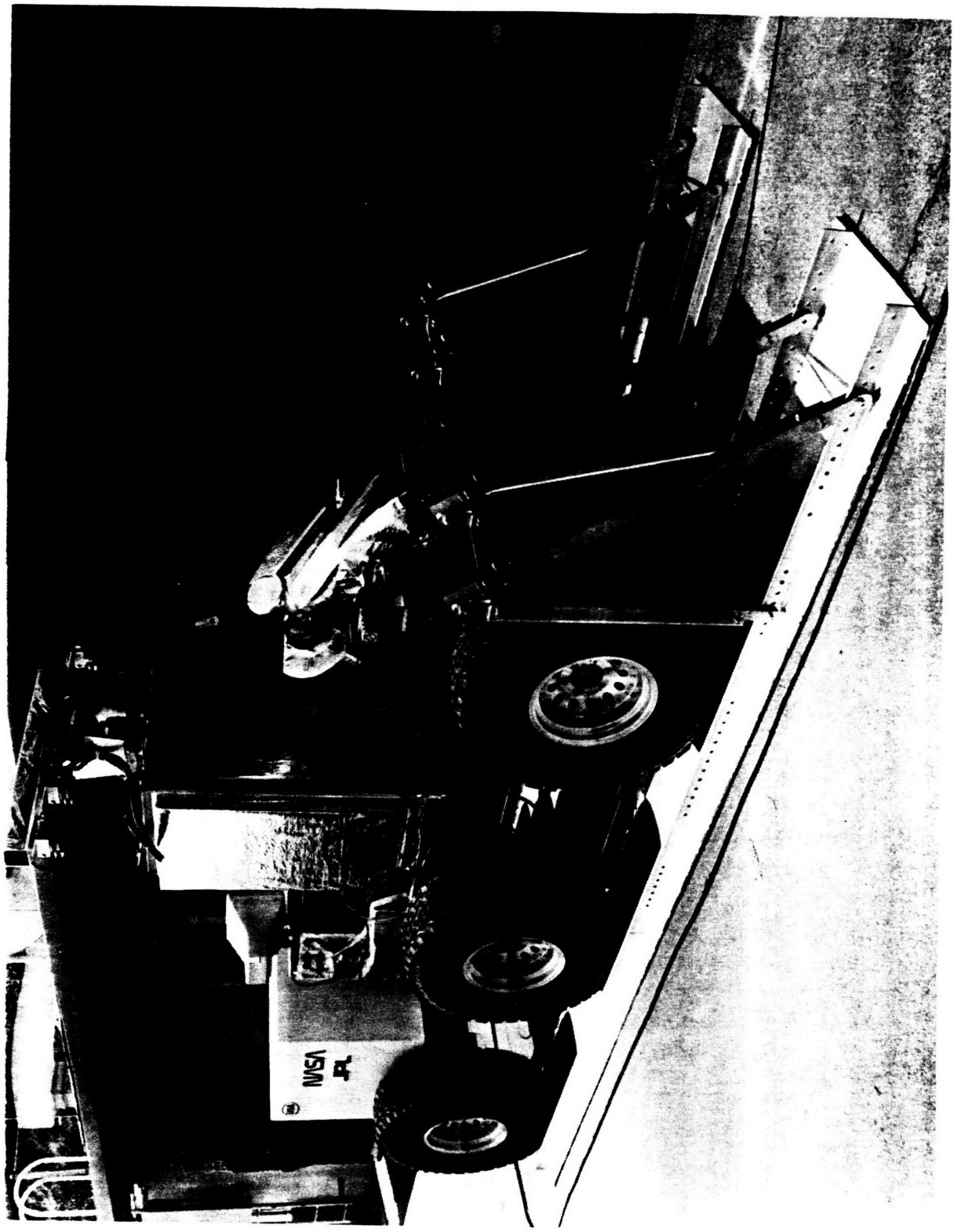

Figure 5-6
Navtest on Test Equipment

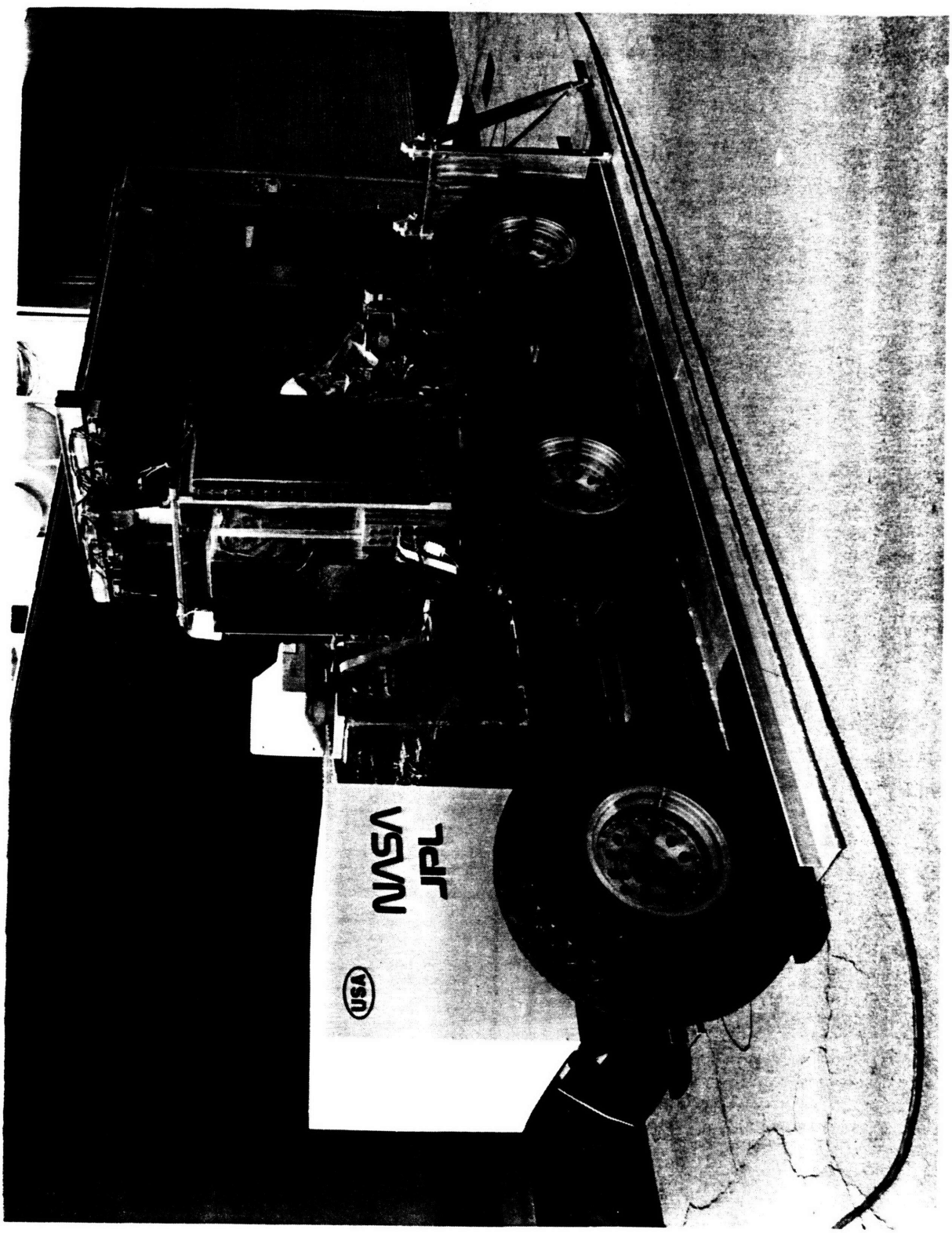

Figure 5-7
Navtest on Equipment (Rear View)

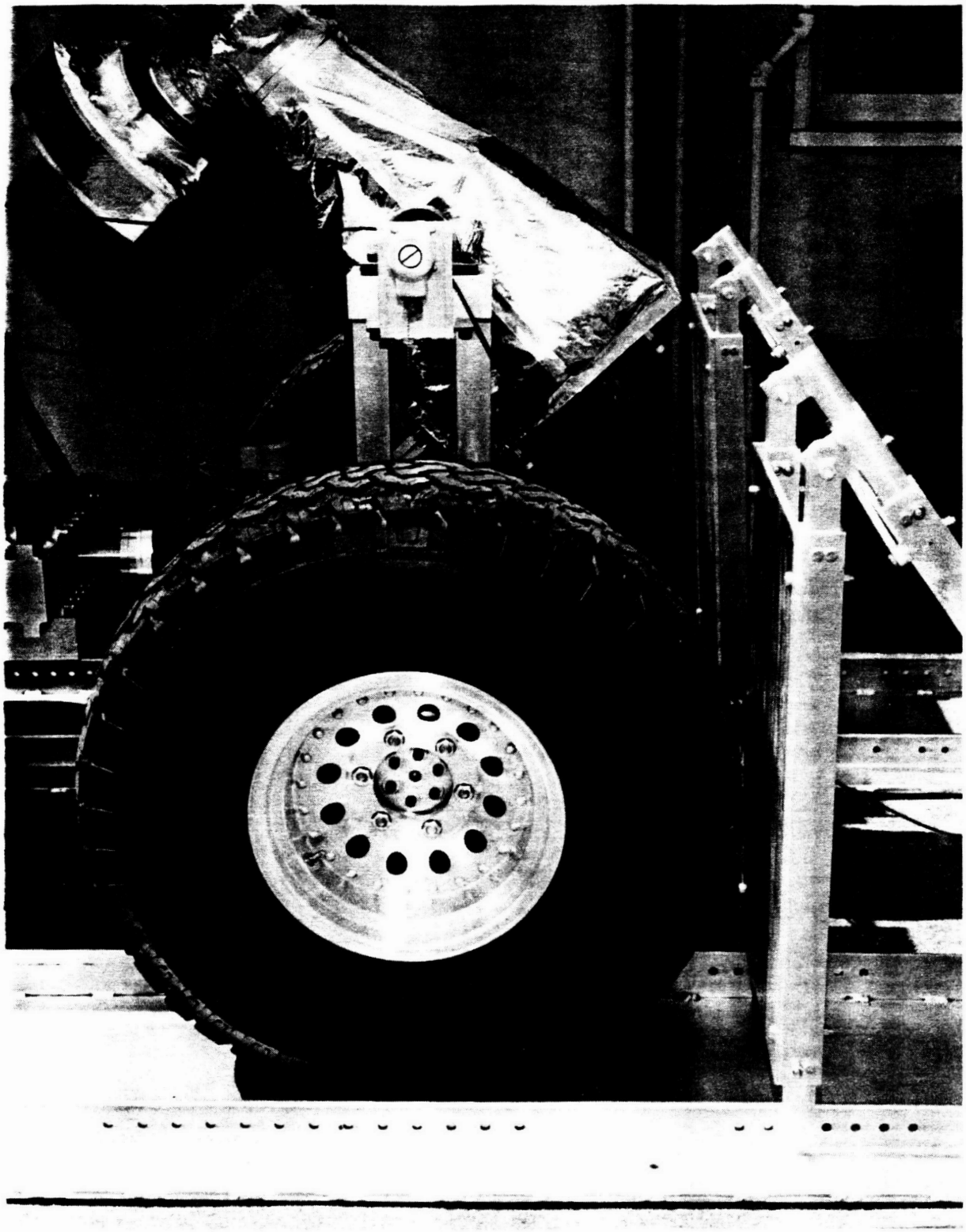

Figure 5-8
Navtest on Equipment (Wheel Closeup)

6. CONCLUSIONS AND RECOMMENDATIONS

6.1 Uses of the Computer Model

The tests described in section 4.3 demonstrated the applicability of the quasi-static modelling technique, and in particular, the model as implemented in the Mathematica code, to the problem of a 2-D vehicle assaulting an inclined plane. While only this situation of the inclined plane has been investigated to this depth, other tests performed concurrently with this thesis have shown the more general applicability of the model to more complex obstacles and vehicle geometries [Lind90].

The use of this result should not be underestimated. The computer model allows for infinite variation of geometry (in two dimensions). By making minor modifications of a given geometry, the sensitivity of performance to the geometrical parameters can be identified. The alternative approaches would be extensive testing using a modifiable model, a complex analysis of the performance change due to the geometrical modification, or a linearized perturbation analysis. Parametric optimization can be more easily conducted using the computer code.

A change in the test (e.g. traction to surmount a 0.5 meter bump rather than a 1.0 meter step) would necessitate a recalculation or reformulation using the analytic approach or a modification of the test fixture for a physical model. A different obstacle simply requires reentering the relevant terrain parameters into the computer model to produce the new results and optimize for the new terrain.

This computer model can be used for evaluation as well as for design. If a set of vehicle designs are to be compared, the relevant geometry of the vehicle and the test terrain can be entered and run, with the vehicle requiring the lower tractive coefficient the winner. Furthermore, a simple routine can be written (given the global terrain and

vehicle geometries as inputs) to yield the vehicle orientation at a given discrete step along that terrain. Such code has been written [Moreno89] for the Navtest to be integrated with the navigation software, and a simple "terrain follower" was also written to be coupled with this computer model [Lind90]. By stepping the vehicles across the terrain, a profile of the required traction at each of those points can be generated. This simulation can be used as a more general evaluation of the capabilities of configurations than just single tests. The implementation of such an obstacle course physically would be costly and little information besides Go/NoGo at various points along the course would be found.

6.2 Continuation with the Scale Model

While the computer code does generate a great deal of useful information about the capabilities of a variety of configurations, it is limited to two dimensions. During the course of this work, three-dimensional effects did indicate that the total vehicle performance is not indicated by the two-dimensional approximation. Furthermore, the surfaces of planetary bodies are not likely to be covered with many objects which happen to strike a pair of wheels at the same height and angle at the same time. Thus, the scale model can still prove useful in investigating these effects and later correlating it to a 3-D computer model or it could be the source of an empirical model.

Another use for the scale model in mobility is determining the sensitivity of tip-over to a variety of parameters, including the height of the center-of-mass. One of the prime failure modes for such multi-body vehicles as the Navtest is tip-over of one of its bodies through excessive roll while surmounting a 3-D obstacle. Finding the safety limits of this motion allows rotational stops to be implemented on the Navtest, thus reducing the risk of damage to the prototype. Finding these limits with the scale model is safe, easy, and much cheaper than repairing the full-scale vehicle.

Further correlation work can also be performed. While some of the computer-predicted effects seem intuitive, others may not, as in the crossing of the middle-forward and rear-forward curves near a 108° degree wall (see section 3.4.3). Some of the more non-linear behaviors of vehicles may be reconsidered, at least to get an idea of the magnitude of errors induced by the modelling assumptions.

Lastly, the model can be modified to test the boundaries of the assumptions made earlier. For example, the torque capability could be lowered by changing the power source such that the vehicle motors might slow appreciably and perhaps stall. Various tires could be installed to test the tire stiffness and constant uniform torque assumptions.

6.3 Continuation of Prototype Testing

The ultimate goal of this work is to allow the design and evaluation of full-scale vehicles. The testing of the actual Navtest vehicle both strengthens confidence in the computer model and allows the incorporation of the computer predictions into the vehicle navigation system.

While the computer and scale models do demonstrate a correlation, many readers will not be satisfied that the model predicts the behavior of an actual full-sized vehicle until that correlation is also demonstrated. The assumptions which were made to allow the development of the computer and scale models may not hold on the actual vehicle, although they all seem to be reasonable. Even if the assumptions are found to be valid, the Navtest can be used to determine the magnitudes of the errors associated with the assumptions. The vehicle could also be used to allow the empirical development of a model of the effects of flexible soil on performance.

A table of expected performance parameters can be generated from the computer model and loaded onto the vehicle to allow the correction of non-optimal performance (e.g. unwarranted power distributions among motors) and the detection of dangerous situations. By carefully modelling the vehicle behavior, deviations outside those bounds can alert the navigation and perception systems, as well as ground controllers, to the potentially catastrophic situation.

6.4 Summary

The data shown in this thesis clearly indicates the potential applications of the quasi-static approach, and has developed the background for a future assessment of the uses of scale models. The reader is cautioned to examine the assumptions made, and only to use the model if the assumptions apply or the vehicle is insensitive to other parameters. The model should be applicable to a wide array of rover configurations; if additional modules are constructed to handle non-rigid terrain or non-linear deflecting tires, the model could be applied to almost any foreseeable situation. It can be used for both design and evaluation purposes, is easy to use, and can be run in a reasonable amount of time on personal computers or workstations which support Mathematica or similar environments.

References

[Baladi84] Baladi, G.Y., Rohani, B., Barnes, D.E., *Steerability Analysis of Multi-Axle Wheeled Vehicles, Report I: Development of a Soil-Wheel Interaction Model.* Department of the Army, Waterways Experiment Station, Corps of Engineers, January 1984

[Bekker69] Bekker, M.G. *Introduction to Terrain-Vehicle Systems.* University of Michigan Press, Ann Arbor, 1969.

[Bernard88] Bernard, D., "Tire/Road Modelling at Low Speeds." JPL Interoffice Memorandum 343-88-501, 31 May 1988

[Bickler89] Bickler, Donald, "Status of 'Rocker Bogie' Model" JPL Interoffice Memorandum 3526-89-351, 8 November 1989

[Bourke89] Bourke, R., Kwok, J., Friedlander, A., AIAA Paper 89-0417 "Mars Rover Sample Return Mission" *27th Aerospace Sciences Meeting,,* Reno Nevada, 9-12 January 1989

[Carr81] Carr, Michael H. *The Surface of Mars.* Yale University Press, New Haven, 1981

[Gao89] Gao, C., Kuhlmann-Wilsdorf, D. ASME Paper 89-Trib-47 "On Stick-Slip and the Velocity Dependence of Friction at Low Speeds" *STLE/ASME Joint Tribology Conference*, Fort Lauderdale, Florida., 16-19 October 1989

[Jindra66] Jindra, Frederick, "Obstacle Performance of Articulated Wheeled Vehicles" *Journal of Terramechanics*, Vol. 3, No. 2, 1966

[JPLD-6688] JPL D-6688 "A Robotic Exploration Program: In Response to the NASA 90-Day Study on Human Exploration of the Moon and Mars", 1 December 1989

[Lind90] Lindemann, R.L., "Quasi-Static Mobility Analysis Tool for the Design of Lunar/Martian Rovers and Construction Vehicles" JPL Interoffice Memorandum 3525-90-225, in publication

[Moore87a] Moore, Henry J., "Preliminary Mars Surface Models" March 1989, unpublished

[Moore87b] Moore, Henry J., (Hutton, R.E., Clow, G.D., Spitzer, C.R.) *U.S. Geological Survey Professional Paper 1389: Physical Properites of the Surface Materials at the Viking Lander Sites on Mars*. U.S. Government Printing Office, Washington D.C., 1987

[Moreno89a] Moreno, Carlos, "Pathfinder Planetary Rover Preliminary Expectation Generation Model Requirements and Interfaces." JPL Interoffice Memorandum 3526-89-052, 1 March 1989

[Moreno89b] Moreno, Carlos, "Pathfinder Planetary Rover: Mobility" *NASA Intercenter Progress Review* 13 December 1989

[Piv89] Pivirotto, Donna L., et. al. *US Planetary Rover Status*, JPL D-6693, 24 August 1989

[Scott89] Scott, Ronald, Personal Communications - *Fall 1989* Professor of Civil Engineering, California Institute of Technology.

[Wolfram88] Wolfram, S., *Mathematica: A System For Doing Mathematics by Computer* Addison-Wesley Publishing Company, Redwood City, California 1988

Appendices

Appendix A
Mathematica Programs

This appendix contains listings of three of the many Mathematica programs written for this thesis. The first is called "Simple 4 Wall" and it includes the equations necessary to solve the simple four-wheeled vehicle climbing up a vertical wall, as in Figure 3-7.

The second program was developed to see the effects of flexibility in tires on vehicle performance. The corresponding analysis and results may be found in section 5.1. Note how the system is solved iteratively, not simultaneously as the complete nine equation system is too much to be handled in the 8 Mb memory of the Mac IIcx used.

The final program is the generalized analysis package (without tire deflection) for generic six-wheeled vehicles on arbitrary terrain geomerty. The program is configured in the example to give traction required for a variety of wall angles hitting the front wheels. The data is then listed, plotted, and curve fitted to obtain an expression for tractive requirement as a function of wall angle.

Appendix A.1
SIMPLE 4 WALL

Rigid Simple 4 vehicle
Driving front wheel up wall.

```
(* Initializing Parameters*)
a = .
h = .
L = .
N1 = .
N2 = .
u = .
W = .
q = .

equations =                          (* equations of static equilibrium *)
          {u N1 + N2 - W == 0,

           u N2 - N1 == 0,

           u N2 r + N1 L Sq + u N1 (r + L Cq) - W ((L-a) Cq - z Sq) == 0 }
(*********************************************************************)



r = 1                        (* Normalizing dimensions to one radius *)
L = 8                        (* Vehicle Length  *)
a = L/2                      (* C.G. at midpoint *)
Sq := h/L
Cq := Sqrt[1-(h/L)^2]
z = r

y := Solve[equations,{N1,N2,u}]              (* the y variable holds the solution *)

answers = Table[{h,u/.y[[2]]},{h,0,2,.1}]  ;     (*answers stores the smallest positive
                                                       root                  *)
```

```
TableForm[answers]                    (* table of heights and required
                                         tractions to achieve equilibrium
                                         at that height *)
```

(* Sample Tabular Output *)

0	$\frac{4}{5}$
0.1	0.7889
0.2	0.777928
0.3	0.767082
0.4	0.756354
0.5	0.745742
0.6	0.735241
0.7	0.724846
0.8	0.714553

```
ListPlot[answers]                     (* Sample graphical output *)
```

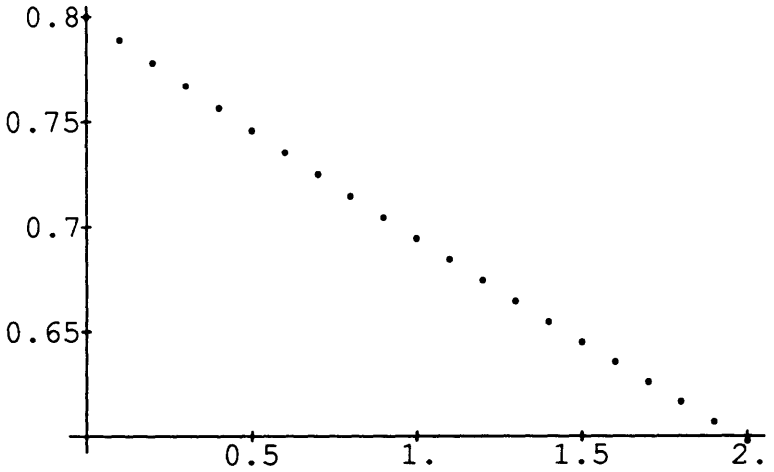

Appendix A.2
Flex-MID

Flexible MID
6-wheel NAVTEST Driving into Wall against MIDDLE AXLE

Flexible Tires (linear spring model)
- axles held level

```
(* Initializing Parameters*)
a = .
b = .
c = .
d = .
h = .
r1 = r2 = r3 = r0          (* All wheels nominally set to standard radius *)

h1 = h2 = h3 = h           (* The vehicle is nominally set to level  *)
(*************************************************************************)
r11 = 12                   (* seed value for r not equal to ro *)

k = 400                    (* spring constant of tires *)

r0 = 17.25                 (* Navtest value of nominal tire radius *)

a = 29.25                  (* Navtest vehicle dimensions  *)
b = 30
c = 6.5
d = 39.3
h = 5.75
f = 13.45

wb = 935.25                (* Navtest Weight Distributions *)
wf = 1542.75
(*************************************************************************)
```

The following procedure is set up to solve the equations of static equilibrium in terms of the normal forces and the coefficient of traction required

```
proc := {r11 = r1;

      y = Solve [
            {wf + wb - f1 - f3 - u f2  == 0,

             f2 - u (f1 + f3) == 0,

             f1 (a+b+c) + u f1 (r1+h1) + u f2 (r2+c) - f2 h2 - wf (c+b) == 0,

             wb d + u f3 (r3+h3) - f3 (d+f) == 0 },
                                                  {f3,f2,f1,u}];


        r1 = r0 - f1 /k   /. y[[3]];          Adjust radius due to flexibility
                                              and normal forces
        r2 = r0 - f2 /k  /. y[[3]];

        r3 = r0 - f3 /k   /. y[[3]];

        h1 = h - (r1 - r0)(a+b+c)/(a+b);      Adjust axle heights to keep vehicle
                                                  on the ground
        h2 = h + (r1 - r0)((a+b)-(a+b+c))/(a+b);

        h3 = h2 + r0 - r3   }
While [Abs[r1-r11]>0.0001, proc]        (* iterate until error is small *)

(* Output results *)
Print [u /. y[[3]]," ",r1," ",r2," ",r3," ",r11]

0.777209   17.25   17.25   17.25   17.25

        END OF FLEX-MID
```

APPENDIX A.3
SIX WHEELED VEHICLE
Quasi-Static Analysis Package

formulated by Randy Lindemann
adapted by Howard Eisen

```
phi = .                          (* current wall angle variable *)

dir = -1.0                       (* +1 indicates forward, -1 reverse  *)

psi3 = 0 Degree //N;             (* second and third wheels set to level terrain *)
psi2 = 0 Degree //N;
psi1 = (dir phi Degree) //N      (* first wheel wall angle varies *)

philow :=25                      (* range of wall angle to be studied *)
phihigh := 125
```

EQUATION PARAMETERS

```
/******************  This first set of numbers  ***************/
/***************  represent the traversal variables  ************/

h1 = 0              (* axle height off ground *)
h2 = 0
h = h1 - h2

/*****************    This second set   **********************/
/**   of variables represents the vehicles geometric constants   ****/

a = 29.25
b = 30
c = 6.5
d = 39.3
e= 5.75
f = 13.45
g = 0.0
j = e
r1 = 17.25
r2 = r1
r3 = r2
wb = 935.25
wf = 1542.75;
```

```
/******************  These represent the  ****************/
/*******  simplifying variables used in the cubic equation  ******/

VarA :=    { thef = ArcSin[h/(a+b)];
             hyp = (e^2 + (f+d)^2)^0.5;
             h3 = -c Sin[thef] + e Cos[thef] + h2;
             theb = ArcSin[h3/hyp];
             thetbo = ArcSin[e/hyp];
             thetbp = theb - thetbo}

VarB :=  { r1x = c Cos[thef] + e Sin[thef] + (a+b)Cos[thef] + r1 Sin[psi1];
           r1y = c Sin[thef] - e Cos[thef] + (a+b)Sin[thef] - r1 Cos[psi1];
           r2x = c Cos[thef] + e Sin[thef] + r2 Sin[psi2];
           r2y = c Sin[thef] - e Cos[thef] - r2 Cos[psi2];
           r3x = -hyp Cos[theb] + r3 Sin[psi3] ;
           r3y = c Sin[thef] - e Cos[thef] - h2 - r3 Cos[psi3]   }

VarC :=  { rm1x = (b+c)Cos[thef] - (j-e)Sin[thef];
           rm1y = (b+c)Sin[thef] + (j-e)Cos[thef];
           rm2x = -d Cos[thetbp] - g Sin[thetbp];
           rm2y = -d Sin[thetbp] + g Cos[thetbp];
           A := dir Cos[psi3];
           B := -Sin[psi3];
           C := dir Cos[psi2];
           DD := -Sin[psi2];
           EE := dir Cos[psi1];
           F := -Sin[psi1];
           G := dir Sin[psi3];
           H := Cos[psi3];
           J := dir Sin[psi2];
           K := Cos[psi2];
           L := dir Sin[psi1];
           M := Cos[psi1]    }
```

EQUATIONS OF STATIC EQUILIBRIUM

```
eqnset := { eqns = { 0.0 == n3(mu A + B) + n2(mu C + DD) + n1(mu EE + F) ,

                     wb + wf == n3(mu G + H) + n2(mu J + K) + n1(mu L + M),

                     0.0 == r3x n3(mu G + H) - wb rm2x - r3y n3(mu A +B),

                     -rm1x wf == r1y n1(mu EE + F) - r1x n1(mu L + M)  +
                                 r2y n2(mu C + DD) - r2x n2(mu J + K)   } }
```

Solving loop

(* This procedure handles loading of variables, sets up the equations defined above, and solves for required traction.

The values are then loaded into the table 'answers' and the wall angle is incremented by 5 degrees *)

```
proceed := { VarA;VarB;VarC;eqnset;
                    ans = Solve[eqns,{mu,n1,n2,n3}];
                    mu2 := mu /. ans [[3]]   }

  answers = Table [{phi/.proceed,mu2},{phi,philow,phihigh,5}];
```

TableForm [answers] **(* display a set of answers *)**

Graphic Output

Curve fit to a polynomial to obtain an analytic approximation, if desired

ansfit = Fit [answers,{1,x,x^2,x^3,x^4,x^5,x^6},x]

```
1.1288 - 0.125461*x  +  0.00597451*x^2  -  0.000137057*x^3 +
0.00000170035*x^4  -  1.07664*10^-8*x^5  +  2.7714*10^-11*x^6
```

Show[gr,Plot[ansfit,{x,25,125}]]

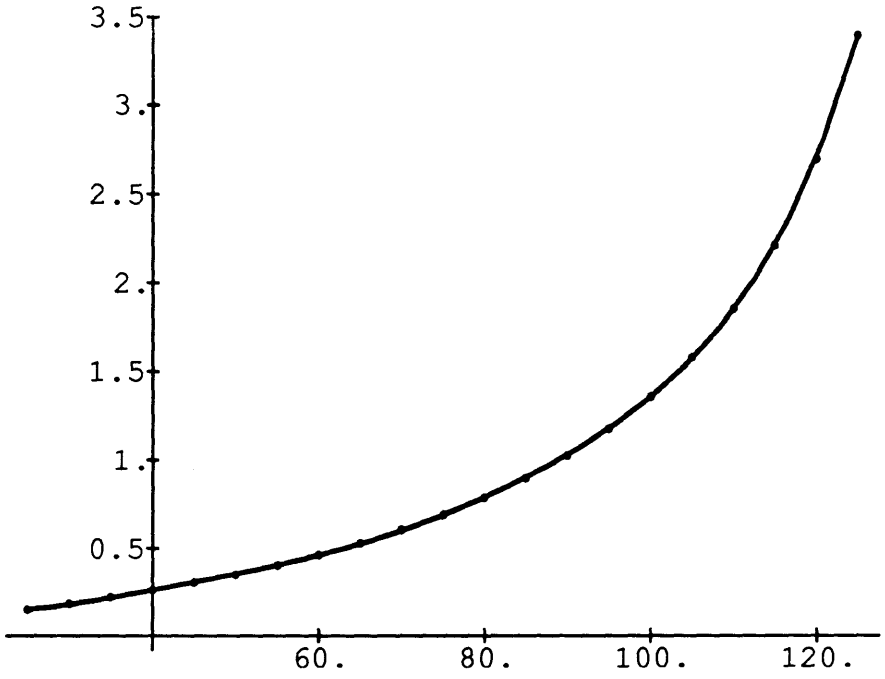

Appendix B
Scale Model Fabrication Drawings

The following pages contain copies of the original drawings prepared by the author in the design and fabrication of the 1/7 scale model. The design was performed by the author with assistance from Donald Bickler and the model was fabricated primarily by the JPL machine shops, although the author did modify several components himself.

JPL

PAGE 1 OF 4

(PREPARED BY)	(DATE)	(REPORT NO.)
HOWARD JAY EISEN 4-9360	9/29/89	
(CHECKED BY)	(DATE)	(PROJECT)
		NAVTEST 1/7 SCALE MODEL

TITLE ROLL AXIS SUPPORTS

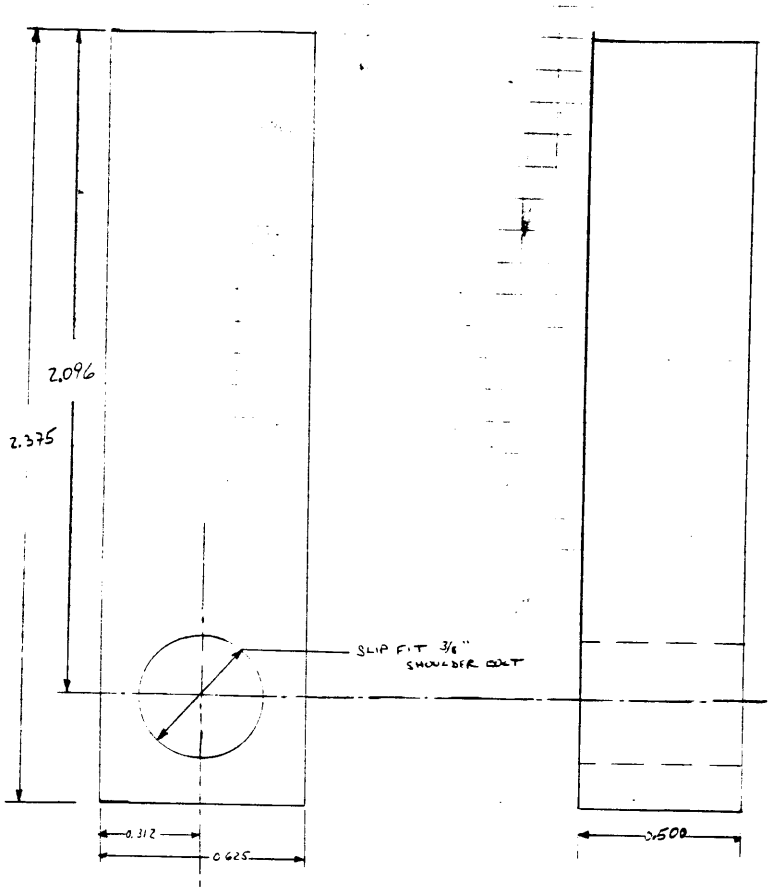

SCALE 2/1

ALL DIMENSIONS IN INCHES

TOLERANCES: LINEAR [illegible] ±.001

DIA [illegible]

ALUMINUM

ACCOUNT # 505-30501-0-2050

QTY: 2

SUPPLY 2 3/8 [illegible] SHOULDER BOLTS;

JPL

(PREPARED BY)	(DATE)	(REPORT NO.)
HOWARD JAY EISEN 4-9360	9/29/89	
(CHECKED BY)	(DATE)	(PROJECT)
		NAVTEST 1/7 SCALE MODEL

TITLE
ROLL AXIS SUPPORTS

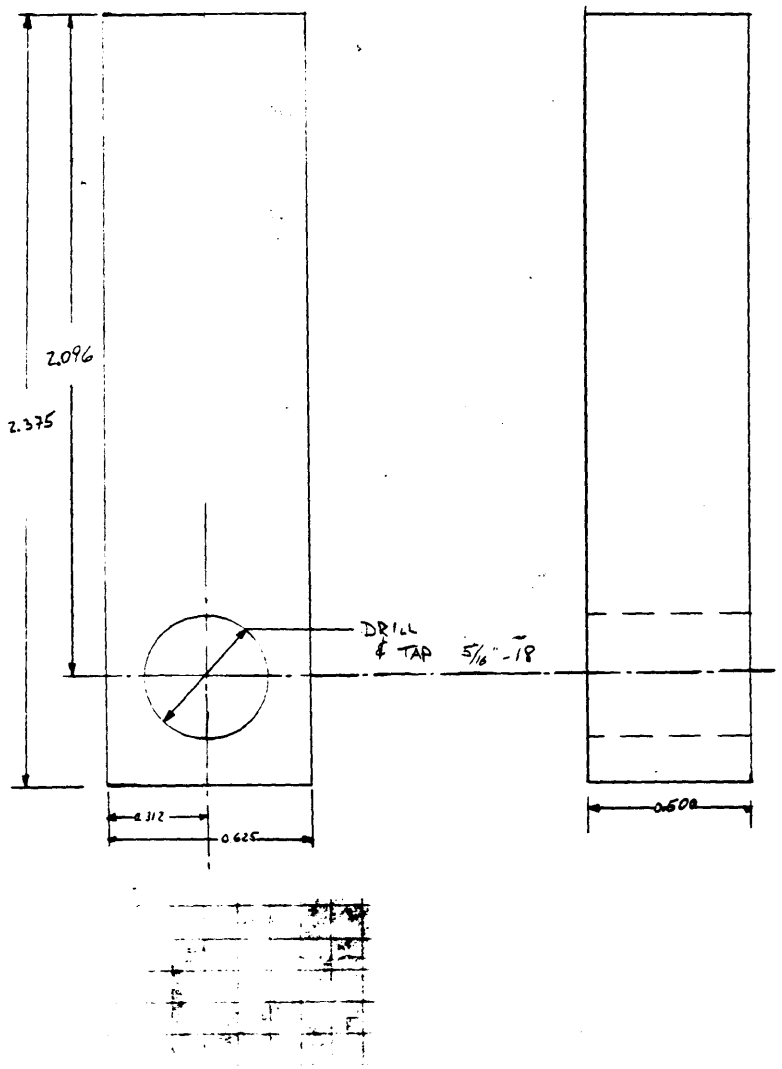

SCALE 2/1
ALL DIMENSIONS IN INCHES
TOLERANCES: LINEAR DIM ±.001
DIA +.002 -.000
ALUMINUM

ACCOUNT # 505-30501-0-2050

QTY: 1

JPL

PAGE 3 OF 4

(PREPARED BY)	(DATE) 10-19-89	(REPORT NO.)
(CHECKED BY) HOWARD EISEN 4-9360	(DATE)	(PROJECT)

TITLE PITCH-ROLL COMBINATION BLOCK

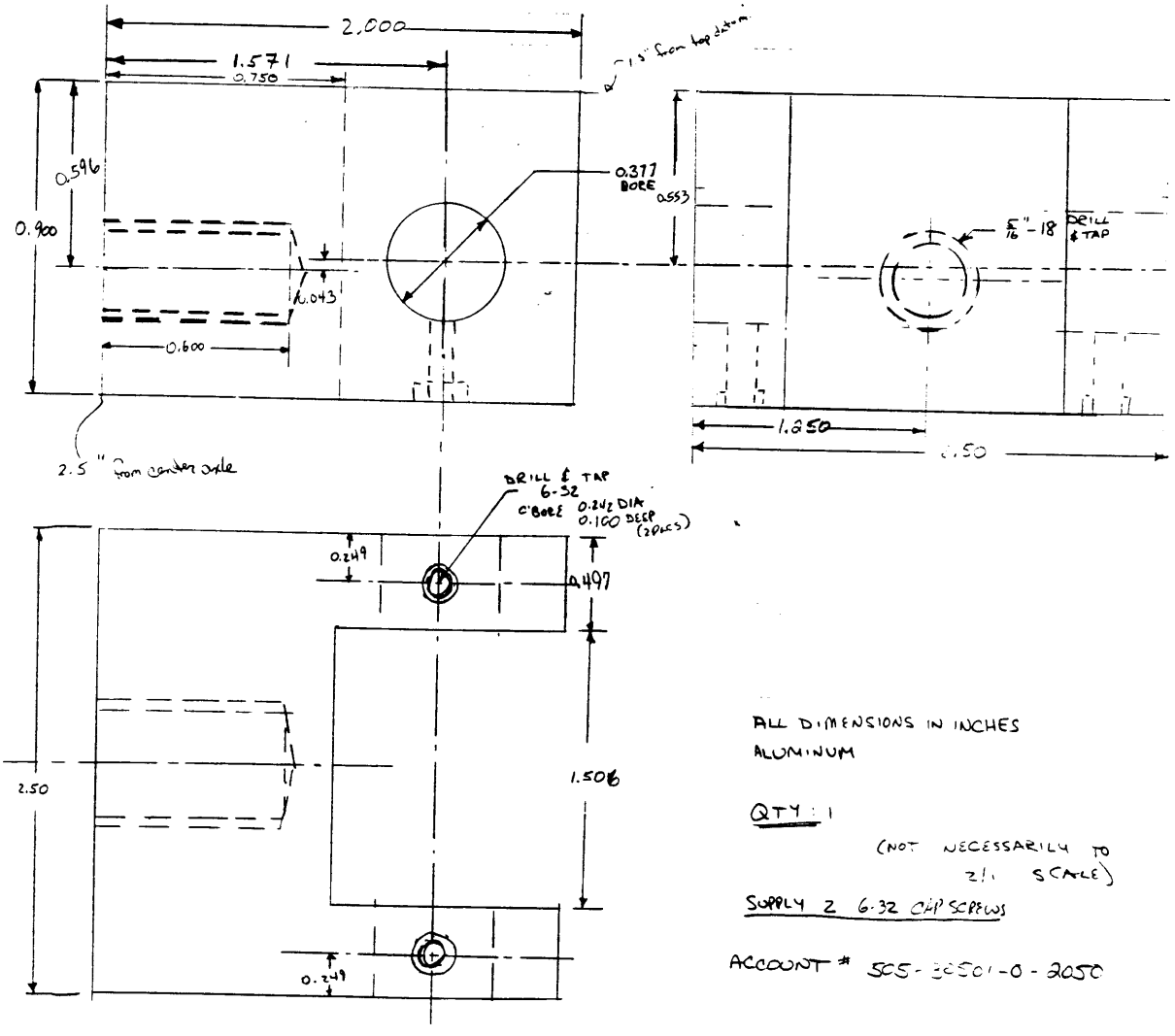

ALL DIMENSIONS IN INCHES
ALUMINUM

QTY: 1

(NOT NECESSARILY TO 2/1 SCALE)

SUPPLY 2 6-32 CAP SCREWS

ACCOUNT # 505-30501-0-2050

JPL

(PREPARED BY)	(DATE) 10-20 89	(REPORT NO.)
(CHECKED BY)	(DATE)	(PROJECT)

TITLE PITCH AXIS SUPPORT

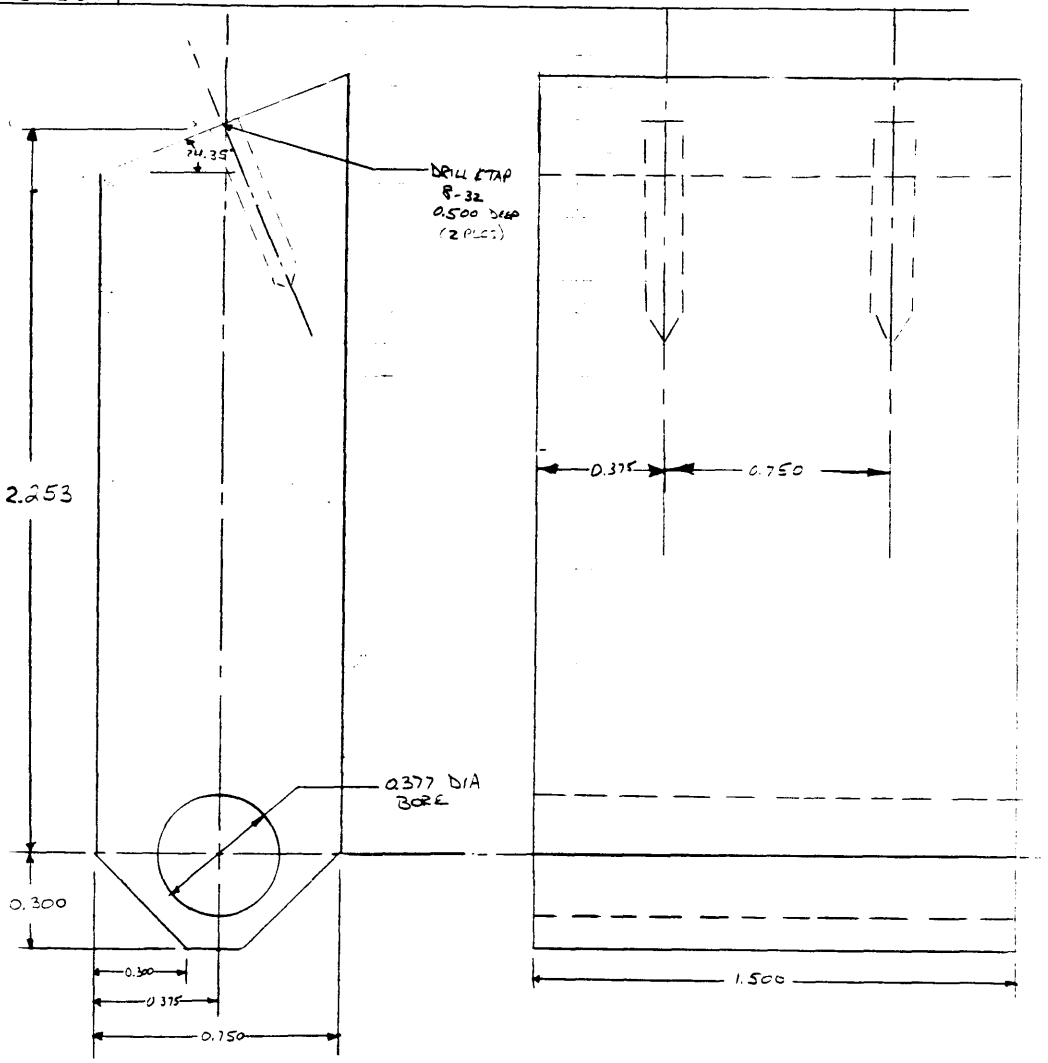

ALUMINUM

QTY - 1

ALL DIMENSIONS IN INCHES
SUPPLY 8-32 CAP SCREW

ACCOUNT # 505 3050-0-2052

JPL

PAGE _____ OF _____

(PREPARED BY)	(DATE) 11-7-69	(REPORT NO.)
(CHECKED BY)	(DATE)	(PROJECT)

TITLE WHEEL - STROT ASSEMBLY

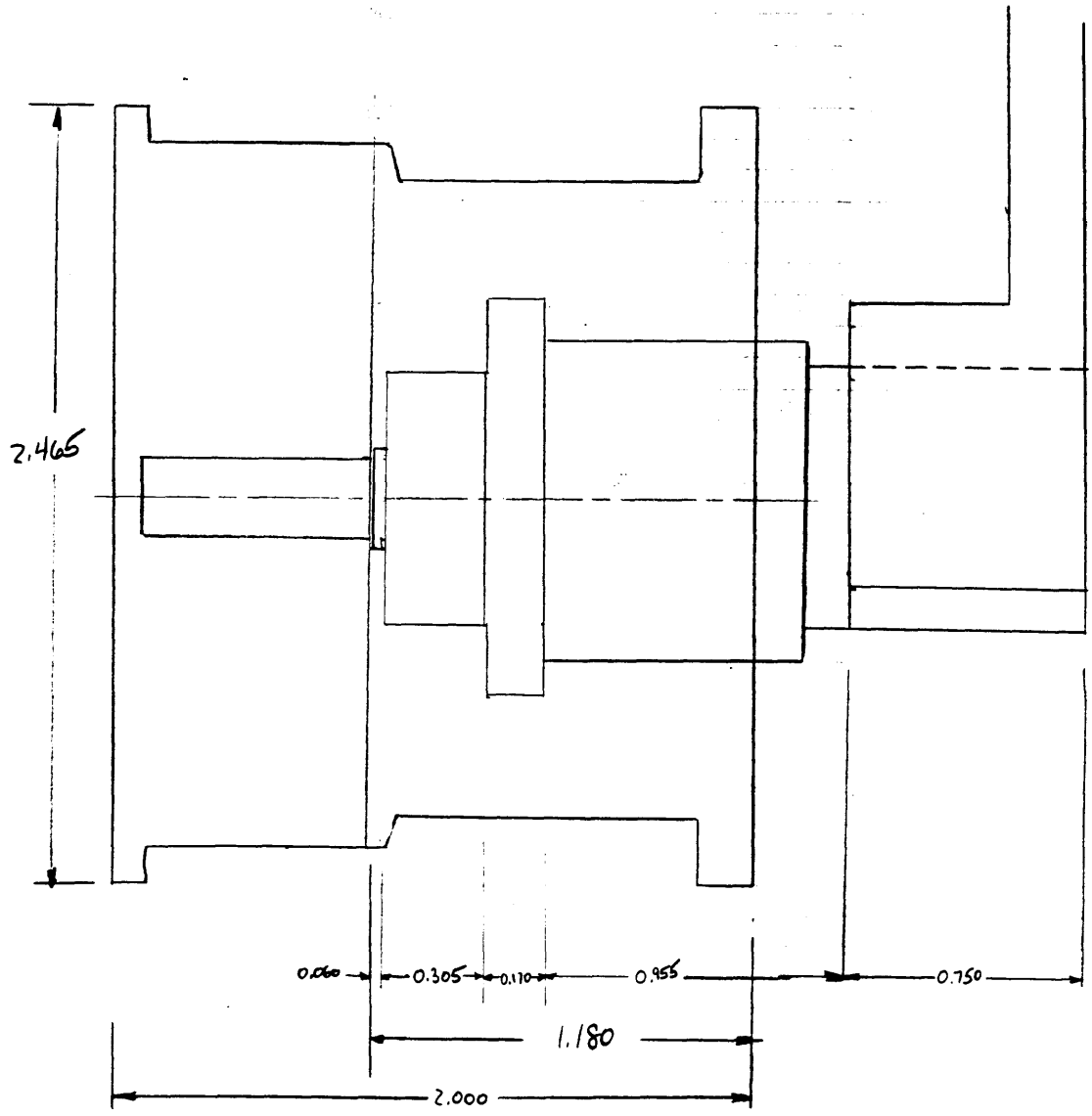

JPL

PAGE _____ OF _____

(PREPARED BY)	(DATE)	(REPORT NO.)
HOWARD JAY EISEN	11-7-89	
(CHECKED BY)	(DATE)	(PROJECT)
		MRSR/PAR NAVTEST 1/7 SCALE MODEL

TITLE
FRONT / REAR BODY PLATES

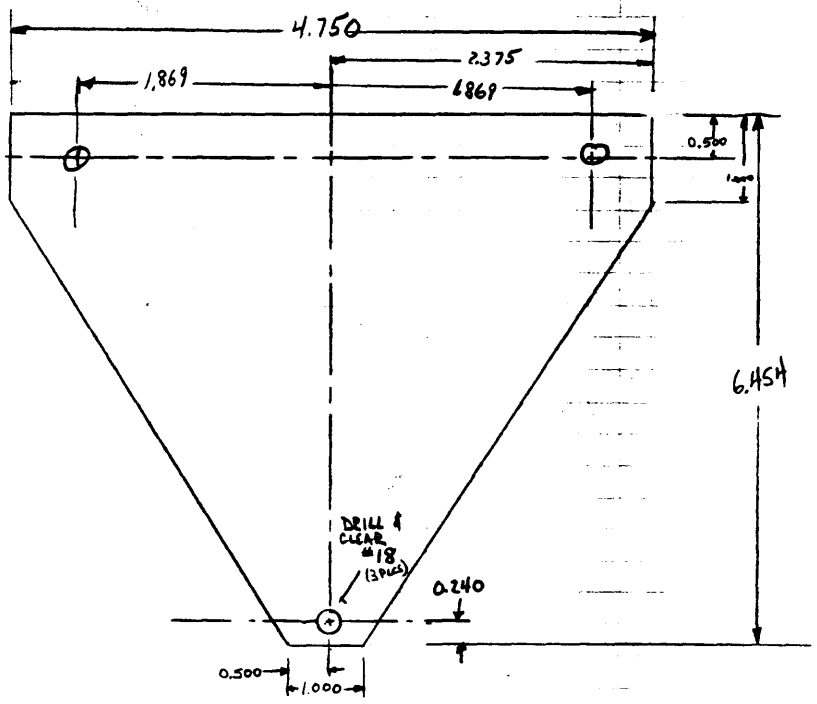

ALUMINUM
THICKNESS 1/8"

QTY: 2

ACCOUNT 505-30501-0-2050

JPL

PAGE _____ OF _____

(PREPARED BY)	(DATE)	(REPORT NO.)
(CHECKED BY)	(DATE)	(PROJECT)

TITLE

CENTER BODY PLATE

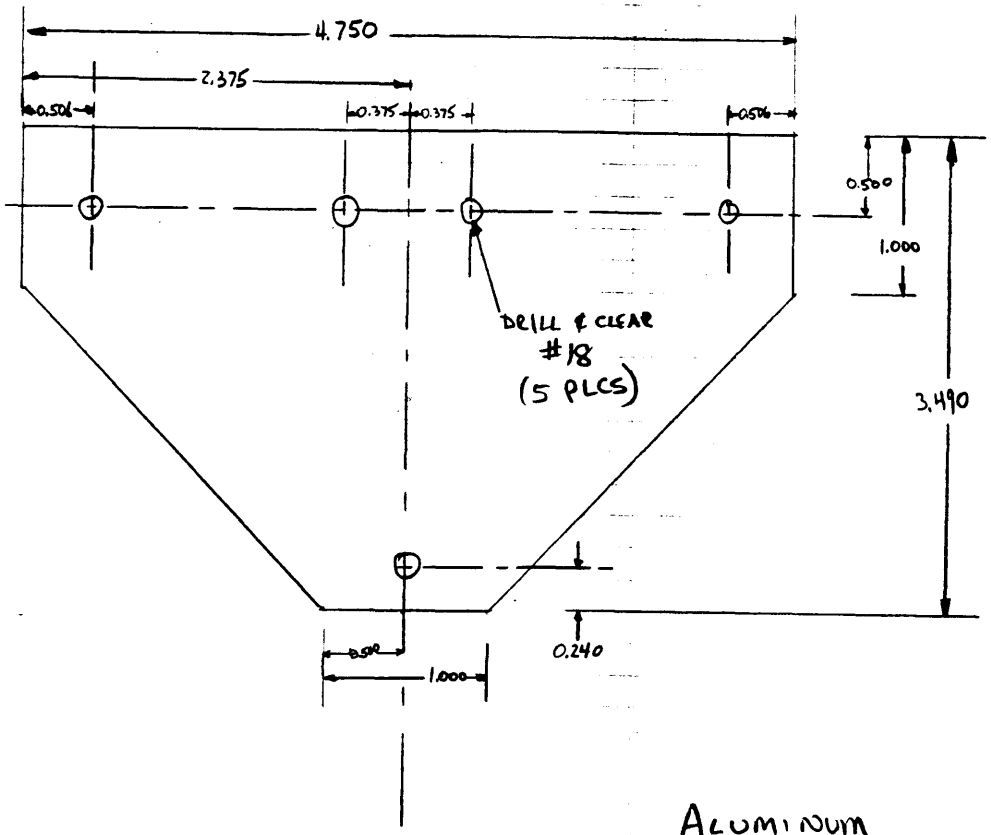

ALUMINUM
THICKNESS 1/8"
QTY: 1

ACCOUNT: 505-30501-0-2050

JPL

PAGE _____ OF _____

(PREPARED BY)	(DATE)	(REPORT NO.)
(CHECKED BY)	(DATE)	(PROJECT)

TITLE

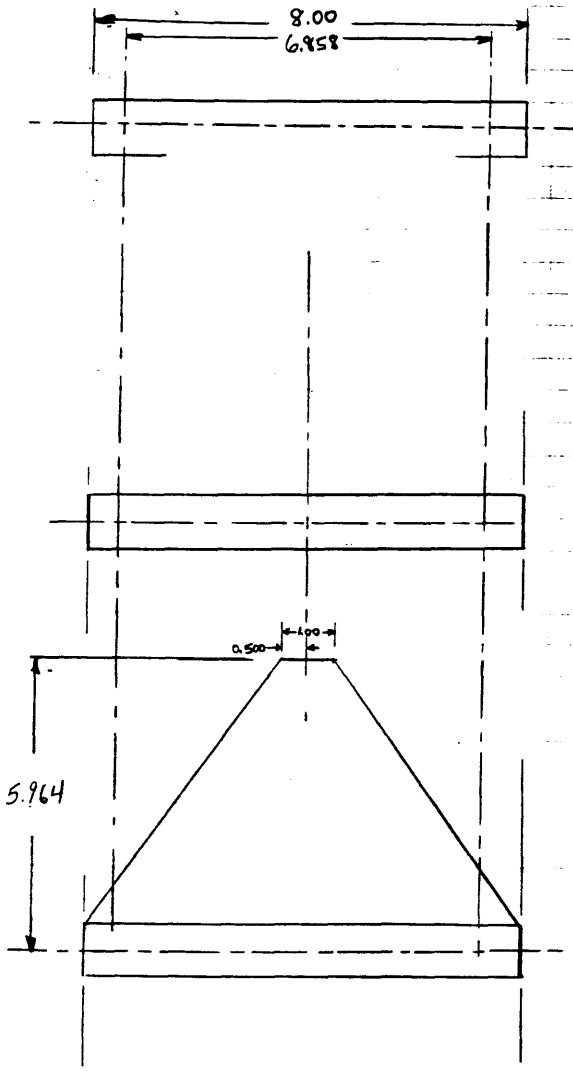

Aluminum 0.125" THICK

JPL

(PREPARED BY)	(DATE) 11-9-89	(REPORT NO.)
(CHECKED BY)	(DATE)	(PROJECT)

TITLE

STRUT MODIFICATION

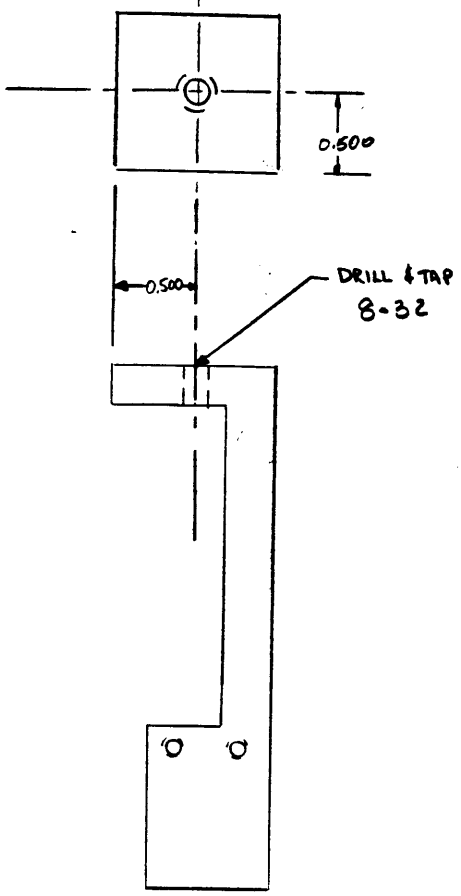

SUPPLY SIX (6)
8-32, 1/2" LONG
ALLEN HEAD CAP SCREWS

QTY: 6

ACCOUNT 505-3501-0-2050

Appendix C
Tire Test Equipment and Safety Analysis

This appendix contains two sets of information related to the tests performed with the tires of the Navtest vehicle. The first shows the fabrication drawing of the "axle" and "mounting wheel" designed to support the tire and provide the appropriate weight loading through attachment to the Instron load cell. The second part of the Appendix shows the safety analysis which the author performed on the equipment to insure that the ultimate factor of safety for the test apparatus was greater than five.

JPL

PAGE 1 OF 1

(PREPARED BY)	(DATE)	(REPORT NO.)
HOWARD EISEN 4-9360	10-20-89	
(CHECKED BY)	(DATE)	(PROJECT)
		BOB HINES 4-2255

TITLE

TIRE PRESSURE / DEFLECTION AXLE

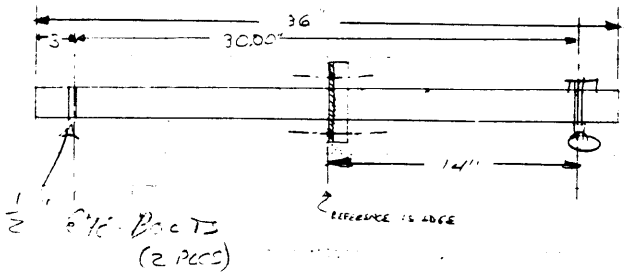

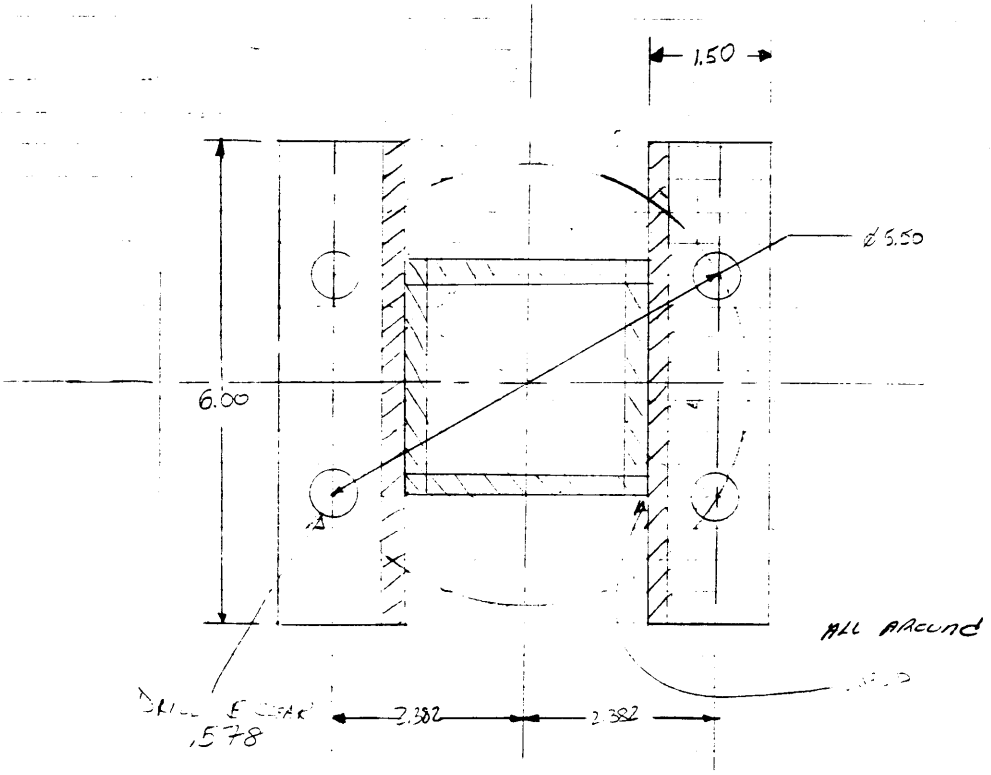

3" x 3" x 1/4 RECTANGULAR TUBING
5" x 3" x 1/4 ANGLE

AMOUNT #

505-30501-1-2050

E-061

JPL

PAGE _____ OF _____

(PREPARED BY)	(DATE)	(REPORT NO.) DEFLECTION TEST EQUIPMENT
(CHECKED BY)	(DATE)	(PROJECT) MRSR/PPR SCALE MODEL STUDY

TITLE

WHEEL MOUNTING FLANGES

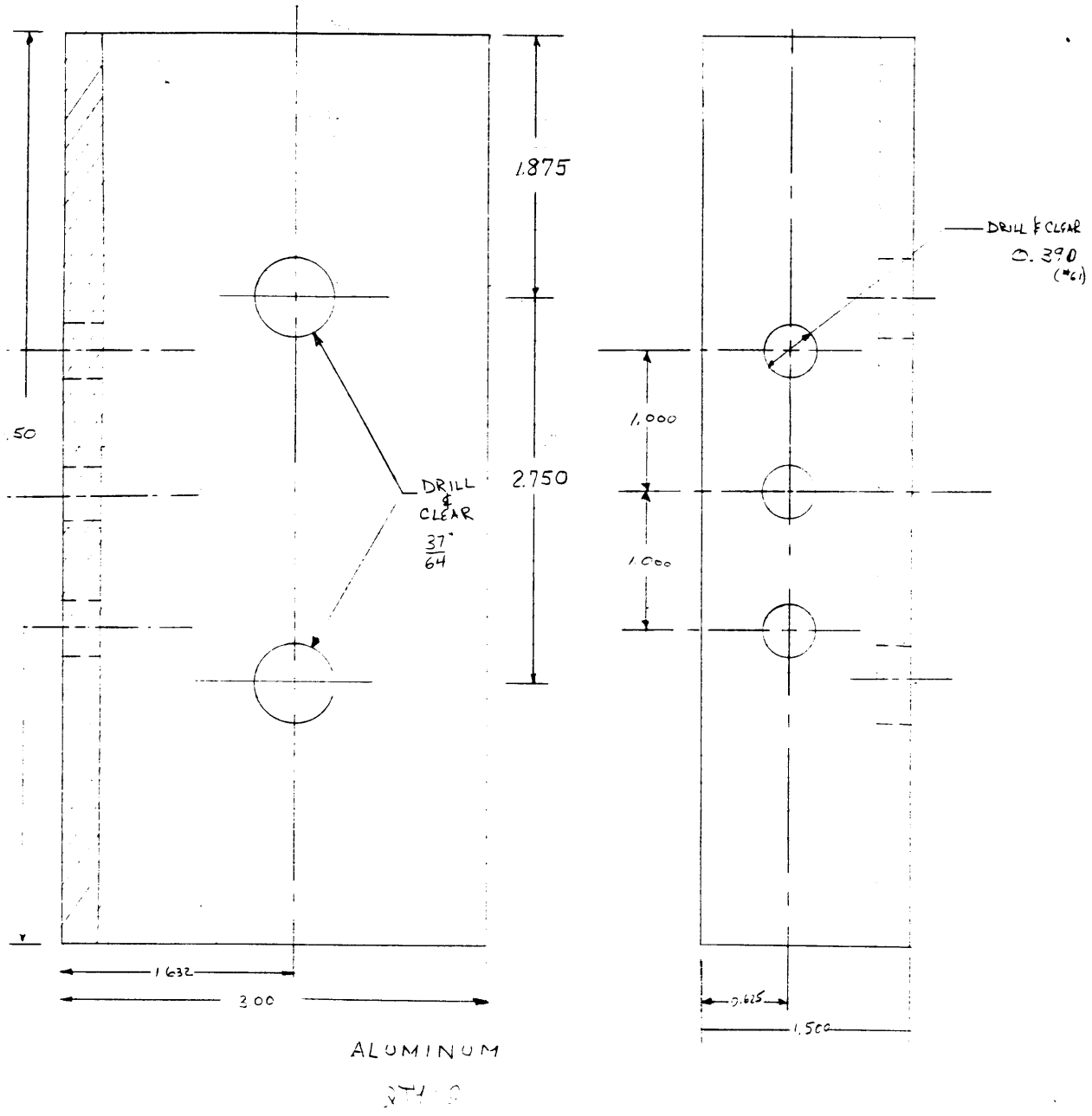

ALUMINUM

JPL

PAGE 1 OF 2

(PREPARED BY)	(DATE)	(REPORT NO.) TIRE DEFLECTION TEST PLAN
(CHECKED BY)	(DATE)	(PROJECT) MRSR/PAR SCALE MODEL STUDY

TITLE
SAFETY ANALYSIS

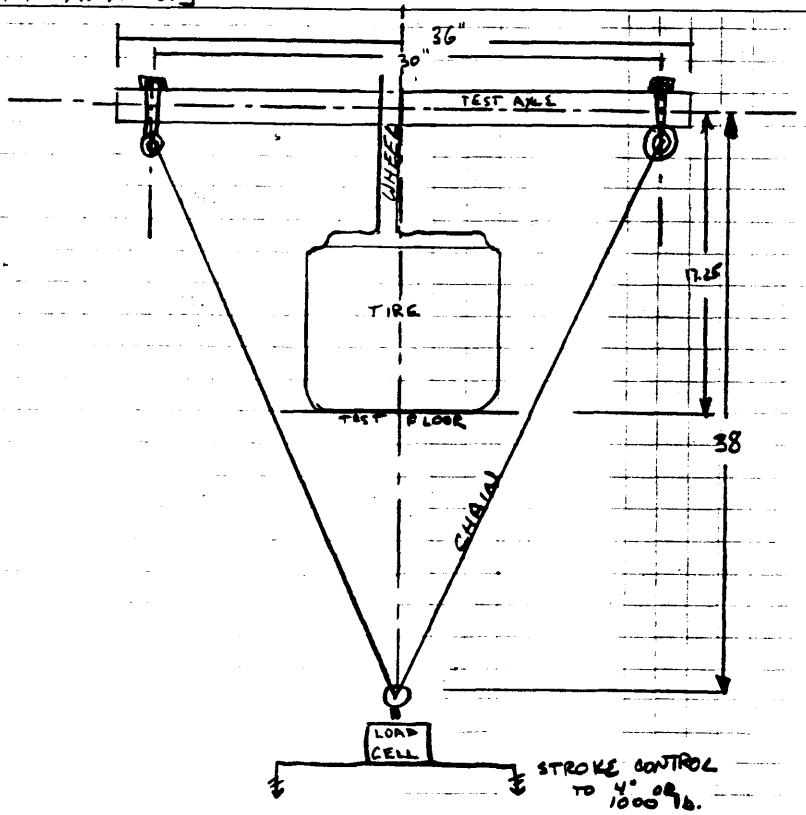

39" CHAIN P = 545 lb
STEEL
TESTED TO
4200 lb ULTIMATE
2200 lb YIELD
UFS = 7.7

AXLE: 3" x 3" x 0.25" SQUARE TUBING $c/I = 0.429$

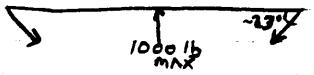

BENDING LOAD: 500 lb x 15" = 7500 in-lbs

$\sigma_b = \frac{Mc}{I} = 3218$ psi

COMPRESSION LOAD: 212 lb

$\sigma_c = \frac{P}{A} = 77$ psi

$\sigma = 3295$ psi

UFS = 11.5 (6061-T6 σ_u = 38 ksi)

EYEBOLTS: 3/4" DIA

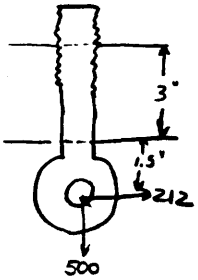

+EYEBOLT MOMENT 212 lb · 3" = 636 lb-in
$\sigma = 264$ psi
$\sigma_y = 3559$ (UFS = 10.7)

$F_1 = 106$ lb
$F_2 = 318$ lb

$\tau_2 = \frac{P}{A} = \frac{318}{(.75)(.25)} = 1696$ psi

∴ EYEBOLTS WILL NOT RIP OUT IN SHEAR

CLASSIFICATION

JPL 7000 5 (REV 11/83)

JPL

PREPARED BY)	(DATE)	(REPORT NO.)
CHECKED BY)	(DATE)	(PROJECT)

TITLE

EYEBOLTS: BENDING: M_{max} moment = 212 × 1.5 = 318 in-lbs

$c/I = 24.14$

$\sigma_b = \frac{Mc}{I} = 7676$ psi

TENSION: $\sigma = P/A = 1131$ psi

$\sigma_T = \sigma_b + \sigma_T = 8807$ psi (UFS = 5.7 for $\sigma_{ult} = 50$ ksi STEEL)

PULL-THROUGH: Assuming Aluminum bearing strength of 38 ksi, for UFS > 5,

$\sigma < 7600$ psi

$\sigma = \frac{P}{A} < 7600$ psi

$A > .066$ in^2

with 3/8" bolt, WASHER DIA > 7/8"

BOLT CAN HOLD

USE THICK 1.25 - 1.5" WASHER TO PREVENT LOCAL DEFORMATION.

Appendix D

Navtest Mobility Equipment and Safety Analysis

The mobility test apparatus for the Navtest vehicle was designed with the expectation that the Navtest would be available for evaluation. A safety analysis was performed on the equipment to ensure that a large (>5) factor of safety existed. The failure of any of the restraining components could prove to be a fatal accident considering the mass and power of a vehicle such as the Navtest, operating near its threshold. The design of the floor rails is shown first, then the safety analysis, and finally the end-caps for the wall supports which were modified to minimize bolt-bending loads at the joints. The aluminum rails were chosen as they provide ease of attachment to the upright supports and good torsional stiffness. The holes were cut at a spacing optimized by the author to provide a good range of possible angles with a high level of precision on adjustments. The 0.516" holes were cut at a spacing of either 1.5" or 1.75" to allow a two degree change in the wall angle, without sacrificing the structural integrity of the aluminum by overcutting.

JPL

PAGE ____ OF ____

(PREPARED BY)	(DATE)	(REPORT NO.)
HOWARD JAY EISEN x49360		FULL SCALE TEST EQUIPMENT
(CHECKED BY)	(DATE)	(PROJECT)
		MRSR/PPR SCALE MODEL SNOW

TITLE

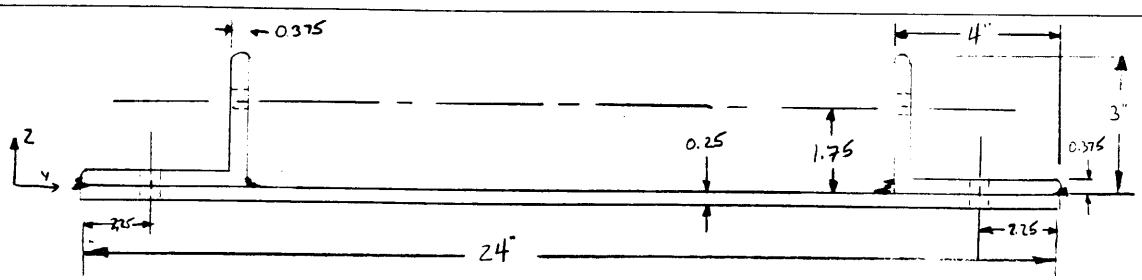

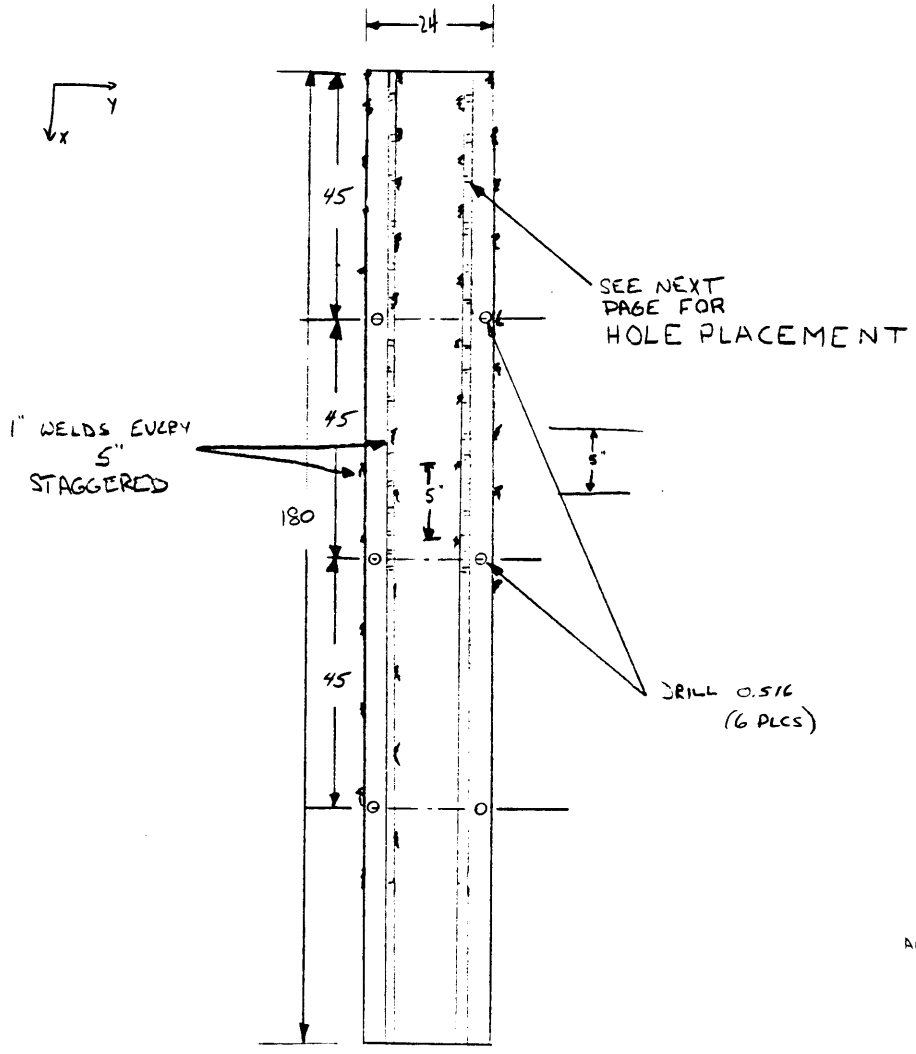

ALL DIMENSIONS IN INCHES

ALUMINUM
GR-W 2

JPL

PAGE _____ OF _____

(PREPARED BY)	(DATE)	(REPORT NO.)
(CHECKED BY)	(DATE)	(PROJECT)

TITLE

HOLE PLACEMENT

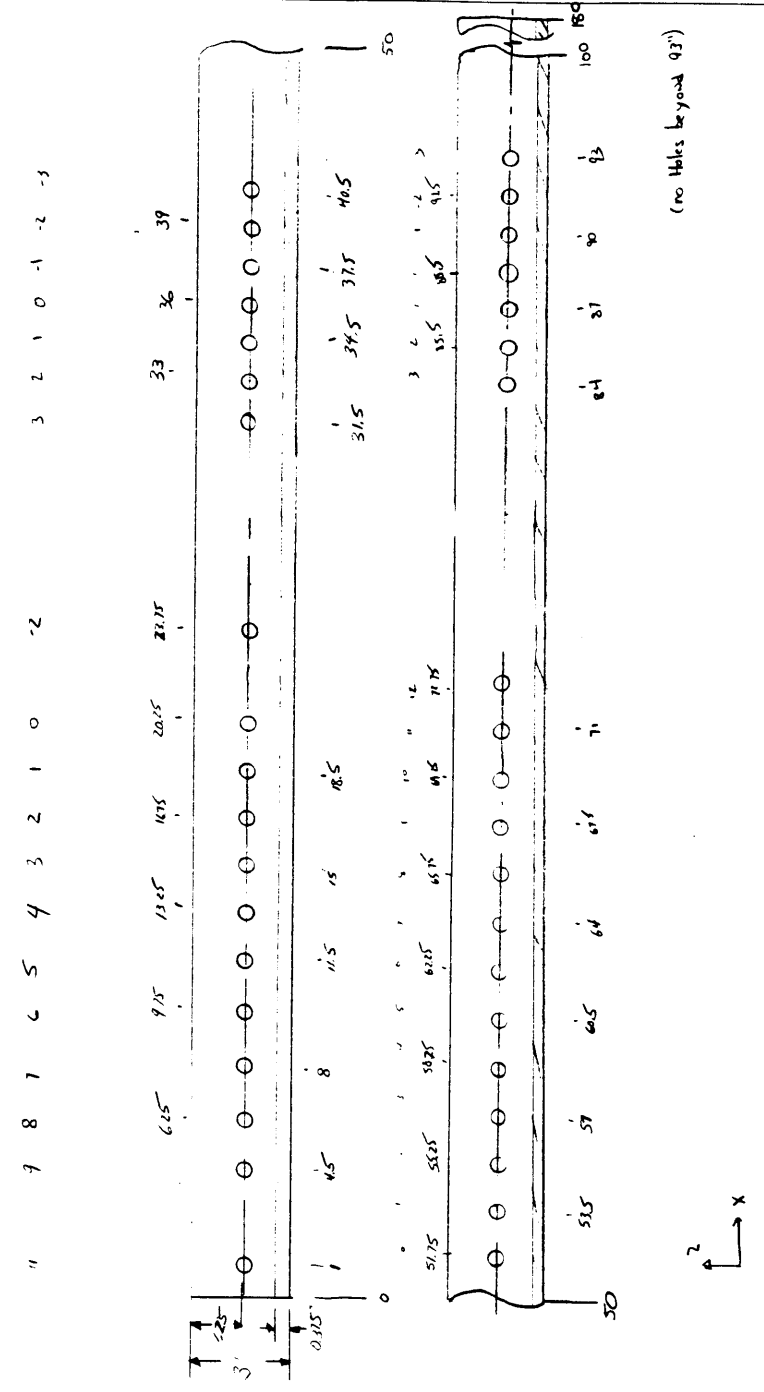

JPL

PAGE 1 OF

(PREPARED BY)	(DATE) 11-14-89	(REPORT NO.)
(CHECKED BY)	(DATE)	(PROJECT)

TITLE

FAILURE / SAFETY ANALYSIS FOR TEST STAND

$$\tan\theta = \frac{b\sin\alpha}{b\cos\alpha + \ell}$$

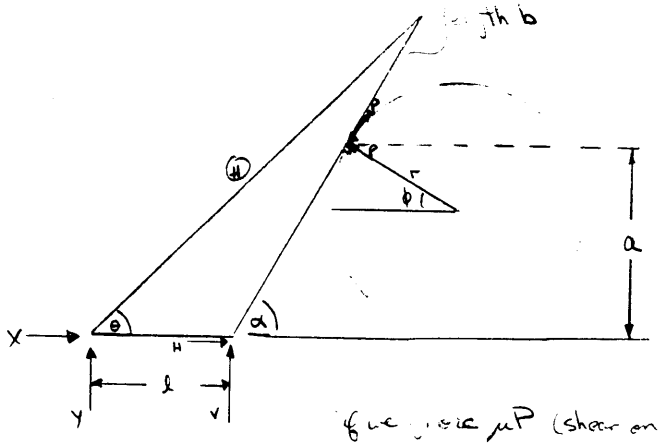

$\alpha + \phi = 90°$

$\phi = 90 - \alpha$

$a = r + r\sin\phi$

$a = r(1+\cos\alpha)$

If we ignore μP (shear on the wall-to-ice interface)

Σ_H: $X + H - P\sin\alpha = 0 \rightarrow H = P\sin\alpha - X$

Σ_V: $Y + V + P\cos\alpha = 0 \rightarrow V = -Y - P\cos\alpha$

Σ_M: $Y\ell - Pa\frac{1}{\sin\alpha} = 0 \rightarrow Y = \frac{Pa}{\ell\sin\alpha} = P\frac{r}{\ell}\frac{1+\cos\alpha}{\sin\alpha}$

No Moment on Ⓗ: $\frac{X}{Y} = \cot\theta \rightarrow X = Y\cot\theta = P\frac{r}{\ell}\frac{1+\cos\alpha}{\sin\alpha}\cdot\frac{b\cos\alpha+\ell}{b\sin\alpha}$

take $W = 2600$ lb

$\mu \sim 0.9$

$P \sim 1100$ lb / side

$b = 35'$

FAILURE MODES:

Bending and Tension in Wall

Compression in support Ⓗ / Buckling

Bending and Tension in Floor

Floor bolt rip-out

For $\alpha = 60°$ (Worst Case)

$X = 2255$

$Y = 2055$

$H = -1302$

$V = -2615$

SELECTED MEMBERS

Ⓗ and wall supports $2\times2\times\frac{1}{4}$ SQ TUBE

FLOOR RAILS : $3\times4\times\frac{3}{8}$ ANGLE

6061-T6 Aluminum (Mcks T

(PREPARED BY)	(DATE) 11-14-89	(REPORT NO.)
(CHECKED BY)	(DATE)	(PROJECT)

TITLE

BENDING AND TENSION IN WALL

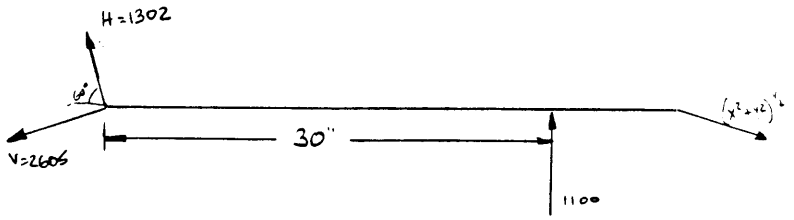

TENSION LOAD = $(H\cos 60° + V\sin 60°) = (x^2+y^2)^{1/2}\cos(60 - \text{Arctan}(\frac{y}{x})) = 2907\ lb = P$

Moment = $30"(H\sin 60° + V\cos 60°) = 30"(175\,lb) = 5250\ in\cdot lb = M$

$$2\sigma_{max} = \frac{Mc}{I} + \frac{P}{A} \qquad \text{(2 supports/wall)}$$

	A	c/I	σ_{max} (psi)	UFS	δ_{max} (x=20)
3x3x¼ SQ TUBE	2.75 in²	0.429	1655	25	0.015
2½x2½x¼ SQ TUBE	2.25 in²	0.650	2353	18	0.027
2x2x¼ SQ TUBE	1.75 in²	1.097	3710	11	0.057

COMPRESSION AND BUCKLING OF SUPPORT (A)

Compression Load = $(X^2+Y^2)^{1/2} = 3053\ lb = 1527\ lb/support$

$\sigma = \frac{P}{A}$, $\sigma < 8400$ psi (UFS=3), $A > 0.182\ in^2$ /support

Euler Buckling $P_E = \frac{\pi^2 E I}{L^2}$ $\quad L = 45\ in$

$I > 0.148\ in^4$ (UFS=5) per support

	A	I	UFS	EL
2x2x¼ SQ TUBE	1.75 in²	0.9115 in⁴	30.8	0.004 in

(PREPARED BY)	(DATE) 11-14-89	(REPORT NO.)
(CHECKED BY)	(DATE)	(PROJECT)

TITLE

BENDING OF FLOOR RAILS

BOLTS @ 45, 90, 135

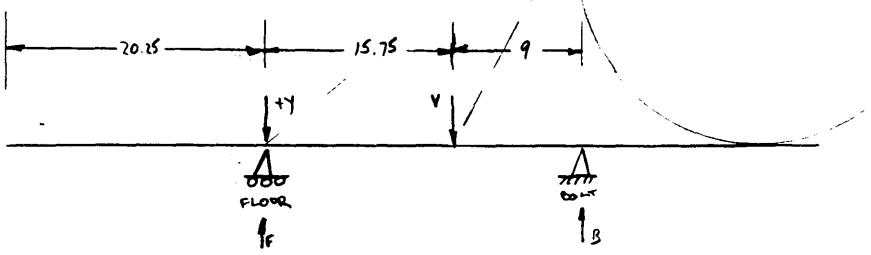

$\uparrow + \Sigma F_{forces}$: $F - Y - V + B = 0$

$\circlearrowleft + \Sigma M_{moments}$: $(F-Y)(24.75) - V(9) = 0$

$\Rightarrow$ $F = 1107$, $B = -1657$

$F - Y = 941$

SHEAR DIAGRAM

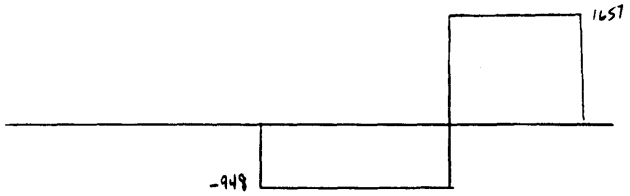

MOMENT DIAGRAM

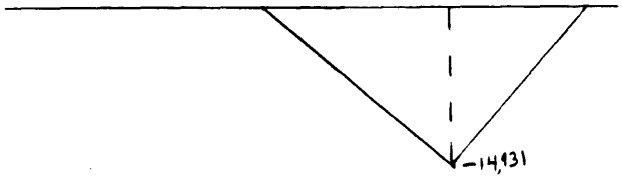

CROSS-SECTION OF FLOOR

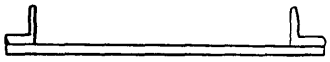

$M_{max} = -14931$ in-lb

$m = 7466$ in-lb / side

$\sigma = \frac{Mc}{I}$

	A	$\frac{c}{I}$	σ	$\delta_{(at\ V)}$	
4x4 x $\frac{1}{4}$ ANGLE	1.94	0.91	6784	.011	(IGNORING FLOOR
3x4 x $\frac{3}{8}$ ANGLE	2.48	0.667	4980	.008	PLATE
4x3 x $\frac{3}{8}$ ANGLE	2.48	1.149	8578	.018	INERTIA)

JPL

(PREPARED BY)	(DATE) 11-15-89	(REPORT NO.)
(CHECKED BY)	(DATE)	(PROJECT)

TITLE

TENSION IN FLOOR RAILS

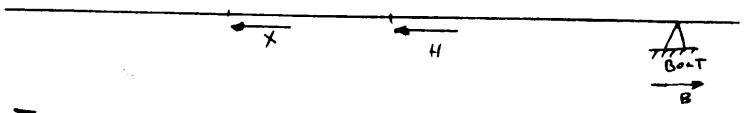

$\Sigma_{M=0}$: $-X - H + B = 0$

$B_M = 953$ lb

$\therefore P_{XH} = X = 2255$ lb/rail → worst case, MAXIMUM TENSILE + MAXIMUM BENDING AT TOP OF RAILS AT PT. H.

$P_{HB} = B_H = 953$ lb/rail

	σ_{BEND}	A	$\sigma_{TENSILE}$	σ_{TOTAL}	UFS	
4x4 x $\frac{1}{4}$	6784	1.94	581	7365	5.7	
3x4 x $\frac{3}{8}$	4980	2.48	455	5435	7.7	✓
4x3 x $\frac{1}{8}$	8578	2.48	455	9033	4.6	

BOLT RIP-OUT

Largest force held by any bolt pair. $(H^2+V^2)^{1/2} = 2912$

$(X^2+Y^2)^{1/2} = 3053$

$B = 1912$

$(X^2+Y^2)^{1/2} = 3053$ lb total = 1527 lb/support

$\frac{1}{2}$" dia bolts

	support ④	floor rails
	2x2 x $\frac{1}{4}$ sq tube	3x4 x $\frac{3}{8}$ ANGLE
BOLT SHEAR AREA:	A_B .25 in^2	A_B = 0.1875
	σ = 6106 psi	σ = 8141
	UFS = 6.9	UFS = 5.2

$\therefore$ BOLTS will not tear through supports or floor rails

JPL

PAGE _____ OF _____

(PREPARED BY)	(DATE)	(REPORT NO.)
(CHECKED BY)	(DATE)	(PROJECT)

TITLE

Bolt Bending

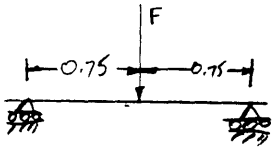

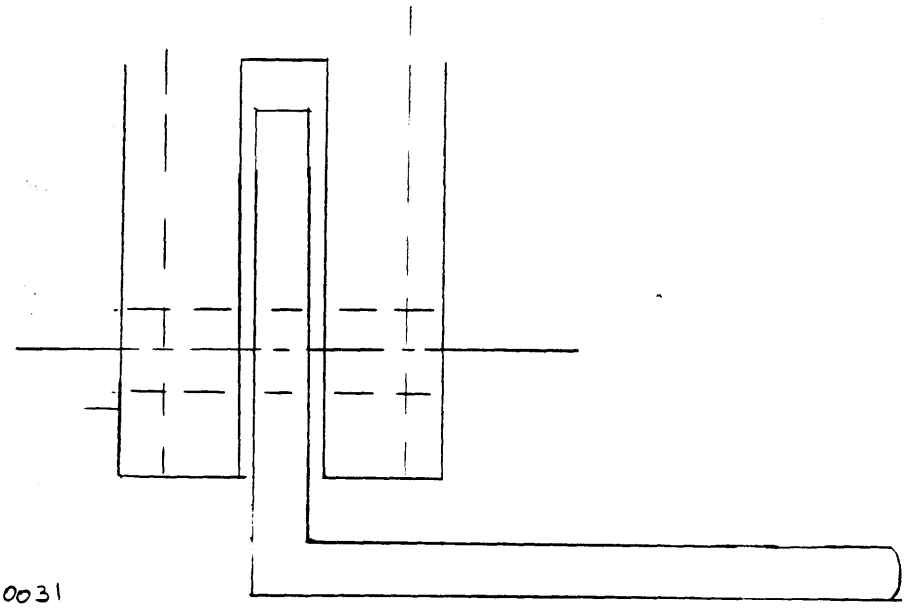

F = 1527 lb maximum

$M = \frac{F}{2}(0.875)$

$M = 668$ in-lb

For a $\frac{1}{2}$" bolt, $I = 0.0031$
$c = 0.25$

$\sigma = \frac{Mc}{I} = 54{,}420$ in-lb

.. NEED EXISTS FOR BETTER JOINT DESIGN

CLASSIFICATION

(PREPARED BY)	(DATE)	(REPORT NO.)
(CHECKED BY)	(DATE)	(PROJECT)

TITLE

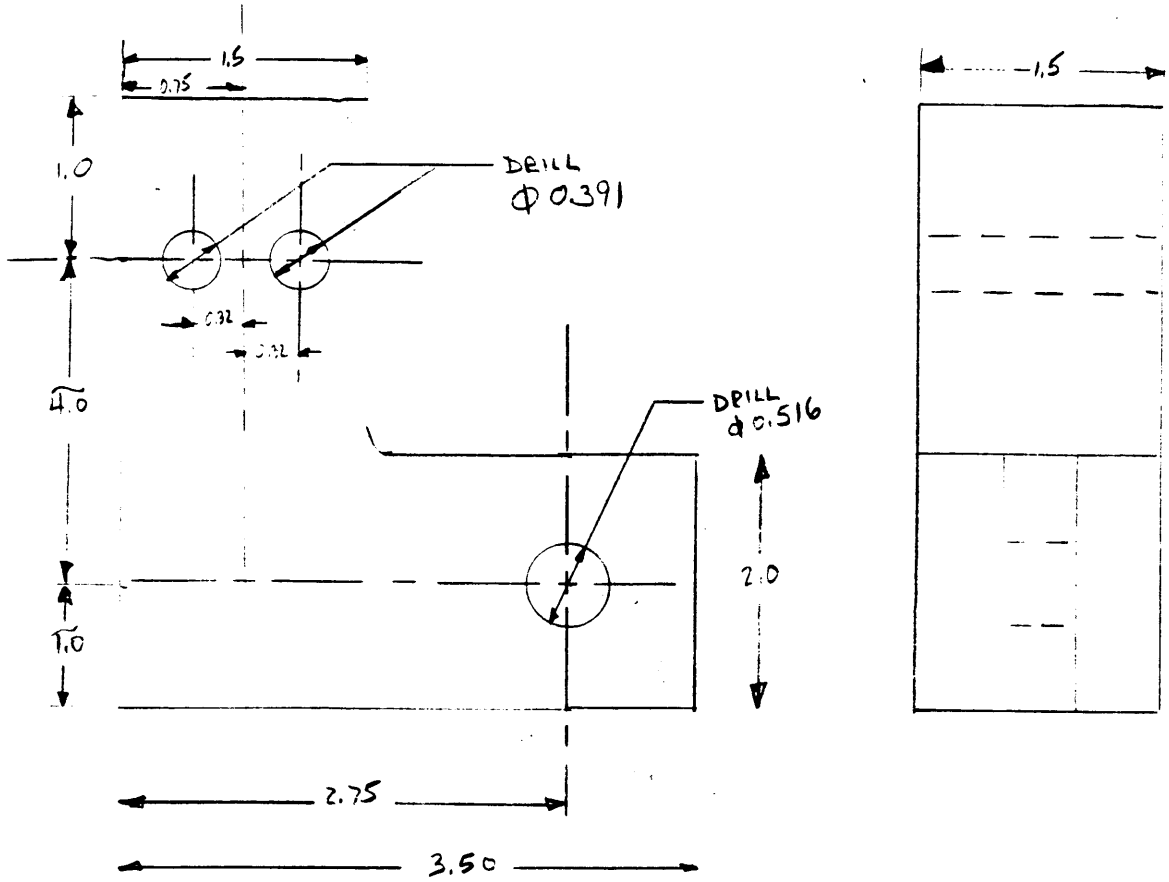

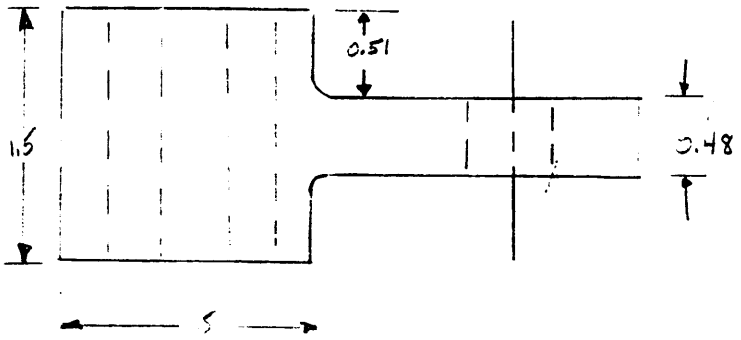

QTY 4

ALUMINUM

JPL

PAGE 1 OF 1

(PREPARED BY)	(DATE)	(REPORT NO.)
Howard Eisen x4-9360		
(CHECKED BY)	(DATE)	(PROJECT)

TITLE

STRUT END-CAPS

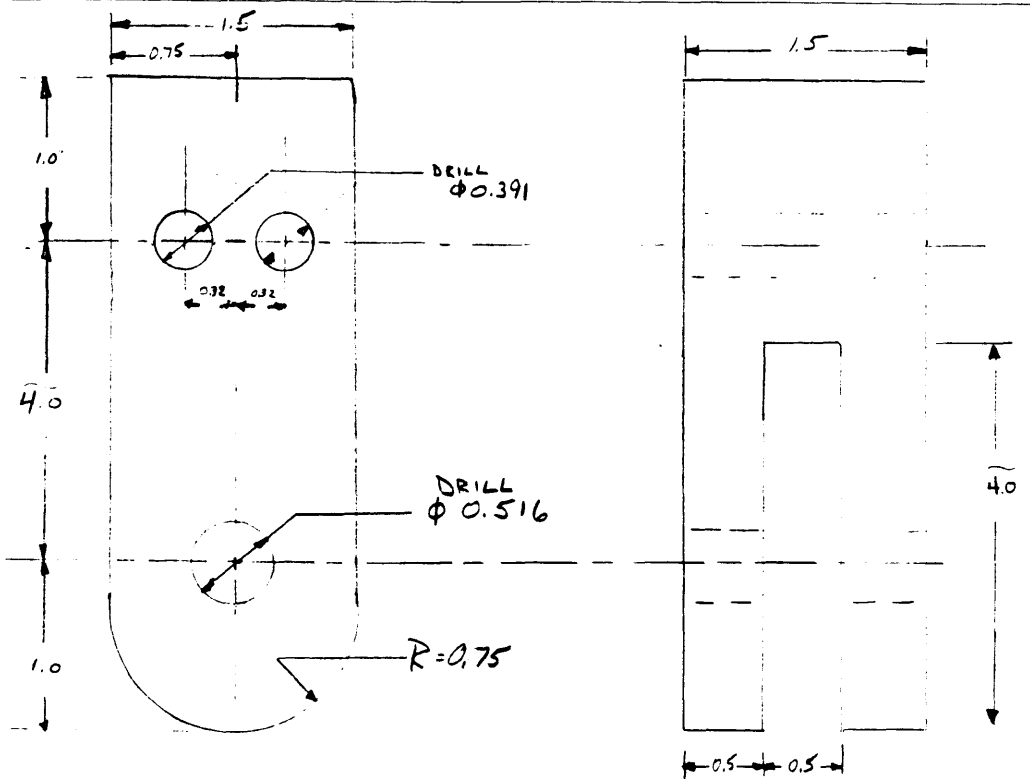

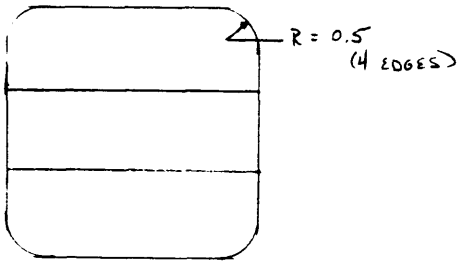

ALUMINUM

QTY: 12

Supply 12-½" x 2" STAINLESS BOLTS + NUTS

ACCOUNT 294-1R201 - 5520

JPL

PAGE _____ OF _____

(PREPARED BY)	(DATE)	(REPORT NO.)
(CHECKED BY)	(DATE)	(PROJECT)
TITLE		

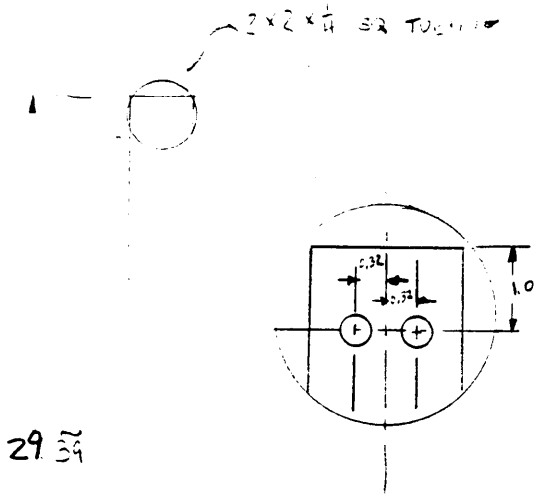

29.39

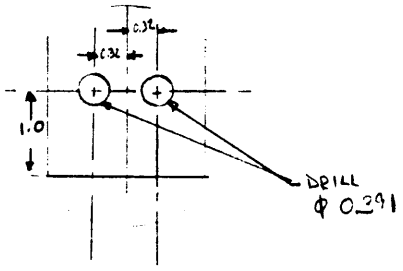

QTY. 4

ALUMINUM

ACCOUNT 294-[illegible]